ACCELERATION AND HEATING OF PLASMAS DUE TO RECONNECTION OF MAGNETIC LINES OF FORCE

by

Shoichiro FUKAO

February 1974

ACCELERATION AND HEATING OF PLASMAS DUE TO RECONNECTION OF MAGNETIC LINES OF FORCE

by

Shoichiro FUKAO

February 1974

Department of Electrical Engineering

Kyoto University, Kyoto, Japan

ACKNOWLEDGEMENTS

The author wishes to express his sincere and hearty appreciation to Professor Takao Tsuda, Hokkaido University, for his continual guidance, stimulating supervision throughout the present work and his careful reading of the manuscript.

The author also wishes to express his hearty appreciation to Professor Emeritus Ken-ichi Maeda who provided the original motivation to take up the ionospheric physics and helped him kindly and patiently during the course of the present work.

The author is deeply indebted to Professor Iwane Kimura for his continual advice and encouragement. Acknowledgement is due to Professors Susumu Kato and Toru Ogawa for their useful and critical discussions and for enlightenment on the attitude of a research.

The author is grateful to Professor Tatsuzo Obayashi, Dr. Atsuhiro Nishida and Mr. Kiyoshi Maezawa, University of Tokyo, for their many discussions and stimulating suggestions.

Several valuable advices of Drs. Toshiyuki Yonezawa and Nobuo Matuura, the Radio Research Laboratories, Tokyo, and Professor Takeo Sakurai are also gratefully acknowledged.

It is also a pleasure to acknowledge Professor Karl Schindler, Ruhr-Universität, Bochum, for the stimulating helpful discussions.

The author wishes to thank Drs. Hiroshi Oya and Kazuaki Takao for their interest in this work.

Thanks are also due to colleagues in the Department of Electrical Engineering and the Ionosphere Research Laboratory of Kyoto University.

Part of the computation was performed at the Data Processing Centers, Kyoto and Hokkaido Universities ; the rest at National Center for Atmospheric Research, Boulder, Colorado.

PREFACE

In the last two decades surprising successes have been achieved in a variety of fields in space science under favor of the progress in rockets and artificial satellites. The topic with which we will concern ourselves in this thesis, i.e., acceleration and heating of plasmas , are those that have never failed to fascinate scientists to their mysterious mechanisms. We may now be proud of our success, but, at the same time, we should know that it is only a glimpse of what the universe still shrouds in mystery.

In this thesis the magnetic field and flow with an X-type neutral point or stagnation point are studied in terms of the *reconnection of magnetic lines of force.* In its somewhat intuitive concept, the reconnection mechanism involves two important physical processes : acceleration and heating of plasmas ; and penetration of an electric field parallel to a plane at rest.

The original stimulus for considering the reconnection process was derived from the solar-flare phenomenon, but recently there has been considerable interest as a possibly important process in strong radio sources and star formation and in the study of geomagnetic storms. Some attempts have also been performed in order to simulate the flare events in laboratory devices, which means in itself the acceleration and heating of plasmas due to the release of magnetic energy.

In chapter 1, we describe a concept and kinematics of magnetic lines of force, together with the way in which a pair of antiparallel magnetic lines of force reconnect with each other at a neutral point.

We will also mention solar flares and geomagnetic storm events shortly.

Chapter 2 deals with the classification of magnetic neutral points in an infinitely conducting fluid. The X-type magnetic neutral point, with which we will mainly concern ourselves, can be appropriately classified as one of the neutral points. The probable existence of spiral and node types of neutral points, and their physical implication as well, are tentatively discussed.

Chapter 3 is given to the critical survey of the current models for the stationary-state reconnection at X-type neutral points. Each model will be examined whether it can describe the explosive phase of the largest solar flares, during which 10^{32} ergs of the kinetic energy are likely to be carried away by a plasma of 10^{16} g ejected at some 1500 km/sec. There have been two opposing points of view concerning what determines the rate of reconnection. One is to assume the conditions near the neutral point to be predominant, while the other considers the conditions far from the point to be important. Both of them say that it is possible to account for the explosive phase of the largest solar flares. However, we cannot approve of their results, since these theories could not completely succeed in the matching of the solutions which were separately studied in the vicinity of the neutral point and in the region far from it.

Hence in chapter 4, we investigate, though numerically, two dimensional stationary-state solutions of a finitely conducting magnetohydrodynamic (MHD) fluid in which no such clear-cut distinctions are made between the two regions. Although the Reynolds numbers used are much smaller than the actual ones, the resulting solutions exhibit smooth transition in their properties from the diffusive near the neutral point to the convective far from it. We can show that the stationary-state reconnection may be possible even in very highly conducting fluids, and that the overall features are not essentially influenced by dissipations due to finite electrical conductivity or viscosity, but definitely by external conditions such as the applied electric field in the magnetized fluid.

Finally, chapter 5 is devoted to the study of the evolutionary process involving a reconnection of magnetic lines of force. Given an initial antiparallel magnetic field, or a current sheet, to which there is an injection of fluid in a transverse direction, we numerically seek to see how the process of reconnection builds up. The findings of this experiment are : magnetic lines of force can reconnect and grow to the X-type configuration in fluids of any finitely large hydromagnetic and hydrodynamic Reynolds numbers ; the conditions local to the neutral point are less important than the external conditions that set up global flow patterns ; acceleration of fluid in bulk only concerns whether the X-type configuration grows to the comparably large extent or not ; and the electric field at the neutral point due to the rapidly changing magnetic field is less efficient in accelerating charged particles.

In chapter 6, the relevant laboratory experiments are shortly mentioned, together with some complementary remarks to the particle acceleration.

All equations and quantities are in the rationalized MKS system of units unless otherwise mentioned.

CONTENTS

ACCELERATION AND HEATING OF PLASMAS DUE TO RECONNECTION OF MAGNETIC LINES OF FORCE

Chapter 1

GENERAL INTRODUCTION

§ 1. Introduction

We have some concepts which possess no real physical entity but describe the qualitative nature or an intuitive side of a physical quantity or a phenomenon. Such concepts are sometimes useful, for they make it easy to give insight into complicated phenomena and to allow the deduction of general results without excessive calculation.

The concept " magnetic lines of force " belongs to this category. We can neither see nor touch them ; they have no real entity, and accordingly we cannot discriminate some line of force from the other. But, for example, when a charged particle is placed in the magnetic field, we are able to make sure of their existence by the particle's gyration. We could show a more familiar example ; put iron powder on a thin board and move a magnet under it, then we can also ascertain its existence by the alignment of the iron powder along the lines of force.

The concept " magnetic lines of force are *frozen* in highly conducting fluids ", which was advanced first by Alfvén in 1942 (Stern, 1966), can qualitatively describe the evolution of magnetic field in highly conducting fluids. It has often been a powerful tool for the elucidation of the complicated geophysical and astrophysical situations.....

§ 2. Concept of Magnetic Lines of Force

2.1 What are magnetic lines of force ?

The magnetic field B is solenoidal and therefore can be represented by two scalars. Though it may be represented in several ways, it is advantageous, for studying magnetic lines of force, to introduce Euler potentials α and β such that

$$B = \nabla\alpha \times \nabla\beta = \nabla \times (\alpha\nabla\beta) . \qquad (1.1)$$

The line of intersection of a pair of surfaces $\alpha \equiv$ constant and $\beta \equiv$ constant *defines* a line of force characterized by the associated values of α and β. It is informative to touch briefly on the features of Euler potentials (Stern, 1966).

(1) The use of Euler potentials facilitates the introduction of tubes of flux. The flux in the tube with a rhomboidal cross section, defined by the 4 lines of force (α, β), $(\alpha + d\alpha, \beta)$, $(\alpha, \beta + d\beta)$ and $(\alpha + d\alpha, \beta + d\beta)$, is given by

$$d\Phi = d\alpha d\beta . \qquad (1.2)$$

(2) A pair of Euler potentials α and β are not uniquely defined, and an alternative choice of $h(\alpha, \beta)$ and $g(\alpha, \beta)$ are possible for a given pair of potentials, provided $\partial(g, h) / \partial(\alpha, \beta) = 1$.

(3) Since the representation is not linear, the superposition of Euler potentials due to several sources is not in general valid. As a result, it is not possible to derive the potentials α and β analytically, except in some simple field configurations. One such case for which the potentials can be derived analytically is provided by a two-dimensional field, where B neither depends on z nor has a component in its direction. One may then choose

$$\beta = z \ ,$$

$$\alpha = A(x, y) \ ,$$

hence

$$B = \nabla A(x, y) \times \nabla z \ . \qquad (1.3)$$

It may be said, in plainer words, that each equi-potential contour of A represents the corresponding magnetic line of force. Superposition of potentials exists in this case, all of them sharing the same β.

(4) Magnetic lines of force characterized by families of Euler potentials are often not closed and therefore attain infinite length in a bounded region of space. We can easily give an instance, e.g., magnetic lines of force which come from both a current flowing along a circle r = R in the z = 0 plane and a filamentary current along the z-axis of a cylindrical coordinate system. The α-surfaces are toroidal rings and β-surfaces an archimedean screw with its axis twisted around the circle and its ends, in general, not meeting.

2.2 Kinematics of magnetic lines of force

An alternative description of a magnetic field which changes in time in a known way is possible by assuming a velocity to the associated lines of force. Here we will mention the *motion* of magnetic lines of force.

The surfaces of α and β which are convected with the fluid define a velocity of the lines of force, v. Since the rate of change in α and β, as observed by a particle moving with the fluid's velocity v, vanishes, they satisfy

$$\frac{\partial \alpha}{\partial t} + v \cdot \nabla \alpha = 0 \ , \qquad (1.4a)$$

$$\frac{\partial \beta}{\partial t} + v \cdot \nabla \beta = 0 \ . \qquad (1.4b)$$

A velocity satisfying this condition can always be found (Northrop, 1963), such that

$$v = \left(\frac{\partial \beta}{\partial t} \nabla \alpha - \frac{\partial \alpha}{\partial t} \nabla \beta \right) \times \frac{B}{B^2} \ . \qquad (1.5)$$

This definition is not concerned with the velocity component parallel to B, which we set equal to zero customarily. The normal component is then regarded as the velocity of a line of force.

However the solution of Eq. (1.5) is not unique. We have pointed out that there exist many equivalent choices of α and β describing the same B. Therefore we can transform Euler potentials from time to time without altering the physical picture. The velocity corresponding to this transformation may always be added to the velocity (1.5). Such a velocity merely relabels the lines and is termed a " relabeling velocity " (Stern, 1966).

Thus, the definition based on Euler potentials is not entirely satisfactory to define the velocity of the lines of force. We therefore broaden the definition and regard as a " velocity of lines of force " any velocity V satisfying

$$\frac{\partial B}{\partial t} - \nabla \times (V \times B) = \frac{1}{\mu_0 \sigma} \nabla^2 B \ . \qquad (1.6)$$

It can be shown that V consists of three components : a convection velocity v, a relabeling velocity u and a slippage velocity w (Sweet, 1950). Convection of magnetic lines of force with the fluid's velocity v is assumed to satisfy*

---

* Newcomb (1958) showed that v satisfies all verifiable consequences associated with the concept of the motion of lines of force, e.g., line preservation and flux preservation.

$$\frac{\partial B}{\partial t} - \nabla \times (v \times B) = 0 . \qquad (1.7)$$

It may alternatively be said that the change of magnetic field in an infinitely conducting fluid is equivalent to the convection of magnetic lines of force with the fluid's velocity. It may be verified that v of Eq. (1.5) is one of the particular solutions.

Since any relabeling velocity u expresses no variation in the field, it is determined from the equation

$$\nabla \times (u \times B) = 0 . \qquad (1.8)$$

The general solution has the form

$$u = \frac{\nabla \Psi \times B}{B^2} , \qquad (1.9)$$

with Ψ a scalar and $\nabla\Psi$ normal to B.

A velocity of slippage, w, due to finite electrical conductivity is defined by*

$$-\nabla \times (w \times B) = \frac{1}{\mu_0 \sigma} \nabla^2 B . \qquad (1.10)$$

The solution to this equation is given by

$$w = \frac{B \times (\nabla \times B)}{\mu_0 \sigma B^2} . \qquad (1.11)$$

The slippage velocity is proportional to the magnetic body force acting on the fluid. One thus gets the picture of a viscous interaction between the fluid and the lines of force, with the lines exerting a

---

* It is apparent that w includes u (Sweet, 1950), but here they are considered separately.

force on the fluid proportional to their relative velocity. The order of magnitude of w is $(\mu_0 \sigma L)^{-1}$, which is used to indicate the time of decay of a given magnetic field.

§ 3. Reconnection of Magnetic Lines of Force

3.1 Schematic picture

Is it possible for magnetic lines of force to be broken off and reconnected again ? The answer of this question is that it is actually possible only at the magnetic neutral point where $B = 0$. This will now be examined schematically.

Taking the neutral point as the origin, the magnetic field B near a neutral point O may be expressed by the lowest order term of a Taylor expansion

$$B = a \cdot r \tag{1.12}$$

where r is the radius vector to O and a is a constant diadic ($a^T = \nabla B|_o$; T denotes transpose). In this order of approximation, there is no diffusion, i.e., $\nabla^2 B = 0$. Hence magnetic lines of force move only with the relabeling velocity w in such a field in which there is no fluid motion. If such a magnetic field pervades initially, magnetic lines of force do not change the pattern as a whole. Near a neutral point, the relabeling velocity is larger and diverges at O, but at large distances from O it diminishes rapidly to a negligible magnitude. As a consequence, no matter what the flow velocity of the conducting fluid is, there will always exist a small neighborhood of O in which the convection of lines of force by the fluid velocity can be neglected, compared with the relabeling velocity. Here we consider the magnetic lines of force near an X-type neutral point as shown in Fig. 1. The possible existence of this neutral point will be studied

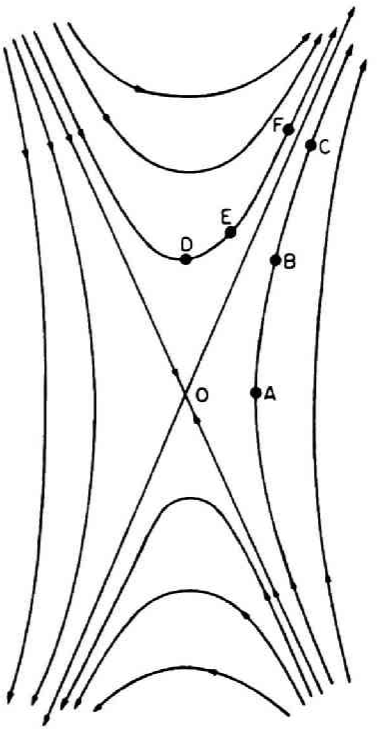

Fig. 1

Schematic configuration of magnetic lines of force near an X-type neutral point. O denotes a neutral point.

in chapter 2. Consider a line of force which initially passes points A,B,C near O. A time interval Δt later the line will move a distance $w\Delta t$. Far from O this shift is negligible, so that if one defines a line by its portion far from O one will be still observing essentially the same line. Near O, however, there will be a real change, with the points A,B,C moving to D,E,F. The point A turns a corner at O by the infinite slippage velocity to reach D while B and C transform smoothly into E and F. This is, what we call, the manner that a pair of oppositely directed lines of force, which go toward the neutral point, are broken off and reconnect with each other at the neutral point.

3.2 Physical meaning

There is no actual change induced before and after the reconnec-

tion in such a field as the one mentioned in the preceding section. It is only a formal relabeling of the magnetic lines of force. When we call for the reconnection in an actual magnetohydrodynamic fluid or in a magnetized plasma, it involves the drastic change both in the field and in the fluid, having the key to the following two processes (Fukao and Tsuda, 1973a).

(1) *Acceleration of particles.* Stored magnetic energy is converted into kinetic and thermal energies of plasmas.

(2) *Quasi-stationary penetration of an electric field parallel to a plane at rest.* If magnetic lines of force grow to an X-type configuration, the fluid is injected from opposite sides, and the electric field is induced parallel to a plane at rest where the incident flow collides. The electric field may exist quasistationarily, since the magnetic energy is carried away by the fluid ejected perpendicular to the injected flow. It is possible for the electric field to be transported along the highly conducting magnetic lines of force across the plane to regions where the electric field has not penetrated before. The detail will be cleared up in the following descriptions.

We add a few comments on nomenclature. Some call the process of reconnection the " annihilation of a magnetic field ", and others, call it the " merging of magnetic lines of force ", according to the images they make of the process or the situation in which it actually occurs. However, we give here a general name " reconnection of magnetic lines of force " to the phenomena that involve neutral points in conducting fluids to bring on such results as mentioned above.

§ 4. Some Roles of Reconnection in Space and Laboratory Plasmas

4.1 Applications to the astrophysics

Astrophysical interest in neutral points dates from an observation by Giovanelli (1947) that solar flares occur preferentially in

the vicinity of neutral points of sunspot fields. This excellent idea —— which still lacks complete confirmation because of the difficulty in identifying neutral points on the sun —— led Dungey (1953 ; 1958 ; 1963) to develope a theory of reconnection which described the acceleration of charged particles in terms of the induced electric field near an X-type neutral point (see, chapter 3, § 2).

Reconnection process has also been considered to be possible in the formation of chromospheric spicules (Uchida, 1969), in the detachment of the magnetic field of an intersteller cloud from the surrounding field (Mestel and Strittmatter, 1967), in X-ray stars (Parker, 1968), and even in galactic flares (Sturrock and Barnes, 1972).

The original stimulus for considering the reconnection of magnetic lines of force was certainly derived from the solar-flare phenomenon, but now it appears on the stage playing a crucial role in the Universe.

We will briefly mention the solar flare phenomenon in the following section which is not only a probable result of the reconncetion but a splendid manifestation of a variety of plasma instabilities. Recently, we have also obtained under favor of the progress in space vehicles, many pieces of observational evidence of the reconnection near and within the earth's magnetosphere. We will, first, give a short account of them in the next section.

4.2 Reconnection near and within the earth's magnetosphere

4.2.1 Observational evidence

There is *indirect* but strong observational evidence for reconnection between the interplanetary and geomagnetic fields. For example, it has been found that geomagnetic disturbance at ground level tends to be greater when the interplanetary magnetic field has a southward

component (see, e.g., Arnoldy, 1971, and references therein). Sonnerup and Cahill (1968) have reported several examples of rotational discontinuities occurring at the magnetopause, especially during magnetic storms ; this is consistent with the occurrence of a significant amount of reconnection on these occasions. Moreover, the dayside magnetopause is found to be closer to the earth when the AE index is large (Meng, 1970) and the interplanetary magnetic field is directed southward (Arnoldy, 1971). In addition, observations of energetic solar particles over the polar caps, in the geomagnetic tail, and in interplanetary space, suggest that the geomagnetic lines of force in the tail are reconnected with interplanetary magnetic lines of force and that this reconnection usually takes place less than about 0.1 AU (AU : astronomical unit of distance, 1AU = 1.495×10^8 km) beyond the earth's orbit (e.g., Domingo and Page, 1971 ; Morfill and Quenby, 1971 ; Van Allen et al., 1971).

Observational evidence has also been obtained for a continuous, but non-uniform, inward shift of the dayside magnetopause by $2R_E$ (R_E : earth radius) during a 2-hour period in which the solar wind momentum flux is thought to have remained constant (Aubry et al., 1970). This inward motion occurred immediately after the direction of the interplanetary magnetic field changed from northward to southward. Moreover, the average position of the magnetopause was closest to the earth when the southward component of the interplanetary magnetic field in the magnetosheath attained its greatest intensity. The inward shift did not produce any compression of the magnetospheric cavity, implying that magnetic flux was transferred from the dayside of the magnetosphere to the geomagnetic tail. Aubry et al. suggest that the erosion of the dayside magnetic flux and the enhancement of the tail magnetic flux, in the absence of an increase in solar wind pressure, may be referred to an increased tangential drag on the geomagnetic cavity resulting from the southward component of the interplanetary magnetic field.

Magnetic neutral line was actually observed in the magnetospheric

tail. Nishida and Nagayama (1973), in what appears to be a very important piece of work, have found that all across the local-time sector of $|y| \leq 15R_E$ (in the solar magnetospheric coordinate), the neutral line is formed somewhere between x = -10 and $-30R_E$ within abount 10 minutes of the onset of the substorm expansion phase.

4.2.2 Model of the magnetosphere

These observational evidence seems in favor of the Dungey reconnection model of the magnetosphere (Dungey, 1963). As sketched in Fig. 2 , there is quite a change in topology when the interplanetary field switches from southward to northward. When the interplanetary

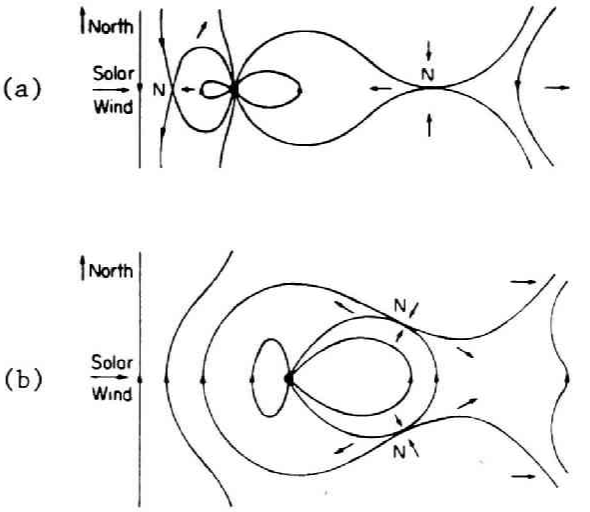

Fig. 2 The Dungey's model of the magnetosphere for : (a) the southward interplanetary field and (b) the northward interplanetary field. N denotes a neutral point. Arrows indicate the direction of plasma flow. A pair of antiparallel magnetic lines of force are carried toward the neutral point from both sides and following reconnections are ejected in the transverse direction. No attempt has been made to draw these diagrams to scale (after Dungey, 1963).

field is southward there are magnetic lines of force with two, one and no feet on the earth, but when the interplanetary field is northward lines of force either intersect the earth twice or not at all. Thus, in the Dungey model the magnetosphere is open for southward interplanetary fields and closed for northward interplanetary fields.

Another difference between the northward and southward models, is the role played by the reconnection between the interplanetary and geomagnetic fields. For southward interplanetary fields flux is added to the tail by this reconnection ; for northward interplanetary fields flux is removed from the tail. Either process is a steady state, however, since flux is removed from the tail for southward fields by reconnection at a magnetic neutral point in the tail, and added to the tail for northward fields by convection from the dayside.

We have already mentioned the observations of solar energetic particles, but both solar electron data (West and Vampolar, 1971) and solar proton data (Evans and Stone, 1971) indicate that the tail is open *at all times*, regardless of the sign of the north-south component of the interplanetary magnetic field (Morfill and Scholer, 1972). Thus, the Dungey model for northward fields is not consistent with these results. The theoretical reconnection models at the magnetopause are now investigated using, for example, a modified Dungey model (Morfill and Quenby, 1971 ; Russell, 1972) and a model with a pair of Alfvén shocks in addition to slow shocks at the interface (Nishida and Maezawa, 1971), but not yet well established.

4.3 Mechanisms of the solar flares

Solar flares are complex and transient excitations of the solar atmosphere above magnetically active regions of the solar surface. They involve enhanced emission of γ-ray, X-ray, EUV, visible rays, H_α and mm-, cm- and m-waves, together with solar cosmic rays and plasma ejection. Their mechanism is not yet understood after more than a

century of study since, in 1859, Hodgson and Carrington separately observed the explosive phenomenon on the solar surface (Sweet, 1969). However, we have rapidly advanced in knowledge in the last twenty years mainly due to the increasing opportunities of the direct observation of various emissions and ejections by balloons, rockets and satellites. The resolving power of observations of the magnetic field in the solar atmosphere is also continuously improved to bring about a better understanding.

A proton-producing flare of importance 3^+ typically occurs in a large complex sunspot group during a period of changing magnetic flux. It begins with an enhancement of the atmospheric emission for several minutes, followed by an explosion leading to the ejection into interplanetary space of plasma clouds and high-energy particles. The total optical emission continues to increase for some minutes, and the whole atmosphere remains activated subsequently on a decay time scale of 1 hour. Here we do not restate the main points obtained to date concerning the observational evidence of solar flares ; readers are referred to the review papers by Sweet (1969) and Takayanagi et al. (1973). However, it is informative to point out that 10^{32} ergs of energy are likely to be emitted during the explosive phase, mainly in the form of the kinetic energy carried by a plasma of 10^{16} g ejected at some 1500 km/sec, and that another 10^{32} ergs are emitted in the decay stage, mainly in optical radiation (Parker, 1963). If one is allowed to distribute this amount of energy over the area of the active region, say 10^{19} cm^2, the energy density is estimated at 2×10^{13} $ergs/cm^2$. However, the thermal energy in the column with a height, say 10^9 cm, may amount, at most, to 5×10^9 $ergs/cm^2$ in the chromospheric level where $n_e = 5 \times 10^{12}$ $/cm^3$ and $T = 7 \times 10^3$ °K, or to 10^9 $ergs/cm^2$ in the coronal condensation where $n_e = 4 \times 10^9$ $/cm^3$ and $T \sim 2 \times 10^6$ °K (Takayanagi et al., 1973). This is short of what is required, by some orders of magnitude, hence cannot account for the thermal energy. Pneuman (1968) has considered the magnetoacoustic flux transported from the photosphere, but the flux density 3×10^8

ergs/cm^2/sec is also unfavorable to the buildup time. On the other hand, the magnetic energy available may be sufficient, with B = 500 gauss which is often seen in the active regions of large flares. Thus we may reasonably consider that the explosive phase of a solar flare is attributable to a release of magnetic energy stored by the photospheric motions during the development of an active region.

We have not yet succeeded in theoretical explanation of solar flares, which is a difficult and troublesome task with many aspects. Some of the most fundamental aspects have been described only by incomplete and qualitative theoretical models. Nevertheless the exclusive association of solar flares with active regions shows that at least some aspects of the problem are magnetohydrodynamic. Hence, we will discuss at length in chapter 3 the prevailing models of the reconnection process in reference to the explosive phase but we should not miss the fact that many different mechanisms have also been proposed and investigated along this line (Sturrock and Coppi, 1966 ; Sturrock, 1968 ; Gold and Hoyle, 1960). Possibly the list of these mechanisms has already been complete in the sense that no immediate source of energy has been overlooked which may be relevant for the total flare phenomenon or any important part of it (Schmidt, 1969).

A number of fundamental alternatives for a theory of flares, of course, are still open. They should be given by the different possibilities to store an energy of about 10^{32} ergs in a way that it can be released within about 10^2 sec.

4.4 Reconnection in laboratory plasmas

Some experiments on the reconnection process have been performed in order to simulate the flare events in laboratory devices (e.g., Bratenahl and Yeates, 1970, Syrovatsky et al., 1972 ; Ohyabu and Kawashima, 1972). Now they are still at preliminary stages but we may expect that when the artificial flares are actually realized in

the laboratory plasmas a new mechanism of acceleration and heating of plasmas will fall into our hands. In this sense, the reconnection process has now received considerable attention by many experimenters.

Chapter 2

TOPOLOGICAL STUDY OF MAGNETIC FIELD NEAR A NEUTRAL POINT

§ 1. Introduction

Magnetic neutral points are classified by the number of lines of force passing through them. A bundle of lines of force having a common tangent at a neutral point O is counted as one line only. It has been known that there exist two kinds of neutral points (Dungey, 1953). If there is only one line of force passing through O, it is called (by the shape of lines of force in its vicinity) an O-type neutral point. Alternatively, if three lines of force or bundles of lines pass through O, it is known as an X-type neutral point. All current-free neutral points belong to this class.

These two types of neutral points have considerably been investigated and we will also be concerned mainly with X-type neutral points. However, they are not the whole of the existing neutral points ; we can show the possible existence of other types of neutral points. We do not afford any stability condition, which requires a full understanding of the flow and magnetic field involving the corresponding neutral point.

In what follows, the classification of magnetic field in the vicinity of a neutral point will be strictly re-examined in terms of

---

* See Fukao et al. (1974).

the phase trajectories. Much of what will be said is the extension and the generalization of Dungey's work, but some types of the neutral points which have not been recognized by the pioneers are first proposed here. Then, we mention the volume force acting on the fluid. Finally, we advocates though very intuitively, a new type of evolution of neutral points which may explain higher rates of energy conversion than those expected in X-type neutral points.

§ 2. Topology of Magnetic Lines of Force

Since the magnetic field must be a solution of Maxwell's equation, it must be differentiable, and hence expansible in Taylor series. Taking the neutral point as the origin, the magnetic field (magnetic flux density) B near a neutral point may be expressed by Eq. (1.12), that is,

$$B = a \cdot r \ .$$

Only one constraint on a is as follows : a must have zero trace, because magnetic field is solenoidal.

Here we consider the solution of

$$\dot{r}(\tau) = a \cdot r(\tau) \ , \qquad (2.1)$$

where $\dot{r}(\tau)$ is the derivative with respect to an arbitrary parameter τ. It is apparent that the solution $r(\tau)$ describes a line of force, since $\dot{r}(\tau)$ indicates B itself. Therefore we can show magnetic lines of force in terms of phase trajectories, which satisfy Eq. (2.1).

It is readily seen that a must have at least one real eigenvalue, and that the orthogonal coordinate system (x, y, z) can always be chosen such that the z axis is in the direction of the eigenvector corresponding to the real eigenvalue of a. In such a coordinate system, a may be described as

$$a^* = \begin{pmatrix} a_{11} & a_{12} & 0 \\ a_{21} & a_{22} & 0 \\ a_{31} & a_{32} & a_{33} \end{pmatrix} , \qquad (2.2)$$

where

$$\sum_{i=1}^{3} a_{ii} = 0 \quad (\text{zero trace}) . \qquad (2.3)$$

In this case the current density J in the vicinity of a neutral point is given by

$$\mu_0 J = \begin{pmatrix} a_{32} \\ -a_{31} \\ a_0 \end{pmatrix} , \qquad (2.4)$$

where μ_0 is the magnetic permeability in vacuum and a_0 is defined as

$$a_0 \ (\equiv \mu_0 J_z) = a_{21} - a_{12} .$$

The characteristic equation of a^*, $f_{a^*}(\lambda)$, becomes

$$f_{a^*}(\lambda) = f_A(\lambda) \cdot (\lambda - a_{33}) , \qquad (2.5)$$

where

$$f_A(\lambda) = \lambda^2 + a_{33}\lambda - X ,$$

in terms of X defined as

$$X = a_{12}a_{21} - a_{11}a_{22} .$$

The eigenvalues of a^* are the roots of the characteristic equation (2.5). Figure 3 shows that the eigenvalues are classified into four groups in the plane (a_{33}, X) ; we can determine an a^* at any point in the region where $4X + a_{33}^2 + a_0^2 \geq 0$. Let the two roots of $f_A(\lambda)$ be α and β, which are not necessarily real. We may note that

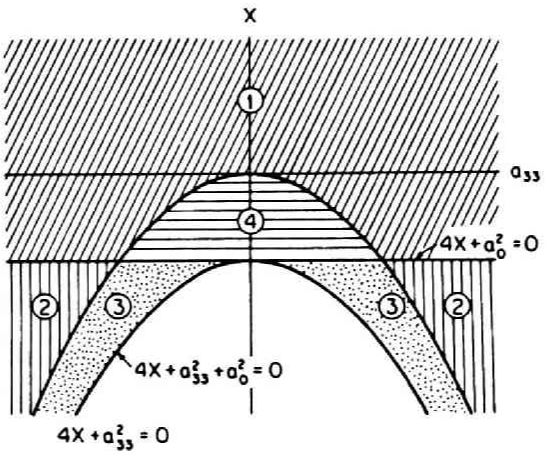

Fig. 3 The grouping of eigenvalues of a^* and C.

$\alpha + \beta + a_{33} = 0$.

As already mentioned, three linearly independent vectors h_1, h_2 and h_3 are chosen such that h_3 is the eigenvector corresponding to a_{33}. And we assume, for simplicity, magnetic fields confined to the plane determined by h_1 and h_2. It may be quite sufficient, if only we illustrate them in the orthogonal cartesian system, since the affine transformation is always possible how much inclined h_1 and h_2 may be. Hereafter h_1 and h_2 are respectively projected onto the x and y axes, and all figures are illustrated in the xy plane.

2.1 Real eigenvalues

Both α and β are real if

$$4X + a_{33}^2 \geq 0 .$$

In this case the roots of Eq. (2.5) can be classified into three cases.

2.1.1 The case of $\alpha = \beta = a_{33}$ (= 0)

This is satisfied if

$$X = a_{33} = 0 . \qquad (2.6)$$

The eigenspace corresponding to the eigenvalue 0 is denoted by W_0. Then there are three cases according to the dimensions of W_0.

(1) When $J = 0$ (i.e., $a_{31} = a_{32} = a_0 = 0$; see Eq. (2.4)), it is readily shown from Eqs. (2.3) and (2.6) that $a = 0$ and, therefore, that dim $W_0 = 3$, which means no field in the whole space.

(2) If $J \neq 0$ and both $\begin{vmatrix} a_{11} & a_{12} \\ a_{31} & a_{32} \end{vmatrix} = 0$ and $\begin{vmatrix} a_{21} & a_{22} \\ a_{31} & a_{32} \end{vmatrix} = 0$ are simultaneously satisfied dim $W_0 = 2$. Either $J_z = 0$ (i.e., $a_0 = 0$) or $J_x = J_y = 0$ (i.e., $a_{31} = a_{32} = 0$) satisfies these conditions. In this case W_0 becomes a plane including the z axis, i.e., $a_{31}x + a_{32}y = 0$ if $|a_{31}| + |a_{32}| \neq 0$. In the case in which $a_{31} = a_{32} = 0$, either $a_{11}x + a_{12}y = 0$ (if $|a_{11}| + |a_{12}| \neq 0$) or $a_{21}x + a_{22}y = 0$ (if $|a_{21}| + |a_{22}| \neq 0$) will take its place. At any rate it is readily seen that the electric current flows parallel to the plane W_0. Then there exist three vectors h_3, h_2 and h_1, each of which satisfies $a^* h_3 = 0 h_3$, $a^* h_2 = 0 h_2$ (h_3 and h_2 are in the plane W_0) and $a^* h_1 = h_2$ (if $J_z = 0$, h_3 is taken instead of h_2), respectively. Therefore the general solution of Eq. (2.1) is expressed as

$$r(\tau) = C_3 h_3 + C_2 h_2 + C_1 (h_2 \tau + h_1)$$
$$= C_1 h_1 + \xi_2 h_2 + C_3 h_3$$

where $\xi_2 = C_1 \tau + C_2$ and C_i's (i = 1, 3) are arbitrary and real constants. These phase trajectories describe the antiparallel magnetic field directed to h_2 (note that, if $J_x = J_y = 0$, h_2 is in the xy plane). The plane W_0 is the so-called magnetic neutral sheet where the magnetic field vanishes.

(3) For the other values of a^*, dim $W_0 = 1$. In this case both $J_z \neq 0$

and $|J_x| + |J_y| \neq 0$ must hold. W_0 is a straight line and identical with the z axis. Then there exist three vectors h_3, h_2 and h_1, each of which satisfies $a^* h_3 = 0 h_3$, $a^* h_2 = h_3$ and $a^* h_1 = h_2$, respectively. Therefore the magnetic lines of force are written by

$$r(\tau) = C_3 h_3 + C_2(h_3\tau + h_2) + C_1(h_3\frac{\tau^2}{2} + h_2\tau + h_1)$$
$$= C_1 h_1 + \xi_2 h_2 + \xi_3 h_3$$

where $\xi_2 = C_1\tau + C_2$ and $\xi_3 = \frac{C_1}{2}\tau^2 + C_2\tau + C_3$. They show that W_0 (the z axis) is the magnetic neutral line along which magnetic field vanishes. In the plane defined by h_2 and h_3 (i.e. $C_1 = 0$) an antiparallel field is formed in the direction of h_3. In any plane parallel to the above, the magnetic lines of force are parabolic. These rather unfamiliar lines of force is formed by the superposition of two antiparallel fields shown in the case of (2).

It is apparent that the lines of force mentioned in (2) and (3) originate only from the current near the neutral point : there is no field induced by externally-applied current, since no field remains when $J \to 0$ (see the case of (1)).

2.1.2 The case of two equal eigenvalues.

This is the case, either if

$$X - 2a_{33}^2 = 0 \quad (a_{33} \neq 0) ,$$

or if

$$4X + a_{33}^2 = 0 \quad (a_{33} \neq 0) .$$

The former condition leads to α(or β) = a_{33}, and the latter, $\alpha = \beta$ ($= -\frac{a_{33}}{2}$). The former case may be shown to be identical with the latter by transforming the coordinate, so that we consider only the latter case. Let's denote the eigenspace corresponding to the eigen-

value $\alpha(= \beta = -\frac{a_{33}}{2})$ by W_α. Then the following two cases should be considered according to the dimensions of W_α.

(1) If $J_z = 0$, dim $W_\alpha = 2$ and W_α becomes a plane given by $2a_{31}x + 2a_{32}y + 3a_{33}z = 0$. Note that, when $J_x = J_y = 0$, W_α coincides with the xy plane itself. Then three vectors h_3, h_2 and h_1 can be chosen such that $a^* h_3 = a_{33} h_3$, $a^* h_2 = -\frac{a_{33}}{2} h_2$ and that $a^* h_1 = -\frac{a_{33}}{2} h_1$; h_2 and h_1 are in the plane W_α. Therefore the general solution of Eq. (2.1) is given by

$$r(\tau) = C_3 h_3 e^{a_{33}\tau} + C_2 h_2 e^{-\frac{a_{33}}{2}\tau} + C_1 h_1 e^{-\frac{a_{33}}{2}\tau} .$$

In the W_α plane all lines of force are straight and go toward the neutral point if $a_{33} > 0$ (Fig. 4a), while outward if $a_{33} < 0$. It is apparent that, in any plane containing the z axis, a saddle is formed (see, for instance, Fig. 5b). The three dimensional configuration does not seem difficult to be visualized.

(2) If $J_z \neq 0$, dim $W_\alpha = 1$. W_α is a straight line given by the intersection of the two planes, i.e., $(2a_{11} + a_{33})x + 2a_{12}y = 0$ and $2a_{31}x + 2a_{32}y + 3a_{33}z = 0$ if $a_{12} \neq 0$. In the case of $a_{12} = 0$ (i.e., $a_{11} = a_{22} = -\frac{a_{33}}{2}$), $x = 0$ (yz plane) should be taken instead of the former of the above two planes. When $J_x = J_y = 0$, W_α is in the

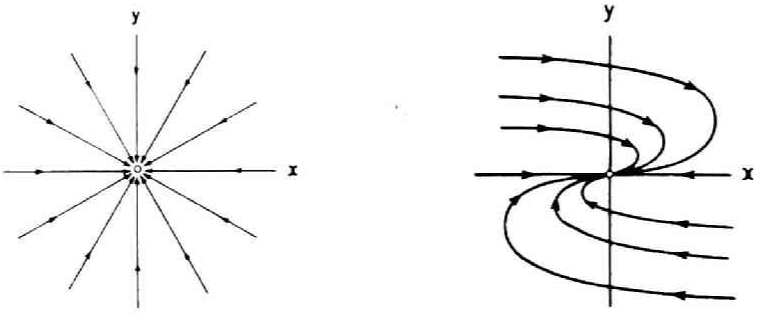

(a) (b)

Fig. 4 Lines of force for the cases $\alpha = \beta < 0$.
(a) dim $W_\alpha = 2$ and (b) dim $W_\alpha = 1$.

xy plane. Then three vectors h_1, h_2 and h_3 can be chosen such that $a^*h_1 = -\frac{a_{33}}{2} h_1$, $a^*h_2 = -\frac{a_{33}}{2} h_2 + h_1$ and that $a^*h_3 = a_{33}h_3$, where h_1 is in the direction of the line W_α. Therefore the general solution of Eq. (2.1) is expressed as

$$r(\tau) = C_1h_1e^{-\frac{a_{33}}{2}\tau} + C_2(h_1\tau + h_2)e^{-\frac{a_{33}}{2}\tau} + C_3h_3e^{a_{33}\tau}$$

$$= \xi_1h_1e^{-\frac{a_{33}}{2}\tau} + C_2h_2e^{-\frac{a_{33}}{2}\tau} + C_3h_3e^{a_{33}\tau} ,$$

where $\xi_1 = C_1 + C_2\tau$. The lines of force in the plane defined by h_1 and h_2 are shown in Fig. 4 b. Note that a saddle is formed in the plane defined by h_1 and h_3.

In this case, when $J = 0$, there are such magnetic fields as shown in (1), which may be referred to some external source currents. When $J \neq 0$ as shown in (2), the fields due to the current near the neutral point are superposed upon the current-free fields.

2.1.3 The case of three different eigenvalues

This is the case if

$$4X + a_{33}^2 > 0 \quad (2a_{33}^2 - X \neq 0) .$$

Let's denote the eigenspaces corresponding to the eigenvalues α, β and a_{33} respectively by W_α, W_β and $W_{a_{33}}$, where $W_{a_{33}}$ is, of cource, identical with the z axis. Both W_α and W_β are also straight lines and W_α, for instance, is given by the line of intersection between the planes $(a_{11} - \alpha)x + a_{12}y = 0$ and $a_{31}x + a_{32}y + (a_{33} - \alpha)z = 0$, if $|a_{11} - \alpha| + |a_{12}| \neq 0$. Otherwise $a_{21}x + (a_{22} - \alpha)y = 0$ is taken instead of $(a_{11} - \alpha)x + a_{12}y = 0$. W_β is similarly determined. Note that, when $J_x = J_y = 0$, both W_α and W_β are in the xy plane. Then the solution of Eq. (2.1) is expressed as

$$r(\tau) = C_1h_1e^{\alpha\tau} + C_2h_2e^{\beta\tau} + C_3h_3e^{a_{33}\tau} ,$$

where h_i's are respectively the eigenvectors corresponding to α, β and a_{33} (therefore they are linearly independent). Three eigenspaces obviously form the principal axes, i.e., lines of force passing through the neutral point. In the plane defined by h_1 and h_2, a node is formed at the neutral point for $\alpha\beta > 0$. In this case all lines of force are directed toward the neutral point for $\alpha, \beta < 0$ (Fig. 5a) and outward for $\alpha, \beta > 0$. A saddle, on the other hand, appears for $\alpha\beta < 0$ (Fig. 5b). In another plane defined by h_1 (or h_2) and h_3,

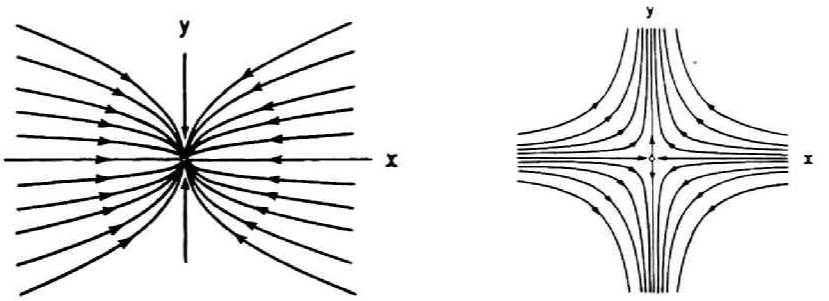

(a) (b)

Fig. 5 Lines of force for the cases (a) $\alpha < \beta < 0$ and (b) $\alpha < 0 < \beta$.

the same is also true. Here, it may be worthwhile to note that, when $J = 0$, the principal axes are orthogonal to each other (since then a^* becomes symmetric). The special case of one vanishing eigenvalue, whose meaning has been extensively discussed by many pioneers, will be discussed later.

2.2 Complex eigenvalues

Both α and β are complex if

$$4X + a_{33}^2 < 0 .$$

The eigenvalues α and β may be written as

$$\alpha = \mu + i\nu \quad \text{and} \quad \beta = \bar{\alpha} = \mu - i\nu \quad \left(\mu = -\frac{a_{33}}{2} \right) ,$$

and the corresponding eigenvectors can be chosen such that they are conjugate with each other, i.e., h and $\bar{h}$. Then the general solution of Eq. (2.1) is expressed as

$$r(\tau) = Che^{\alpha\tau} + \bar{C}\bar{h}e^{\bar{\alpha}\tau} + C_3 h_3 e^{a_{33}\tau} , \tag{2.7}$$

where C is an arbitrary complex number. We put

$$h = \frac{1}{2}(h_1 - ih_2)$$

where h_1 and h_2 are real vectors. Both h_1 and h_2 are in the xy plane if $J_x = J_y = 0$. Since h_1 and h_2 are linearly independent, they compose the bases of the phase space together with h_3. Putting

$$\xi(\tau) = \xi_1 + i\xi_2 = Ce^{\alpha\tau} , \tag{2.8}$$

Eq. (2.7) is expressed as

$$r(\tau) = \xi_1 h_1 + \xi_2 h_2 + C_3 h_3 e^{a_{33}\tau} .$$

If h_1 and h_2 are projected onto 1 and i, respectively, the vector $\xi_1 h_1 + \xi_2 h_2$ corresponds to the complex number given by Eq. (2.8). Putting $C = Re^{i\theta}$, Eq. (2.8) is expressed as

$$\xi(\tau) = Re^{\mu\tau} \cdot e^{i(\mu\tau + \theta)} .$$

Magnetic lines of force in the plane defined by h_1 and h_2, therefore, become logarithmic spirals. They are inward when $\mu < 0$ ($a_{33} > 0$; Fig. 6a), while outward when $\mu > 0$ ($a_{33} < 0$). In the case of $\mu = 0$ ($a_{33} = 0$; Fig. 6b), each line of force becomes a closed trajectory, forming a so-called center of spiral (therefore the z axis is the magnetic neutral line). In the limit $J \to 0$, the closed

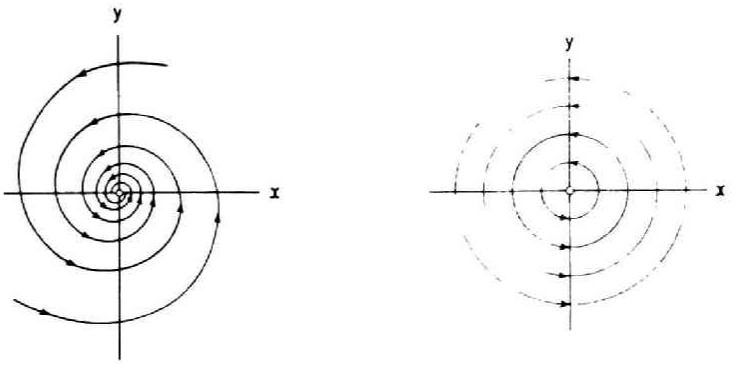

(a) (b)

Fig. 6 Lines of force for the cases in which α and β are complex conjugate. (a) $\mu < 0$ and (b) $\mu = 0$.

lines of force tend to vanish in the whole space, which means that these lines of force are induced by the current near the neutral point. Hence the spiral fields ($a_{33} \neq 0$) may be regarded by considering the limit $a_0 \to 0$ such that they are formed by the superposition of the closed lines of force (Fig. 6b) upon those due to the external source currents as shown in Fig. 4a.

Finally, it may be instructive to consider the case of one vanishing eigenvalue, which is very familiar to us. This condition is given by

$$a_{33} = 0 \quad (X \neq 0) \qquad \text{or} \qquad X = 0 \quad (a_{33} \neq 0) .$$

The latter case is shown as the direct copy of the former by transforming the coordinate, therefore, only the former case is considered. Then the z axis is apparently a neutral line and magnetic field B becomes independent of z. When $J_x = J_y = 0$, $B_x = 0$ and h_1 and h_2 are in the xy plane as shown before. When $X > 0$ (see the case (2.1.3)), a saddle is formed in the planes parallel to the plane defined by h_1 and h_2 (Fig. 5b). This type of magnetic field has been familiar to us as the X-type configuration from its shape. When $X < 0$, the so-called O-type configuration is formed as shown in the case (2.2) (Fig. 6b).

§ 3. Topology of Magnetic Volume Force

The magnetic volume force acting on the fluid is

$$\mu_0 F = \mu_0 J \times B = c \cdot r \ ,$$

where

$$c = (a^* - a^{*T}) \cdot a^* \ .$$

For simplicity, we consider only the case of $J_x = J_y = 0$ ($J_z \neq 0$). Then the magnetic volume force becomes two-dimensional ; it is independent of z and $F_z = 0$. Therefore, they may be expressed as

$$\mu_0 F = c^* \cdot r = a_0 \begin{pmatrix} -a_{21} & -a_{22} \\ a_{11} & a_{12} \end{pmatrix} \begin{pmatrix} x \\ y \end{pmatrix}$$

where a_0 ($= \mu_0 J_z$) is the same as before. Topological patterns of the magnetic volume force, so to say the *force* lines of force, are specified by the eigenvalues of c^* in the same manner as those of magnetic lines of force. The characteristic equation of c^* becomes

$$f_{c^*}(\lambda) = \lambda^2 + a_0^2 \lambda - a_0^2 X \ ,$$

where X is the same as before. They are classified into three groups depending upon $4X + a_0^2 \gtreqless 0$. The descriptions would be the direct copy of those for magnetic lines of force mentioned in section 2. Let the two eigenvalues be α and β. At least one of them must be negative, since $\alpha + \beta = -a_0^2 < 0$. The types or topological patterns of the *force* lines of force are classified and tabulated in Table 1.

In the case of $a_{33} = 0$ (then the magnetic field also becomes two-dimensional as shown in section 2), a saddle-type volume force is formed for the X-type magnetic field when $X > 0$ (i.e., $\alpha\beta < 0$). Let's denote the eigenspaces corresponding to α and β respectively as ξ_α and ξ_β, both of which are apparently straight lines. ξ_α and ξ_β

Table 1 Topological pattern of the *force* lines of force. $a_0 = J_z \neq 0$ is assumed ; otherwise it becomes force-free.

Case	Types of α and β		Topological pattern of *force* lines of force
$4X+a_0^2>0$	real ($\alpha<\beta$)	$\alpha<\beta<0$($X<0$)	node(Fig. 5a)
		$\alpha<0<\beta$($X>0$)	saddle(Fig. 5b)
		$\alpha<\beta=0$($X=0$)	sink
$4X+a_0^2=0$	real ($\alpha=\beta<0$)	dim $W_\alpha=2$	radial line (Fig. 4a)
		dim $W_\alpha=1$	degenerate node (Fig. 4b)
$4X+a_0^2<0$	complex conjugate($\alpha=\mu+i\nu$ and $\beta=\bar{\alpha}$ with $\mu<0$)		logarithmic spiral (Fig. 6a)

are orthogonal to each other, since then, C^* is symmetric as seen from Eq. (2.3) . It will be readily shown that the magnetic force pushes the fluid in the larger wedge of X-type magnetic field so as to squeeze it outwards from the smaller wedge. On the other hand, when $X < 0$ (i.e., $\alpha\beta > 0$), a node-type volume force is formed for the O-type magnetic field. In this case the magnetic force pushes the fluid inwards to the neutral point (or the z axis).

The above result of the classification of magnetic volume forces are shown in Fig. 3 , upon which $4X + a_0^2 = 0$ is superposed. Figure 3 indicates that the ordinary two-dimensional problems ($a_{33} = 0$) are merely the very limited case.

§ 4. Evolution of a Neutral Point

For simplicity, we discuss only the case of $J_x = J_y = 0$. As shown in Fig. 3 , the (a_{33}, X) plane is divided into four domains. If there is no current near the neutral point (i.e., $a_0 \to 0$), both the third and fourth domains will vanish. The topology of magnetic field and volume force in each domain has been made clear in sections 2 and 3.

Some sort of evolution of magnetic neutral point was first discussed by Dungey (1953). He proposed that the rapid increase of the current density, i.e., discharge, would occur near an X-type neutral point, if the pressure gradient was negligible and the conductivity was infinitely large. In our topological analysis the discharge model belongs to the case of $a_{33} = 0$ and $X > 0$ in the first domain : both the magnetic field and volume force are two-dimensional and have the X-type configuration. It is easy to imagine from the preceding discussions that both the fluid and the magnetic field in the larger wedges concentrate in the vicinity of the neutral point, which leads the smaller wedges to become diminished. This folding of the principal axes means that the current density grows at the neutral point. In reality, however, the finite conductivity would diffuse the concentrated magnetic field, arresting the growth of the current density, which enhances the thermal energy (or the pressure) of plasmas in the vicinity of the neutral point. Moreover, the force due to the increasing pressure gradient would keep the fluid from concentrating further. Hence, it may be expected that a steady state could be attained by a balance between the force due to the pressure gradient and the magnetic volume force. This is alternatively interpreted as the rate of reconnection in the vicinity of the neutral point is balanced with that of the supply of lines of force by the incoming fluid from the exterior. This is the basic mechanism of reconnection at the x-type neutral point, which we will investigate later.

The X-type magnetic field, however, is only a special case in the

first domain in Fig. 3 : there may exist various types of neutral points in three dimensional magnetic field, and the full understanding of their remarkable natures will be required for various astrophysical and geophysical phenomena. That is, however, very difficult, since the problem becomes, in general, an unsteady process in three dimensions. Hence we shall discuss below, though in a simplified way, the quite different types of configuration, that is, spiral types of fields and volume forces in the second, third and fourth domains in Fig. 3.

In the second domain, a node-type magnetic field is formed in the xy plane (Fig. 5a ; the principal axes are not necessarily orthogonal, since $J_z \neq 0$). In the plane containing both the z axis and either of the principal axes in the xy plane, a saddle is formed. The magnetic volume force, on the other hand, is a spiral type in the planes parallel to the xy plane (Fig. 6a). The fluid would easily move along the *force* lines of force, since then the force due to pressure gradient does not effectively keep the fluid from entering spirally along the *force* lines. Hence, if the external conditions are favorable, the field-lines would be wound due to the spiral motion of the fluid to become spiral.

In the third domain, a spiral-type magnetic field is formed in the xy plane (three dimensional configuration is not difficult to be visualized). Remind that this type of magnetic field is formed by the superposition of the field induced by the external source currents (Fig. 4a) upon that by the current near the neutral point (Fig. 6 b). In this domain, a spiral-type magnetic volume force is formed in the planes parallel to the xy plane. If the current density (a_0) is sufficiently small, the lines of force are in such a form as shown schematically in Fig. 7a , where the radial lines of force are more predominant. The corresponding *force* lines of force are shown by dotted lines. The fluid would move spirally along the magnetic *force* lines to carry and wind the lines of force inward with time. This is accompanied with the growth of the current density in the vicinity of

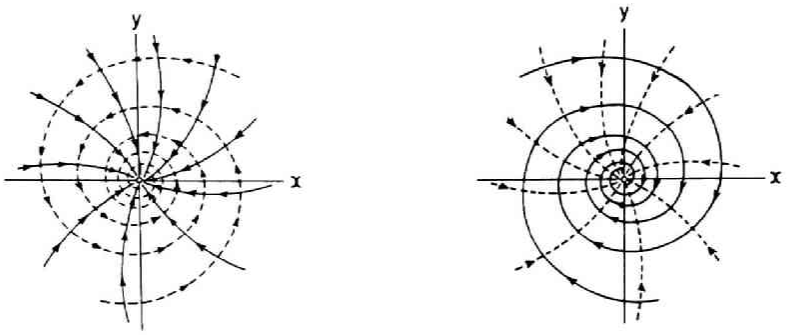

(a) (b)

Fig. 7 Schematic pattern of magnetic lines of force (solid lines) and force lines of force (dotted lines) for the case that J_z is comparably (a) small and (b) large.

the neutral point. If the current density (a_0) grows comparably large, the lines of force are considerably wound as shown schematically in Fig. 7b , where the O-type lines of force become predominant. Then the magnetic volume force becomes similar to a node-type as shown by dotted lines. These magnetic field and volume force are met in the fourth domain. This suggests that the fluid would be pinched radially and that the magnetic lines of force are piled up in the vicinity of the neutral point. If the magnetic energy reserved up to the extreme would lead to the rapid annihilation, we can expect the heating and acceleration of plasmas, sufficient for many phenomena.

It is worthy of notice that, if magnetic lines of force are wound somewhere except near a neutral point, they tend to unwind themselves due to magnetic volume force, while near the neutral point they are wound by themselves.

The above discussions have made clear, though very intuitively, the exotic nature of magnetic neutral points. However, they were restricted only to the vicinity of the neutral point, and in reality, the external conditions seem to play a crucial role in any type of evolution of magnetic neutral points.

§ 5. Concluding Remarks

The classification of magnetic neutral points was strictly re-examined in terms of the phase trajectories. It is the extension and the generalization of Dungey's work (1953), but the probable existence of some types of neutral points —— spiral and node —— was pointed out first. The solutions describe only the vicinity of the neutral point, and in practice one of them will adapt itself to that of the outer region.

We also tentatively discussed the evolution of magnetic neutral point for the spiral configuration of magnetic field and volume force, which is quite different from the X-type configuration. Then we pointed out that the current density may grow (or the magnetic energy may be reserved) extremely near the z axis due to the spiral motion of the fluid. The magnetic energy reserved up to the extreme may lead to an abrupt release when the fluid is pinched radially. This would be difficult, however, to be discussed quantitatively, since the problem is essentially an unsteady process of three dimensional magnetic fields, in which the external conditions must be always taken into consideration.

Chapter 3

A CRITICAL SURVEY OF CURRENT RECONNECTION MODELS

§ 1. Introduction

Before considering the individual proposed mechanisms it may be useful to examine one-dimensional behaviors of two opposing antiparallel magnetic lines of force (Petschek, 1964 ; Yeh and Axford, 1970). In the incompressible, unsteady hydromagnetic fluid in which $B = (0, B(x, t), 0)$, with $B(x, 0) = -B(-x, 0) \equiv$ constant (in Cartesian coordinates), the fluid is stationary and B satisfies

$$\frac{\partial B}{\partial t} = \frac{1}{\mu\sigma} \frac{\partial^2 B}{\partial x^2} .$$

The fluid intensity is

$$B \propto \operatorname{erf}\left(\sqrt{\left(\frac{\mu\sigma}{t} \right) \frac{x}{2}} \right) . \qquad (3.1)$$

The instantaneous thickness of the current sheet $\delta \sim \sqrt{t/\mu\sigma}$. In this case the antiparallel magnetic lines of force do not become reconnected, in the strict sense of the word, but only annihilated as they merge at the neutral line or sheet $x = 0$. The surplus of the magnetic energy is directly converted into heat by Joule dissipation. The rate of merging is given by the rate at which magnetic lines of force diffuse towards the neutral sheet, which in turn is proportional to

$1 / \delta$. Since δ increases with time, rapid conversion of magnetic energy into other forms of energy cannot be expected by the simple diffusion in the absence of fluid motion.

Then we will imagine a uniform flow toward the neutral sheet from either side, together with a sink for un-magnetized fluid there. If $u = (u(x), 0, 0)$ with $u = \mp u_0$ in $x \gtrless 0$, a steady state can be reached such that

$$u \frac{\partial B}{\partial x} = \frac{1}{\mu\sigma} \frac{\partial^2 B}{\partial x^2} .$$

The solution is

$$B \propto \pm (1 - e^{\mu\sigma u x}) \qquad \text{in} \quad x \gtrless 0 . \tag{3.2}$$

The thickness of the current sheet $\delta \sim 1 / \mu\sigma u_0$ is held constant by a balance between the convection and the diffusion of magnetic lines of force. A high rate of merging is possible under the large gradient of the magnetic inductance. However, the example quoted here is not actual because of its postulated sink. In a more realistic situation the fluid must be removed from the neutral sheet and the process is never limited to the one-dimensional problem.

In what follows, we will discuss the prevailing models of reconnection in relation to the explosive phase of largest solar flares which seems to be the most splendid manifestation of the process in space. In section 2 we consider the special instability of a neutral point or line discussed by Dungey (1953) and by Chapman and Kendall (1966). Dissipation in a homogeneous current sheet of Sweet (1958) and the wave mode dissipation in a current sheet discussed by Petschek (1964) will be described in sections 3 and 4, respectively. In section 5 there follows a group of proposals of Sonnerup (1970) and Yeh and Axford (1970). Finally we will mention the nonsteady current sheet of Syrovatsky (1966, 1969).

§ 2. Discharge at a Magnetic Neutral Point

Dungey (1953) has argued a remarkable behavior of a pressure-less fluid in the vicinity of a magnetic neutral point. If initially both a fluid motion and an electric current vanish, so that magnetic lines of force are rectangular hyperbolas, a small perturbation amplifies itself and produces a flow diminishing the angle between the principal axes. The current density meanwhile increases, until the electric field (in the fluid's frame) becomes appreciable. Dungey called this as " instability " ; he thought that such a development takes place in solar flares and that the current then becomes a " discharge " accelerating particles to high energies. However, the theory suffers from an essential defect in that the effects of the pressure gradients which are likely to play an important role in controlling the rate of inflow of the fluids are not considered in the process.

To understand Dungey's mechanism one should note that the folding of the principal axes and of the associated system of lines of force is not confined to the neighborhood of the neutral point. The neutral point which resembles in all respects the one investigated by Dungey is realized (Stern, 1966), for example, by two fixed parallel dipoles, directed along the line connecting them and immersed in an infinite homogeneous conducting fluid at rest (Fig. 8) . In this

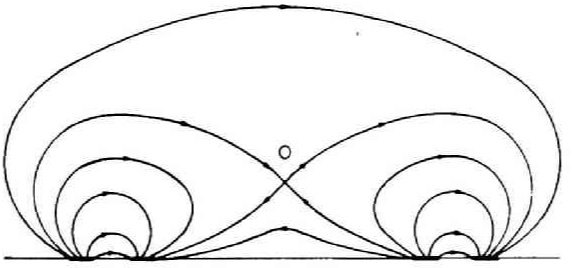

Fig. 8 The neutral point formed between two parallel dipoles (after Stern, 1966).

system, the field is, and remains, a potential field and is therefore stable. Only if the dipoles are allowed to attract each other, i.e., if the lines of force are free to move, the system is unstable and releases the available surplus of magnetic energy. But in this case the system is not in equilibrium to start with and there is no question of stability in the usual sense.

A special solution to the hydromagnetic fluid containing an X-type neutral point has been given with elegance by Chapman and Kendall (1963, 1966) and by Uberoi (1963, 1966). In their model the neutral point is contained in a tube of incompressible conducting fluid with a circular cross section, which is surrounded by a vacuum. Dungey's instability proceeds and the cross section becomes progressively more elliptical with the ratio of minor to major semi-axes tending zero. This solution seems to indicate that a thin current sheet between two approaching magnetic fluxes of opposite polarity will be formed within the travel time of an Alfvén wave, i.e., within less than 10^2 sec in a preflare environment. However, the electric current density is uniform over the cross section and does not become large near the neutral point within a finite time ; that is, the magnetic lines of force do not reconnect at the neutral point (Yeh and Axford, 1970). A more serious limitation arises in that the fluid is decoupled from the magnetic sources by vacuum surrounding the tube. Such decoupling seems unlikely, however, in astrophysical applications.

§ 3. Dissipation in a Homogeneous Current Sheet

The dynamics of a stationary homogeneous current sheet have been studied by Sweet (1958) and then by Parker (1963). See the schematic figure 9 . Two homogeneous antiparallel magnetic fields sandwich the current sheet. Two fields outside the sheet are carried by the fluid toward the sheet at the same rate at which inside the sheet they diffuse toward each other and simultaneously annihilate themselves by

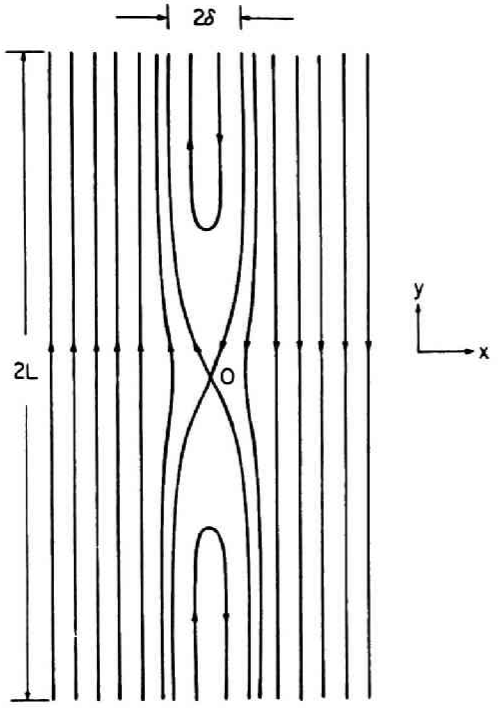

Fig. 9

Magnetic lines of force for Parker's mode (left) and the coordinate to be used (right). The fluid moves toward the null magnetic field region of the current sheet from both sides and is ejected along it. 2L and 2δ are respectively the length and thickness of the current sheet.

Joule dissipation. The fluid outside the sheet moves toward the sheet at the same rate at which it can be squeezed out of the sheet in a direction parallel to the original magnetic lines of force with the Alfvén velocity. The rate is alternatively represented by the reconnection time scale for magnetic flux within a distance from the sheet equal to its extension L along the field, i.e.,

$$\tau = (\tau_A \tau_L)^{1/2} \qquad (3.3)$$

where $\tau_A = L / V_A$ is the time of passage of an Alfvén wave across L and $\tau_L = \sigma\mu_0 L^2$ (σ, electrical conductivity ; μ_0, magnetic permeability) is the ohmic diffusion time for a system of dimension L without a current sheet. For a current sheet of width $L = 10^7$ m in the corona at the level of the type III bursts, i.e., $\rho = 10^{-9}$ kg/m^3 ($= 10^{-12}$ g/cm^3), $\sigma = 2 \times 10^6\ \Omega^{-1}$ ($\sim 2 \times 10^{16}$ esu) and with B = 250 gauss, $\tau_A = 15$ sec and $\tau_L = 3 \times 10^{14}$ sec. This would result in a reconnection time $\tau = 7 \times 10^7$ sec, which was found to be much longer than the

observed time scales of flares. The theoretical time scales could never approach the observed ones unless *ad hoc* dimensions L are assumed extremely smaller than the observable scales. The compressibility of the fluid improves the situation, but if the two fields were not exactly antiparallel or they had no neutral plane, the common component of the fields would accumulate in the sheet and diminish the compressibility of the fluid. The reconnection time is still impossibly long even in the ideal case (cf. Parker, 1963).

It was pointed out, however, by Jaggi (1964) that the tearing mode instability would disintegrate the current sheet into current threads before the sheet became thin enough for the stationary state to be established. Before the onset of the instability, and while the sheet is thicker than its stationary-state thickness, the fluid would be squeezed out from the edges of the sheet without replenishment by ohmic diffusion across the field. Mass continuity then shows that the thickness of the sheet diminishes exponentially with time scale τ_A. Therefore the tearing mode instability becomes effective when its fastest-growth time scale τ_T falls below τ_A. For a sheet of thickness ℓ, $\tau_T = (\tau_a \tau_\ell)^{1/2}$ where τ_a is the Alfvén travel time across ℓ and τ_ℓ, the ohmic diffusion time within the sheet (Furth et al., 1963). Setting $\tau_A = (\tau_a \tau_\ell)^{1/2}$, the thickness of the sheet at the onset of instability is given by $\ell / L = (\tau_A / \tau_L)^{1/3}$, i.e., $\ell = 4 \times 10^2$ m in the example considered. It is at this stage that the ohmic diffusion sets in and that material would diffuse into the sheet. It is not clear how the system would develop subsequently. If it were assumed that a stationary state were maintained such that the stability criterion $\tau_A = (\tau_a \tau_\ell)^{1/2}$ remained marginal, mass continuity within a sheet of constant thickness ℓ determines the incoming velocity as $v = \ell V_A / L = V_A (\tau_A / \tau_L)^{1/3}$. This would lead a reconnection time $(\tau_A^2 \tau_L)^{1/3} = 4 \times 10^5$ sec. Although this is less than the time $(\tau_A \tau_L)^{1/2}$ mentioned above, it is still extremely longer. This is not altered under chromospheric conditions.

According to Sturrock (1968), the sheet would not remain near

marginal stability but would become highly turbulent, the diffusion velocity being governed by the Bohm diffusion coefficient. However, enhanced diffusion thickens up the sheet which thereby tends to removed the tearing mode instability. This supports the assumption that the system cannot depart very far from marginal stability.

§ 4. Slow Shock Dissipation in a Current Sheet

The first stationary-state mechanism fast enough for a flare itself is that of Petschek (1964) comprising a boundary layer framed by two intersecting slow-mode magnetohydrodynamic shocks as shown in Fig. 10. Ohmic diffusion operates only in the small plane current sheet of the intersection region of size $2y^*$.

Two antiparallel magnetic fields outside the boundary layer moves with the fluid toward the boundary layer, so that any line of force

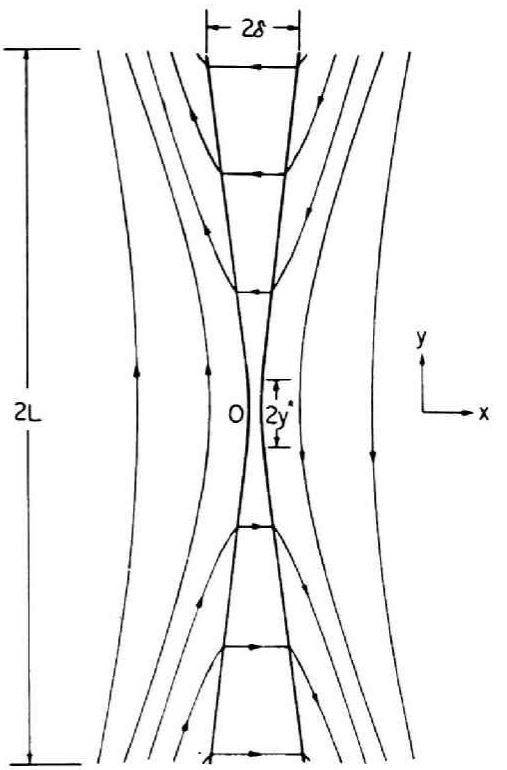

Fig. 10

Configuration of the magnetic field including standing waves. The magnetic lines of force are indicated by light lines. The heavy lines indicate the edge of the boundary layer. For $y > y^*$, the edge of the boundary layer is determined by magnetohydrodynamic waves and is therefore rather sharply defined. The fluid moves toward the boundary layer and is ejected along it (after Petschek, 1964).

reaches the current sheet before it cuts the shock wave anywhere else. Once the fluid has crossed the shock wave, it moves rapidly outward in the y direction together with the reconnected line of force. The direction of the field and fluid motion as well changes discontinuously in the shock waves. In this sense they are a sort of switchoff shocks, though not in its strict meaning. The magnetohydrodynamic shocks directly transform magnetic to kinetic energy by Lorentz forces. They propagate upstream against the incoming fluid, which can move toward the shock at a rate which yields a stationary state of the system. Thus the inflow velocity is the Alfvén velocity reduced merely by geometrical factors which are to be determined from conditions of compatibility between the outer region with the boundary layer. This yields annihilation time scales for the system

$$\tau \sim \tau_A \ln(\tau_L / \tau_A) . \qquad (3.4)$$

Therefore the time scales are longer than Alfvén travel times but only by factors between 10 and 30, and hence they become comparable with the observed time scales of flares. This mechanism also can operate in the presence of a z field. Since logarithms are slowly-varying functions, one can interpret Eq. (3.4) as implying that the electrical conductivity plays only a minor role in this mechanism. Under the coronal conditions mentioned in the previous section $\tau \sim 10^2$ sec, which is of the right order of magnitude. It is even possible at chromospheric level.

However, if the ohmic diffusion in the current sheet is governed by classical electron scattering, it gives the thickness δ of the current sheet $\sim 10^{-6}$ m, which, as Petschek (1964) had recognized, is unreasonable for hydrodynamic approximations to hold, since it is much smaller than the electron gyroradius. The adoption of the anomalous conductivity would lead to a more realistic model for the current sheet (Parker, 1973b), which is self-consistent with the necessary conditions for the instability. It has been pointed out by Friedman and

Hamberger (1968) that the density of current, which constricts itself into the current sheet, violates the two-stream instability criterion. It is suggested that as the sheet is formed, it would settle into a condition near to marginal stability, in which the electrical conductivity is the reduced value given by Buneman (1959). In this case the diffusion region can be wider than the electron gyroradius. The current density yields electron velocities comparable with thermal velocities corresponding to an electron temperature 1.6×10^4 °K. Laboratory experiments, by these authors, of current-driven instabilities at similar densities result in a rough agreement with the anomalous conductivity predicted by Buneman (1959).

The structure of the boundary layer has been subject to some criticism (Green and Sweet, 1967 ; Petschek and Thorne, 1967), and it is deduced that the boundary layer consists of two separate modes ; an outer one is the intermediate shock and an inner one, the slow shock. The intermediate shock allows for the necessary changes in the field direction. It enables us to construct more realistic boundary layers which are smoothly matched to the outer field and fluid motion. Insertion of the intermediate shock makes it possible that an added uniform field in the z direction, which cannot participate in the reconnection process, will not interfere with the reconnection of the y component of the magnetic field in the slow shock as it does in a homogeneous current sheet. It seems to be applicable to any two neighboring plasmas which are driven toward each other and transport magnetic flux of roughly opposite direction.

§ 5. Hydromagnetic Flow in a Similarity Form

In the preceding models efforts were focussed on how the reconnection rate depends on the electrical conductivity of the fluid (e.g., Sweet, 1969). Thus attention was confined to the diffusion region (Parker, 1957 ; 1963) or to the outgoing flow after the

reconnection (Petschek, 1964). Axford (1967 ; 1969), on the other hand, noticed that the reconnection is essentially controlled by the external conditions outside the whole region where two incoming flows merge into two outgoing flows. In support of his view Yeh and Axford (1970) have derived the flow with some kind of similarity property in an incompressible, perfectly conducting and inviscid fluid which shows the direct relationship between the outgoing flow and the incoming flow. These remarkable solutions appear out of the nonlinear equations, apparently as a result of the symmetry of the terms in the flow and magnetic field (Elsasser, 1954).

Figure 11 is a sketch of the magnetic lines of force and streamlines in the similarity solution. The magnetic fluxes are divided into four sectors by the four separatrices (Alfvén discontinuities). In the two inflow sectors the prominent feature is the bending of the lines of force into the separatrices, which is caused by the pressure gradient toward the neutral point. In the two outflow sectors, there

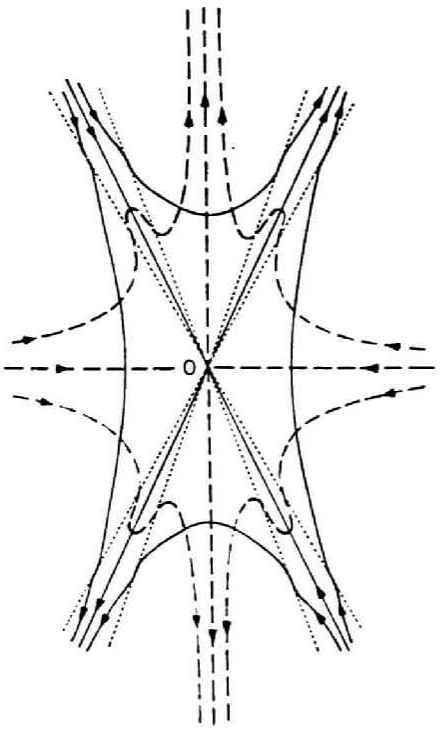

Fig. 11

A sketch of the magnetic field and flow configurations in the similarity solution : the solid lines represent magnetic lines of force, and the dashed lines represent streamlines. The dotted lines show the standing waves (after Yeh and Axford, 1970).

appears the Alfvén discontinuity which is the slow-mode hydromagnetic shocks in the compressible case. The physical origins of the shocks are, as ingeniously pointed out by Petschek, the kinks of the reconnected lines of force at the neutral point. The formation of these kinks is preceded by the bending of the lines of force.

Diffusion is predominant within the place where the diffusion velocity matches the convection velocity of the incoming lines of force. It is, however, the *product* of the electrical conductivity and some scale length that determines a diffusion velocity, and there is no natural scale length for the diffusion region in the magnetohydrodynamic description. Therefore the magnitude of the electrical conductivity adjusts the size of the diffusion region in order to accomodate the surrounding convective flow. It is not actual that the size of the diffusion region limits the convection velocity. Thus, the diffusion region is necessarily small for a highly conducting fluid and/or for a large convection velocity. The outgoing flows are actually unaffected by the details in the diffusion region, but determined directly by the magnitude of the incoming flows or the distribution of the pressure on the external region. In this sense the reconnection rate is essentially independent of the electrical conductivity in the diffusion region, and can have any value up to the Alfvén velocity. Thus the diffusion region is important only in providing a seat for reconnection.

We should bear in mind that, in the similarity solutions for an incompressible fluid, the logarithmic gradient of the pressure in the radial direction is an exact constant. With this constant kept unchanged, the current density would become infinite along the four separatrices where the azimuthal fluid velocity attains the Alfvén speed associated with azimuthal magnetic field. The locations of the singularities were chosen in a manner such that, as the pressure gradient tends to zero, the configuration reduces to the geometry given by Sonnerup (1970), in which one quadrant consists of three uniform flow and magnetic field separated by two Alfvén discontinuities

as shown in Fig. 12 . This configuration differs from the one considered by Petschek by inclusion of the first Alfvén discontinuity, indicated by the line OL in the figure. The second Alfvén discontinuity, OT, was contained in Petschek's model where it was preceded by a region of non-uniform flow and magnetic field. The second discontinuity is compressive in the sense that the fluid pressure increases across it, while the magnetic pressure decreases. Furthermore, it is backward facing relative to the flow, so that it is the trailing wave.

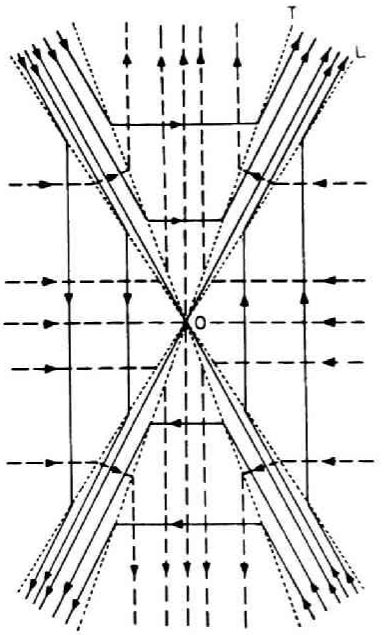

Fig. 12

A sketch of the magnetic lines of force (solid lines) and streamlines (dashed lines) for the vanishing pressure gradient. The lines OL and OT are leading and trailing waves, respectively (after Yeh and Axford, 1970).

On the other hand, the first discontinuity is expansive, i.e., the fluid pressure decreases across it while the magnetic pressure increases. It also appears to be forward facing relative to the flow, and therefore, it is the leading wave. However, the physical meaning has not yet been clarified (Sonnerup, 1970).

Recently, Yeh and Dryer (1973) analyzed a compressible fluid for the case that the compressibility is small, and noticed that the leading wave in Sonnerup's solution corresponds to a expansion wave in which the bending of the magnetic lines of force takes place. In the case of an idealized situation discussed by Sonnerup bending takes

place in a narrow sector, so that the diminutive expansion wave would appear as discontinuity. The magnetic energy seems to be piled up around the separatrices in the expansion phase of the reconnection, and then in the compression phase the energy is converted from magnetic into kinetic and thermal.

The flow reversal in Fig. 11 which is due to the above choice of the locations of the singularities would have no physical meaning and any improvement would not drastically modify the conclusion mentioned above.

Yeh and Axford, however, gave only a rough analysis of the diffusion region and did not notice the particular nature of the outgoing flow in their model, especially the fact that the total pressure at the exit from the diffusion region has a tendency to block the outgoing flow. A more careful matching of the diffusion region to convection region was performed to obtain a tentative conclusion that the highest rate of reconnection is about V_A / 18 (Priest, 1973).

§ 6. Nonstationary-State Current Sheets

In this section, we should mention Syrovatsky (1966 ; 1969) who has casted a doubt on whether a stationary-state current sheet can be established. He examined a pair of parallel currents as shown in Fig. 13 . The configuration is current-free in the vicinity of the origin where the field intensity varies linearly from the origin. Here, the current is assumed to approach each other by a small fraction δ of their initial separation. If the displacement ocurrs slowly enough for the fluid velocity to be less than the local Alfvén velocity, the new configuration will remain current-free except within a sheet of length $\sqrt{2\delta}$ and width r_s, as shown in Fig. 14 ; r_s shows the distance from the origin within which the gas pressure exceeds the magnetic pressure. Thus $r_s^2 = \mu_0 \rho_0 V_s^2 / 2B_0^2$ where ρ_0 is the initial fluid density, B_0 is the typical strength of the field and V_s is the

Fig. 13

Magnetic lines of force and a pair of source currents (I_0) fixed at intervals of 2 (normalized). The coordinate to be used is also shown (after Syrovatsky, 1966).

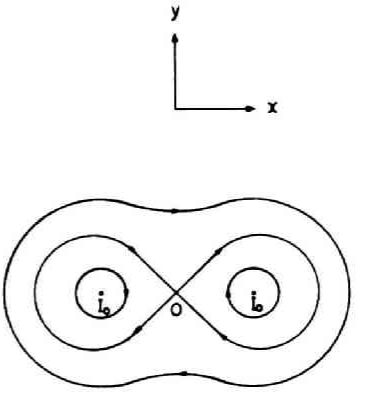

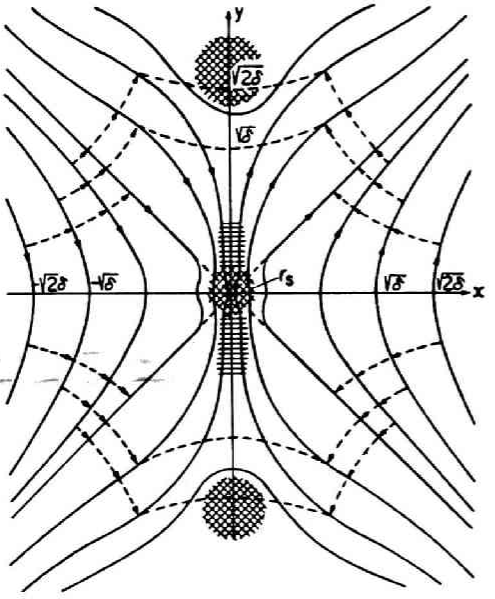

Fig. 14

Magnetic field and fluid motion induced by the displacement of the source currents. The solid lines represent magnetic lines of force, and streamlines are represented by dashed lines with arrows. The other dashed lines form parts of the original magnetic lines of force which are rectangular hyperbolas.

sound velocity. It is further assumed, on the other hand, that the displacement is done fast enough to ensure that the fluid velocity in the neighborhood of the current sheet exceeds V_s. Therefore, outside the current sheet the fluid will not have time to flow along the magnetic lines of force. The frozen-in condition then uniquely determines the fluid displacement outside the current sheet. The rarefaction formula in the current sheet $\frac{h}{\rho} \sim \frac{h_0}{\rho_0}$ has been obtained, where h is the field gradient in the sheet and h_0 is that of the initial time. He argued the onset of the two-stream instability, relativistic runaway electrons, and the conversion of the bulk of the released magnetic energy into high-energy particles. However, the theory suffers from

such a serious defect that the formula is invalid within the current sheet, and that the fluid is in fact more likely to be compressed.

It should be emphasized that the theory proves impossible for a stationary current sheet to be formed (Sweet, 1969). This is apparent from the comparison between the magnetic and the fluid pressures. An upper limit to the fluid pressure in the current sheet is given by that of the fluid within $|x| < \sqrt{2\delta}$ swept up along the x axis by the frozen-in field. If the compression is assumed isothermal, this gives a maximum ratio of compression $\sqrt{2\delta} / r_s$, hence a maximum fluid pressure becomes $\rho_0 V_s^2 \sqrt{2\delta} / r_s$. The field intensity immediately outside the sheet on the x axis is $B_0\sqrt{2\delta}$ (Green, 1965). Therefore the ratio of magnetic pressure at the x boundary of the sheet, to the fluid pressure at the neutral point must exceed $\sqrt{2\delta} / 2r_s \gg 1$. This indicates that the fluid in the sheet should be more compressed, i.e., the current sheet cannot be in equilibrium. A sort of Parker modes can never be attained, although the above discussion cannot entirely preclude possible existence of a Petschek-type configuration. It would be rather closer to the Dungey's (1953) instability at a neutral point. The stability of this configuration, as that of Dungey mechanism, depends upon whether the lines of force are free to move at the boundary. For example, if the pair of line currents in Fig. 13 are fixed, the field remains a potential field and is therefore stable. Only if the currents are released, the system changes itself to that of lower energy. It is the same as the Dungey's case that the system is not in equilibrium to start with.

Chapter 4

A NUMERICAL SOLUTION FOR STATIONARY-STATE RECONNECTION OF MAGNETIC LINES OF FORCE

§ 1. Introduction

The major question to be answered by a steady-state analysis is " What is the maximum rate of reconnection ? " As already mentioned, several arguments have been presented about the maximum reconnection rate, based on the well-established boundary layer technique in hydrodynamics : the diffusion region and the convection region are investigated separately, and then suitably matched with each other. However, they could not succeed in the complete matching in many aspects (Priest, 1973), which is really a controversial problem.

Therefore we discuss here a solution for steady, incompressible, finitely conducting, viscous fluid involving an X-type neutral point of magnetic field, in which no such clear cut distinctions are made between the two regions. It is assumed that the configuration is two-dimensional in the sense that it is invariant with respect to z, as in the pioneering works. In this case, magnetohydrodynamic behaviour depends upon three parameters : externally applied electric field E (equivalently, the Alfvén Mach number M of the incident flow), magnetic Reynolds number R_m and hydrodynamic Reynolds number R. The method of computation is described in Appendix I.A. The nonlinear

---

* See Fukao and Tsuda (1973a).

differential equations involving the fluid velocity and the magnetic field are solved numerically by the over-relaxation method. The solutions are obtained only for moderate values of R_m and R, and instabilities caused by the numerical scheme disturb convergence in cases where their values are very large.

§ 2. Governing Equations

The governing equations are the continuity equation, the equation of motion, Maxwell's equations and Ohm's law :

$$\nabla \cdot u = 0 , \tag{4.1}$$

$$\nabla \cdot B = 0 , \tag{4.2}$$

$$\nabla \times E = 0 , \tag{4.3}$$

$$\mu^{-1} \nabla \times B = J , \tag{4.4}$$

$$E + u \times B = J / \sigma , \tag{4.5}$$

$$\rho(u \cdot \nabla)u = J \times B - \nabla p - \rho\nu \nabla \times \nabla \times u , \tag{4.6}$$

for fluid velocity u, magnetic field B, electric field E, current density J, hydrodynamic pressure p, mass density ρ, magnetic permeability μ, electrical conductivity σ, kinematic viscosity ν. There is no necessity for using the energy equation in the incompressible case. The fluid is characterized by σ and ν which are assumed to be uniform. Since the fluid is incompressible, ρ is also constant.

As mentioned, we assume that the phenomenon concerned is two-dimensional. Then the above equations become

$$\frac{\partial u_x}{\partial x} + \frac{\partial u_y}{\partial y} = 0 , \tag{4.7}$$

$$\frac{\partial B_x}{\partial x} + \frac{\partial B_y}{\partial y} = 0 , \tag{4.8}$$

$$\frac{\partial E_z}{\partial x} = 0 \ , \qquad \frac{\partial E_z}{\partial y} = 0 \ , \tag{4.9a,b}$$

$$\frac{\partial E_y}{\partial x} - \frac{\partial E_x}{\partial y} = 0 \ , \tag{4.10}$$

$$E_x + u_y B_z - u_z B_y = \frac{1}{\sigma} J_x \ , \tag{4.11}$$

$$E_y + u_z B_x - u_x B_z = \frac{1}{\sigma} J_y \ , \tag{4.12}$$

$$E_z + u_x B_y - u_y B_x = \frac{1}{\sigma} J_z \ , \tag{4.13}$$

$$\rho\left(u_x \frac{\partial}{\partial x} + u_y \frac{\partial}{\partial y} \right) u_x = \left(J_y B_z - J_z B_y \right) - \frac{\partial p}{\partial x} - \rho\nu \frac{\partial \omega_z}{\partial y} \ , \tag{4.14}$$

$$\rho\left(u_x \frac{\partial}{\partial x} + u_y \frac{\partial}{\partial y} \right) u_y = \left(J_z B_x - J_x B_z \right) - \frac{\partial p}{\partial y} + \rho\nu \frac{\partial \omega_z}{\partial x} \ , \tag{4.15}$$

$$\rho\left(u_x \frac{\partial}{\partial x} + u_y \frac{\partial}{\partial y} \right) u_z = \left(J_x B_y - J_y B_x \right) - \rho\nu \left(\frac{\partial \omega_y}{\partial x} - \frac{\partial \omega_x}{\partial y} \right) \ , \tag{4.16}$$

where

$$\boldsymbol{\omega} = \nabla \times \mathbf{u} \tag{4.17}$$

is the vorticity. By introducing vector potential A(x, y) and stream function Φ(x, y), we have

$$B_x = \frac{\partial A}{\partial y} \ , \qquad B_y = - \frac{\partial A}{\partial x} \ , \tag{4.18}$$

$$u_x = \frac{\partial \Phi}{\partial y} , \qquad u_y = - \frac{\partial \Phi}{\partial x} , \tag{4.19}$$

and

$$J_z = - \frac{1}{\mu} \nabla^2 A , \qquad \omega_z = -\nabla^2 \Phi \tag{4.20}$$

where

$$\nabla^2 = \frac{\partial^2}{\partial x^2} + \frac{\partial^2}{\partial y^2} .$$

The contour A = constant gives an individual magnetic line of force, while the contour Φ = constant gives streamline. Equation (4.13) then becomes

$$\frac{\partial \Phi}{\partial y} \frac{\partial A}{\partial x} - \frac{\partial \Phi}{\partial x} \frac{\partial A}{\partial y} = E_z + \frac{1}{\sigma \mu} \nabla^2 A . \tag{4.21}$$

Elimination of p from Eqs. (4.14) and (4.15) yields

$$\rho \left[\frac{\partial \Phi}{\partial y} \frac{\partial}{\partial x} - \frac{\partial \Phi}{\partial x} \frac{\partial}{\partial y} \right] \nabla^2 \Phi$$

$$- \frac{1}{\mu} \left[\frac{\partial A}{\partial y} \frac{\partial}{\partial x} - \frac{\partial A}{\partial x} \frac{\partial}{\partial y} \right] \nabla^2 A = \rho \nu \nabla^4 \Phi . \tag{4.22}$$

It follows from Eqs. (4.9a and b) that E_z is constant in the xy plane. We may assume that E_z is a positive constant, E, since the streamlines would be decoupled with the magnetic lines of force if E_z were zero. This means that magnetic lines of force are carried, at a constant rate, into the region of analysis. The above couple of equations are self-contained and can be solved independently from the set of equations that determines the other variables u_z, B_z, E_x and E_y. Eliminating E_x and E_y among Eqs. (4.10) - (4.12) and (4.16), it is readily seen that B_z and u_z must satisfy

$$\rho\Big[\, u_x \frac{\partial}{\partial x} + u_y \frac{\partial}{\partial y} \,\Big] u_z$$

$$- \frac{1}{\mu} \Big[\, B_x \frac{\partial}{\partial x} + B_y \frac{\partial}{\partial y} \,\Big] B_z = \rho\nu\nabla^2 u_z \ , \qquad (4.23)$$

$$\Big[\, u_x \frac{\partial}{\partial x} + u_y \frac{\partial}{\partial y} \,\Big] B_z$$

$$- \Big[\, B_x \frac{\partial}{\partial x} + B_y \frac{\partial}{\partial y} \,\Big] u_z = \frac{1}{\sigma\mu} \nabla^2 B_z \ . \qquad (4.24)$$

These equations, together with appropriate boundary conditions, can be solved using the magnetic field and flow in the xy plane, which are determined by Eqs. (4.21) and (4.22). We shall, however, concern ourselves here with only Eqs. (4.21) and (4.22).

Next we scale the variables. Distance x, etc., are normalized by L, the size of the *whole* domain, magnetic field B by B_0, the intensity of the magnetic field at the boundary where there is an influx of magnetic lines of force ; fluid velocity u_x etc. by V_A, the Alfvén velocity corresponding to B_0 ; electric field E by $V_A B_0$. Accordingly, magnetic potential A and flow potential Φ are normalized by LB_0 and LV_A, respectively. Hereafter, unless otherwise specified, all the variables that appear are understood to have been normalized in this way.

The equations to be solved are scaled to the nonlinear, simultaneous equations :

$$\frac{\partial\Phi}{\partial y}\frac{\partial A}{\partial x} - \frac{\partial\Phi}{\partial x}\frac{\partial A}{\partial y} = E + \frac{1}{R_m} \nabla^2 A \ , \qquad (4.25)$$

$$\Big[\frac{\partial\Phi}{\partial y}\frac{\partial}{\partial x} - \frac{\partial\Phi}{\partial x}\frac{\partial}{\partial y} \Big] \nabla^2\Phi$$

$$- \Big[\frac{\partial A}{\partial y}\frac{\partial}{\partial x} - \frac{\partial A}{\partial x}\frac{\partial}{\partial y} \Big] \nabla^2 A = \frac{1}{R} \nabla^4\Phi \ . \qquad (4.26)$$

where R_m and R are respectively the hydromagnetic and the hydrodynamic Reynolds numbers given by

$$R_m = \sigma\mu V_A L \qquad \text{and} \qquad R = V_A L / \nu \,. \tag{4.27a,b}$$

§ 3. Numerical Results

For simplicity we impose a symmetry condition on both the x axis and the y axis, and solve for the first quadrant only. Figure 15 is a schematic picture of the region of analysis, with magnetic field and streamlines.

A number of computer runs started from the magnetic field and flow, which are given by Sonnerup (1970) for the ideal hydromagnetic fluid (perfectly conducting and inviscid fluid free from thermal conduction). Sonnerup's solutions (shown in Figs. 16 (a) and (b))

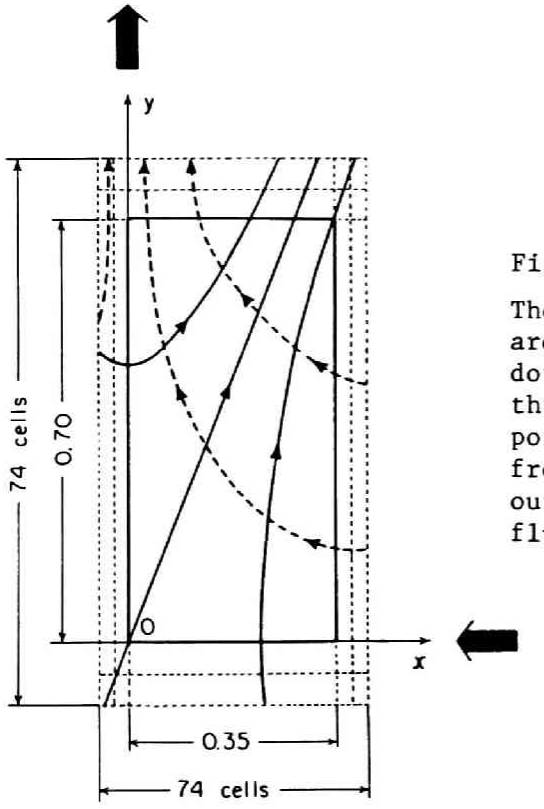

Fig. 15

The region of analysis. Solid lines are for magnetic lines of force and dotted lines for streamlines. The thick arrow pointing to the neutral point 0 shows the injection of fluid from outside, while that pointing outward indicates the ejection of fluid.

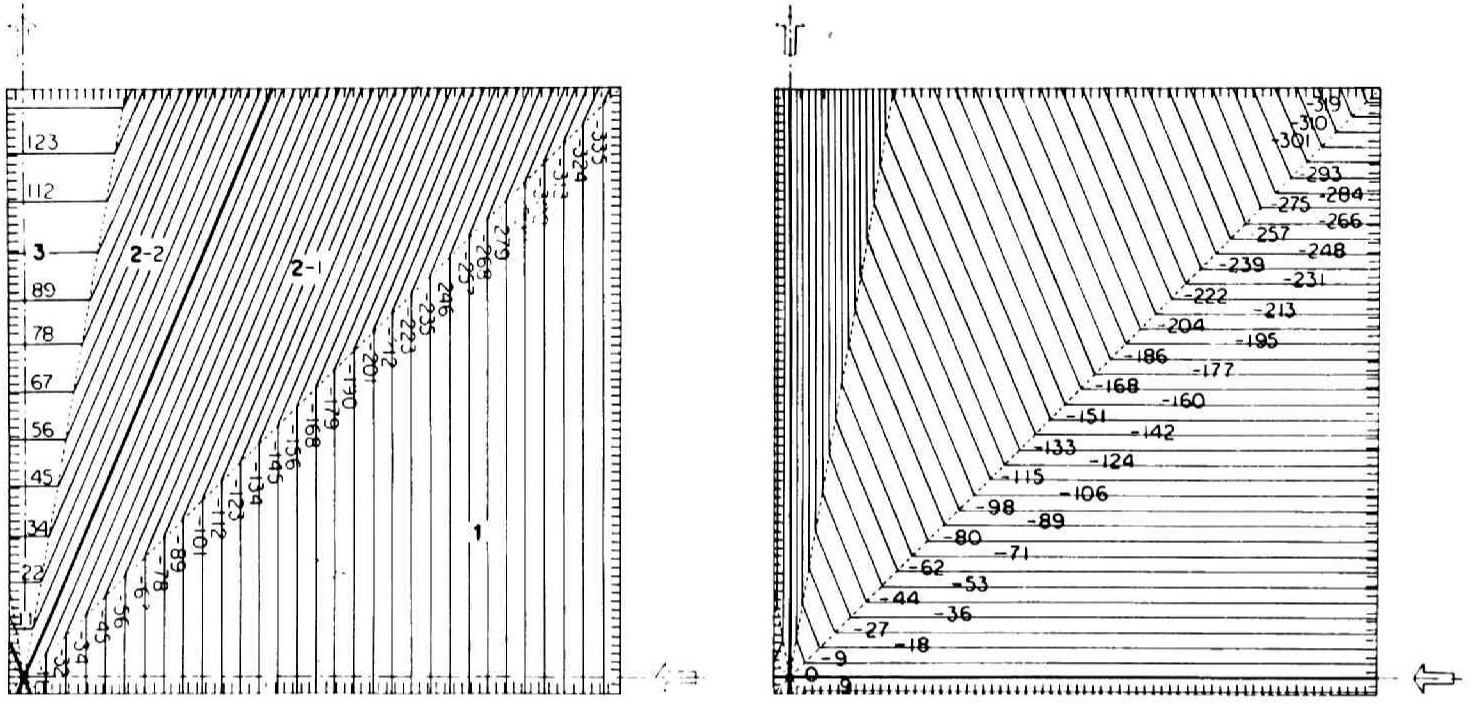

Fig. 16 Sonnerup's solution in an ideal hydromagnetic fluid for M = 0.5. Note the difference of length scale between the vertical and the horizontal directions. The heavy dot at the left bottom corner is the neutral point in the magnetic field, and also the stagnation point of the flow. The heavy lines indicate the ones with zero potential. Two rotational discontinuities divide the flow domain into three regions, each of which contains a uniform flow and magnetic field. (a) Magnetic lines of force. Contours drawn from -3.35×10^{-1} to 1.34×10^{-1}, with a contour interval of 1.117×10^{-2} scaled by 10^3. (b) Streamlines. Contours drawn from -3.37×10^{-1} to 9×10^{-3}, with a contour interval of 8.866×10^{-3} scaled by 10^3.

correspond to the case of M = 0.5. Figures 17 (a) and 18 (a) show the calculated profiles of magnetic lines of force in the cases of M = 0.5 and M = 1.0, respectively, where R_m = 200 and R = 200. The profiles of streamlines are shown in Figs. 17 (b) and 18 (b). We can readily see that the calculated configurations of Figs. 17 (a) and (b) are not altered much from the starting ones of Figs. 16 (a) and (b). There appear two transition layers, which smoothly connect each physical quantity in the regions on either side. The magnetic lines of force with zero-potential keep away from the origin. The streamlines become concave to the neutral point between the two layers, whereas they are straight under the uniform hydromagnetic pressure in the ideal hydromagnetic fluid (Sonnerup, 1970 ; Yeh and Axford, 1970). When the Alfvén Mach number M is larger, the wedge in which the fluid is ejected, as well as the one between the two transition layers, extends more widely throughout the whole regions except in the vicinity of the neutral point. Checking on the cross-section of ejection velocity u_y along the lines parallel to the x axis, one finds that the fluid is ejected at a velocity several times greater than the injection velocity in the narrow region around the y axis. A small increase and decrease appear in u_y along the transition layers far from the neutral point, by virtue of the considerable difference in the tangential component of the magnetic field between the regions adjacent to the layer. Between the two transition layers is the plateau in u_y ; it is clearest in the region far from the neutral point. The magnetic field is intensified in the region between the two transition layers, and a sharp valley is formed along the y axis. The fluid, on the other hand, should expand across the layer that stands nearest to the x axis ; and it should be compressed across the one nearest to the y axis. In this sense (as Sonnerup (1970) suggested) the former is an expansion wave (in the compressible case this would dissolve into a series of isentropic, slow-expansion waves), while the latter is compressive (in the compressible case this would be a slow shock, or perhaps a combination of that and an intermediate wave).

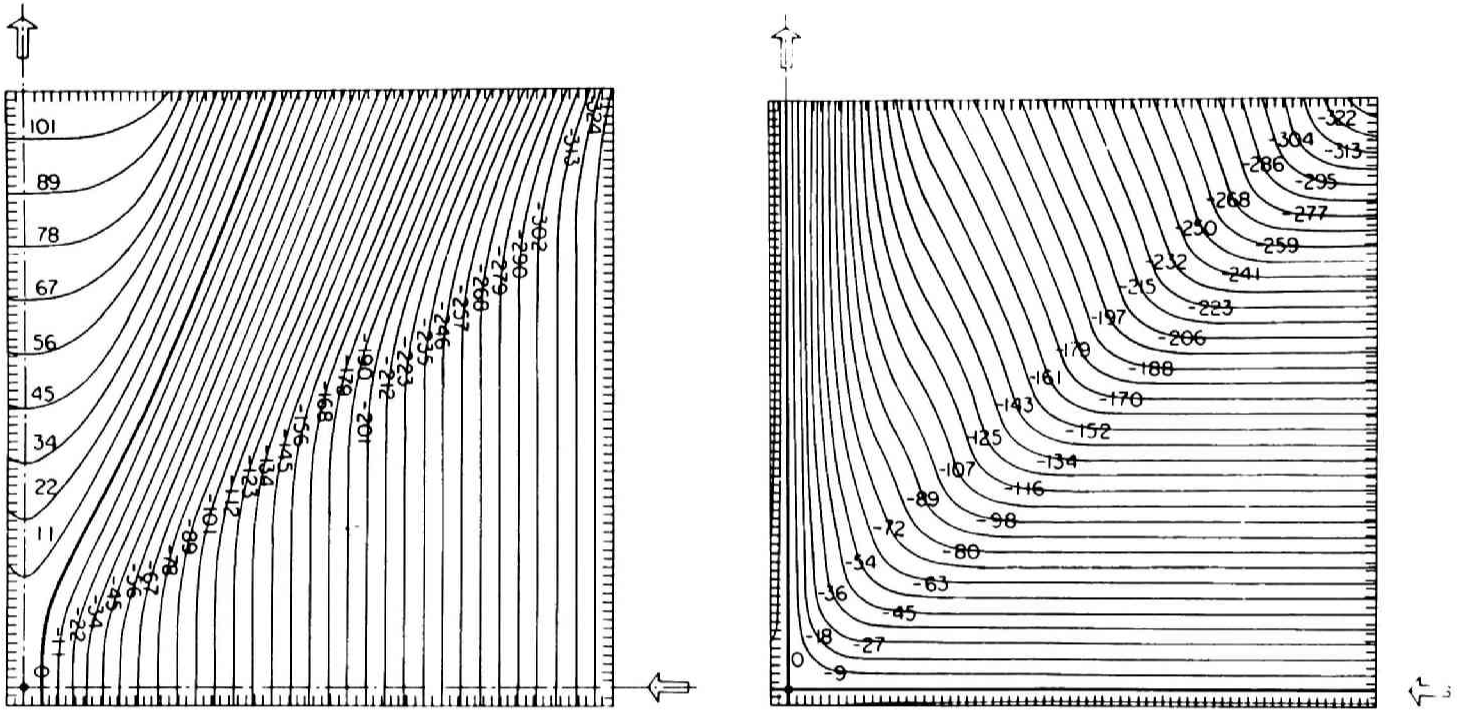

Fig. 17 Calculated results in the case of R_m = 200, R = 200 and M = 0.5. The potential value of each contour is similar to that of Figs. 16 (a) and (b). (a) Magnetic lines of force. (b) Streamlines.

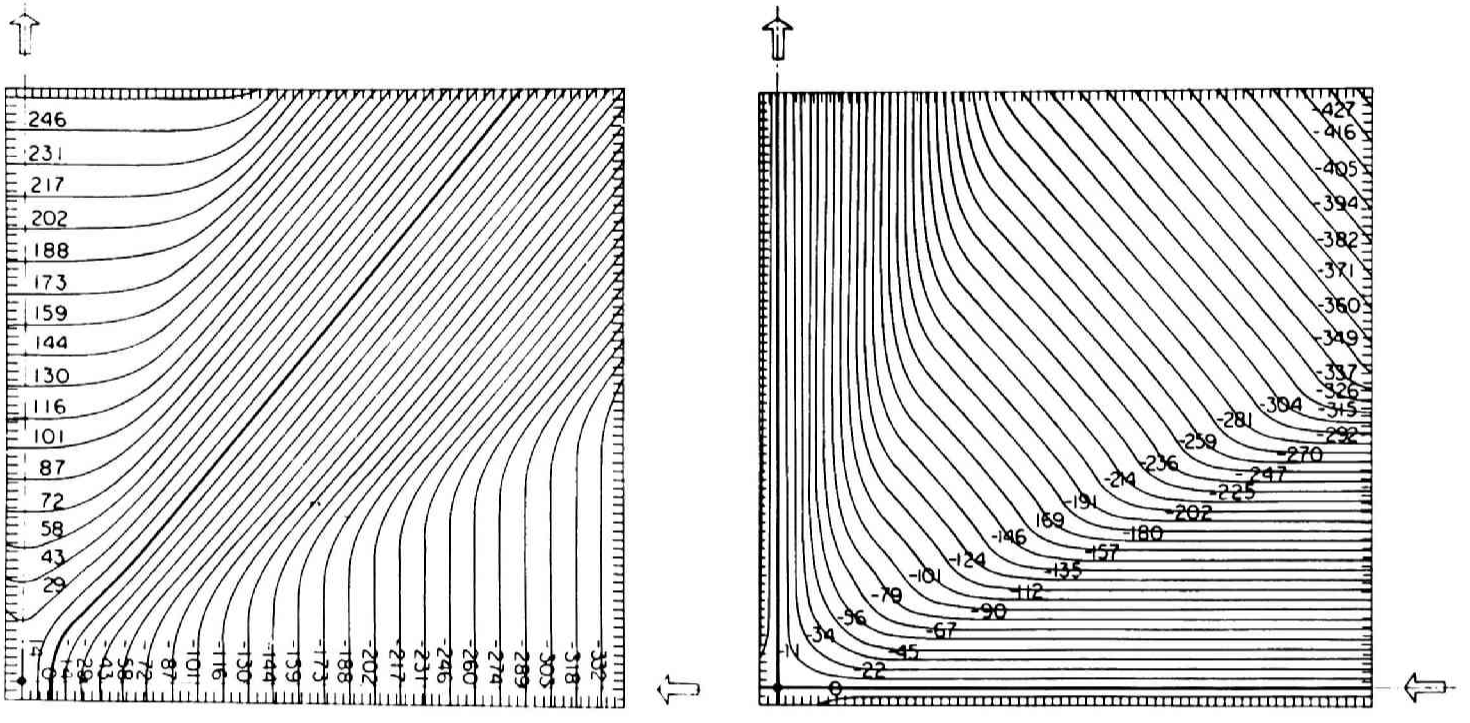

(a) (b)

Fig. 18 The same as Figs. 17 (a) and (b) for M = 1.0.

The accelerated fluid is ejected along the deep valley of the magnetic field. The effects of E, R and R_m will be examined in this order below.

3.1 Electric field

Figure 19 shows the magnetic field B_y along the x axis and B_x along the y axis for differnt R_m's and R's. In the ideal hydromagnetic fluid, magnetic fields B_y and B_x are constant along the x and y axes, respectively, and $B_x / B_y = M / (1 + \sqrt{2})$ (see Eqs. (A5), (A8) and (4.18)). Here we have cases of M = 0.5 and 1.0 when R_m = 200 and R = 200. It is readily seen that the intensity is not constant along the axes, and that B_y is considerably intensified near the neutral point. Each component tends to the respective constant of the ideal hydromagnetic fluid in the regions far from the neutral

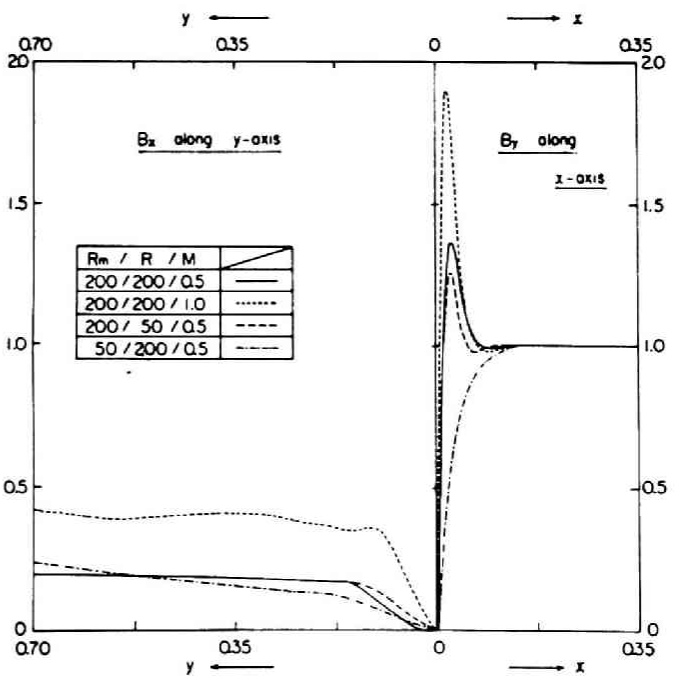

Fig. 19 Magnetic fields B_y along the x axis, and B_x along the y axis for different R_m's and R's.

point. The humped pattern of the variation of magnetic field is remarkable for highly conducting fluid, and is only emphasized when the injection velocity or applied electric field becomes more intense (we shall mention this in section 4, in connection with the motion of magnetic lines of force). In the ideal hydromagnetic fluid, injection velocity is equal to M all over the x axis, and ejection velocity is also constant $1 + \sqrt{2}$ throughout the y axis, regardless of the intensity of injection velocity. It is made clear by our computational study, however, that $-u_x$ increases linearly along the x axis from zero at the neutral point, has a small hump, then tends to the constant of the ideal hydromagnetic fluid. Ejection velocity u_y also increases linearly along the y axis near the neutral point, then has a large hump or the maximum velocity which is considerably larger than that of the ideal fluid. There is little change in the maximum velocity, except the shift of its position inward to the neutral point when the injection velocity is doubled. The ejection velocity tends more rapidly to the constant as the injection velocity becomes larger. In the vicinity of the origin, the rate of decrease of the injection velocity is found to be equal to that of increase of the ejection velocity. This is the same as those known in the usual stagnation flows.

The current density $J_z = -\nabla^2 A$ in the xy plane is shown in Fig. 20 (a) in the case of $R_m = 200$, $R = 200$ and $M = 0.5$. In the vicinity of the origin where magnetic field is null and fluid velocity is stagnated, the Ohm's law $J_z = R_m E$ should be satisfied. In our case, the calculated result at the neutral point is nearly 97, and may satisfy the law, since the exact result is 100. Two antiparallel electric current layers are formed along the two transition layers. The positive current flows so as to cover the magnetic neutral point and to form a current-core in the vicinity of it, while the negative current with somewhat weaker intensity avoids it. This implies, as Sonnerup suggested, that the transition layer corresponding to the positive current forms at the origin, while that corresponding to the

negative current forms in the outer region. The negative current exerts the Lorentz force on the fluid directed outwards, and decelerates the injected flow, co-operating with the hydrodynamic pressure (which does not explicitly appear in the calculation). Note the position of negative current layer in Fig. 20 (a). The steep shear of currents is formed in the vicinity of the origin, especially along the direction of the injection of fluid. As discussed later, this may contribute to the reduction of the electrical conductivity, and seems to support the universal validity of the results obtained using a comparably small R_m (such as 10^2), though in the sun and the interplanetary space values of 10^9 - 10^{10} are familiar. Figure 20 (b) depicts the case of M = 1.0, when R_m and R are the same as before. The two current layers are formed, corresponding to the transition layers in the magnetic field and flow. Both positive and negative currents show enhancement over the case of M = 0.5 and the current in the vicinity of the origin is compressed to the thinner core. The current shear near the origin also becomes stronger. The current is almost free in any other regions.

Figures 21 (a) and (b) show the vorticity $\omega_z = -\nabla^2\Phi$. The vorticity is also dominant near the transition layers in the velocity field, and the intensity along the layer which stands nearest the y axis is considerably larger than that along the other, though the two layers are not so clearly separated near the origin. Note that vorticity is zero on the x and y axes. It is conspicuous that the binocular vortices appear in the transition layer nearest the y axis. The vortex nearest the origin (the first vortex) may be caused because the fluid injected from opposite sides with a super Alfvénic velocity forms, due to its inertia, a flow of wedge-like shape with its peak on the y axis. The other vortex (the second vortex) is excited in the same manner as the one that would be formed in flow passing a wedge-like obstacle. Both of them will be affected by the intensity of viscous force. These are so-called trailing vortices, and give vortex drag to the flow. The variation of ejection velocity

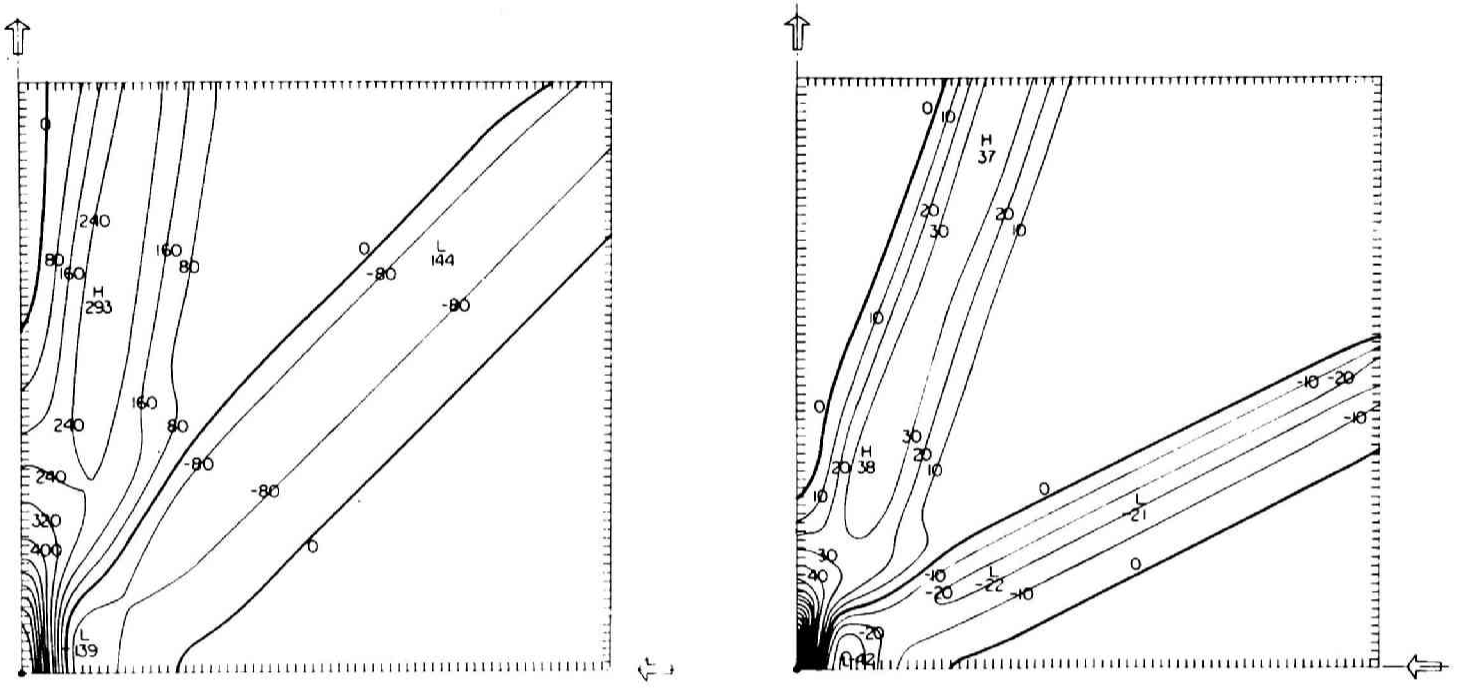

Fig. 20 Current density $J_z = -\nabla^2 A$ in the xy plane for the case of R_m = 200 and R = 200. The dot at the left bottom corner is the position of the neutral point. (a) M = 0.5. Contours drawn from 88.0 to -8.0, with a contour interval of 8.0 scaled by 10.0. (b) M = 1.0. Contours drawn from 190.0 to -40.0, with a contour interval of 10.0 scaled by 1.0.

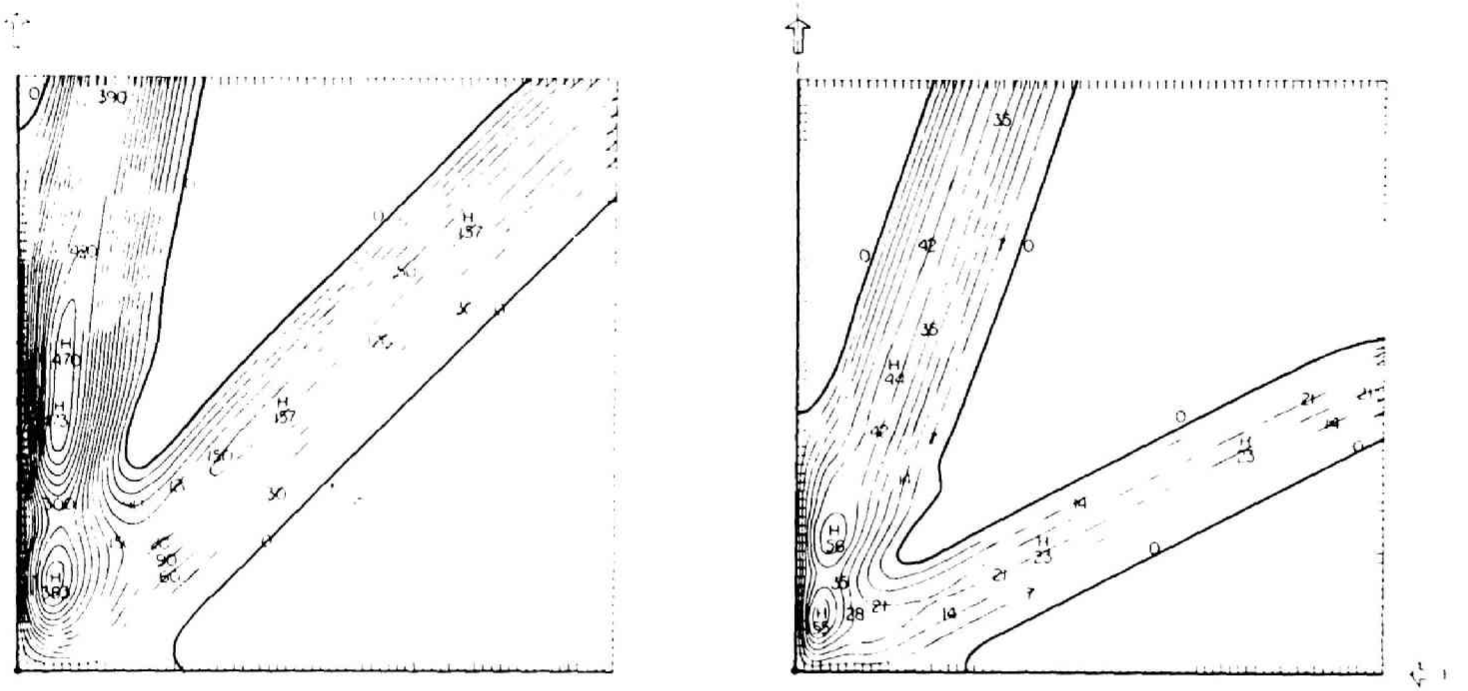

(a) (b)

Fig. 21 Vorticity $\omega_z = -\nabla^2\Phi$ in the xy plane for the case of $R_m = 200$ and $R = 200$. Minus sign is omitted. The dot is the position of the neutral point. (a) M = 0.5. Contours drawn from 0.0 to -45.0, with a contour interval of 3.0 scaled by 10.0. (b) M = 1.0. Contours drawn from 0.0 to 49.0, with a contour interval of 7.0 scaled by 1.0.

along the y axis corresponds quite well to the positions of vortices. The fluid velocity along the y axis increases linearly near the origin, the rate of increase becomes smaller away from the origin (ascribable to drag of the first vortex). As we go farther along the y axis, the comparably large increase is recovered and the rate becomes smaller again, which seems due to the second vortex.

3.2 Hydrodynamic Reynolds number

The variation of viscosity does not cause much difference both in the magnetic field and flow. Slight differences are recognizable, however ; the more viscous the fluid becomes, the peak that appears in the variation of B_y along the x axis is suppressed, and the rate of increase of B_x along the y axis in the vicinity of the neutral point becomes somewhat larger. The same is also true of the fluid velocity (i.e., the maximum ejection velocity decreases a little and the rates of deceleration along the x axis, and acceleration along the y axis in the vicinity of the origin, become somewhat larger). The extent of the current-rich region in the vicinity of the neutral point is compressed a little along the x axis, while it expands along the y axis, forming a slightly flatter core of current. The currents are somewhat localized and intensified, especially near the expansion-wave-like transition layers, as the fluid becomes more viscous. Variations of vorticity exhibit a tendency similar to those of current : the two layers of vorticity are joined together in the vicinity of the neutral point, while those of current are clearly separated. The overall pattern of the variations, including the maximum current at the origin, is apparently not influenced by the change of the hydrodynamic Reynolds number. Thus we can conclude that the viscous effect does not change drastically the features of the reconnection of magnetic lines of force.

3.3 Hydromagnetic Reynolds numbers

Figure 19 includes the case of $R_m = 50$, $R = 200$ and $M = 0.5$, which is less conducting than that of $R_m = 200$. In this case, the intensification of the magnetic field B_y in the vicinity of the neutral point disappears. The intensity B_x along the y axis still increases beyond $y \sim 0.2$, while it remains constant beyond there in the more conducting fluid. When the hydrodynamic Reynolds number is reduced, such that $R = 50$, with the same parameters $R_m = 50$ and $M = 0.5$, there is little change in the feature mentioned above. When the fluid is less conducting, the current intensity is considerably reduced, the region of current in the vicinity of the neutral point expands and reaches the boundary of the numerical domain along the y axis. Accordingly, the current shear near the origin becomes less conspicuous. The expansion-wave-like transition layer does not intersect the x axis, and so does not have a continuous configuration across the injected fluid. The layer of this type should have the origin far from the neutral point, as already mentioned.

Thus the change of hydromagnetic Reynolds number has a great influence on the magnetic field or the current field but little influence on the flow or the vorticity field. The change of the hydrodynamic Reynolds number, on the other hand, seems to have more effect upon the flow than the magnetic field, though both of them are not so susceptible to the hydrodynamic Reynolds number as they are to the hydromagnetic Reynolds number.

§ 4. Discussion and Concluding Remarks

Although we adopt Reynolds numbers that are 10^{-7} - 10^{-8} times smaller than those familiar in astrophysical and geophysical phenomena, the resulting solutions exhibit that the magnetic field and flow make a smooth transition in their properties from the diffusive in the

vicinity of the neutral point to the convective far from it. Electric current-core is formed over the neutral point, and is bordered with a steep current shear around it. Electric current also flows along the two transition layers which divide the reconnection region into three, each of which contains almost uniform flow and magnetic field. The other regions are nearly current-free, and the magnetic field is practically frozen in the fluid there. The magnetic field is, of course, more easily frozen in more conducting fluids. The overall features are affected little by the change of the viscosity, except in the vicinity of the transition layers. As the conductivity becomes larger, the current-core over the neutral point is reduced in area, and the current shear becomes steeper. The current shear may contribute to reducing the effective electrical conductivity locally, as described below, and the reduction may become more remarkable as the conductivity becomes higher. Although we inevitably use unnaturally small values of the hydromagnetic Reynolds number, universal validity may be supported by the results : we expect effective electrical conductivity to be reduced near the neutral point, even if the conductivity is extremely large, and the magnetic field to be nearly frozen in the fluid far from it, even if conductivity is moderate. In this sense, the reconnection of magnetic lines of force is always possible, not only in the dissipative fluids but also in highly conducting ones. It is revealed, however, that conductivity, as well as viscosity, inherent in the fluid has no influence on the reconnection rate ; this rate is determined entirely by the external conditions corresponding to the parameter M of our computation. Thus we may conclude that the rate of reconnection does not depend on conductivity and viscosity, but on external conditions, such as the externally applied electric field or the injection velocity of the fluid, as was indeed suggested by Yeh and Axford (1970).

Next we mention the selective reduction of the electrical conductivity in the vicinity of the neutral point. In the collision-free plasma there are at least two possible mechanisms that might cause

the conductivity to remain finite. One is the wave-particle interactions between the streaming electrons and low-frequency ion waves. Interactions between an electron and the ions are more influential than those between electrons in determining the magnitude of conductivity. Since the energy of ion waves is mainly in the regime of ion acoustic waves, the excitation of ion acoustic waves is of interest. The other mechanism is due to the finite flight time during which the charged particles are exposed to, and accelerated by, the external electric field. Speiser (1970) estimated the magnitude of these *inertial* conductivities when applied to the geomagnetic tail. He found that they are about 8 - 11 orders of magnitude smaller than the collisional conductivity, and suggested that the wave-particle interactions exert a small influence on the effective conductivity.

The simplest version of the inertial conductivities is as follows. Ohm's law involving the inertia effect is

$$\frac{m}{ne^2}\frac{dJ}{dt} = E + v \times B - \frac{J}{\sigma_c} , \tag{4.28}$$

where the collisional conductivity

$$\sigma_c = \frac{ne^2}{m}\tau_c , \tag{4.29}$$

using the mean collision time τ_c. Near the neutral point where the magnetic field is weak and the flow velocity is small, Eq. (4.28) can be approximated as

$$\frac{dJ}{dt} = -\frac{J}{\tau_c} + \frac{\sigma_c}{\tau_c} E , \tag{4.30}$$

which is solved for zero initial current such that

$$J = \sigma_c (1 - \exp(-t/\tau_c)) E . \tag{4.31}$$

So an effective conductivity σ_i is defined as

$$\sigma_i = \sigma_c (1 - \exp(-\tau_i/\tau_c)) , \qquad (4.32)$$

where the time τ_i is, from particle aspect, identical with the average flight time of the particles in the system (Speiser, 1970). If $\tau_i \gg \tau_c$, the inertial conductivity σ_i is the same as σ_c. If $\tau_i \ll \tau_c$, on the other hand,

$$\sigma_i = \frac{\tau_i}{\tau_c} \sigma_c , \qquad (4.33)$$

and σ_i assumes arbitrarily small values as $\tau_i \to 0$. Note that the inertial term for the steady state is

$$\frac{dJ}{dt} = v \cdot \frac{dJ}{dr} , \qquad (4.34)$$

which is negative in the y direction. In the vicinity of the neutral point this may be sufficiently larger than the collisional term, since much steeper shear of currents is to be expected in fluids more conducting than those discussed above. Therefore, it is suggested that electrical conductivity is reduced effectively in the vicinity of the neutral point even in very highly conducting fluids, and hence, the current there remains finite.

We add a few comments concerning the hump shown in Fig. 19 , or the intensification of magnetic field in the vicinity of the neutral point. As mentioned the velocity of a magnetic line of force consists of two components : convection with fluid velocity, and slippage with diffusion velocity due to finite electrical conductivity (we do not concern ourselves with relabeling of magnetic lines of force). Convection carries magnetic lines of force with no variation in the fluid, while diffusion is proportional to the magnetic body force acting on the fluid, as well as to the reciprocal of conductivity. The

diffusive transport is efficient in the vicinity of the neutral point and the convective transport far from it. Therefore, if conductivity of a fluid is sufficiently small, magnetic lines of force, convected into the deceleration or the stagnation region of the flow, will be entirely carried away from there by the diffusive transport ; hence, no humps appear as in the case of $R_m = 50$. On the other hand, if a fluid is so conducting that all lines of force, convected into the stagnation region, cannot be carried away by diffusive transport, they are piled up there. In such a fluid a hump or intensification of magnetic field is induced as in the case of $R_m = 200$. This is more remarkable in the more conducting fluid and in the case of larger fluid velocity.

Chapter 5

A NUMERICAL SOLUTION FOR THE EVOLUTION OF RECONNECTION

§ 1. Introduction

In this chapter we present transient incompressible magnetohydrodynamic solutions to investigate the evolution of reconnection in a highly conducting viscous flow.

We start with a current sheet, i.e., antiparallel magnetic lines of force. There is then an influx of flow from both sides, transverse to the null magnetic field-region of the current sheet. The lines of force will be locally pressed against the other parallel lines of force and we may expect reconnection to begin.

We use two-dimensional incompressible MHD equations which are numerically solved with every nonlinear term retained. Numerical studies certainly have some drawbacks ; for instance, it may be said that we search for a particular solution in a particular situation. We nevertheless make an attempt on the lines described because there has been no self-consistent solution to date of the evolutionary process of reconnection in the fluid of finitely high conductivity.

If we analyze the points of interest of the evolutionary process, they are as follows.

---

* See Fukao and Tsuda (1973b).

Confirmation of reconnection. We want to confirm that individual lines of force can indeed join across the region of null magnetic field. This confirmation can be made by use of a magnetic vector potential which turns out to be a scalar in case of two dimensions. Each magnetic line of force is labeled with its potential value whereby the identity of individual lines of force is retained.

Speed of growth. If reconnection occurs, then there is the formation of the so-called X-type configuration of magnetic field. We need to know the speed of growth, or the time scale of the reconnection process involving the neutral point.

Controlling conditions. What are the conditions that control the growth of the reconnection or the formation of the X-type configuration of magnetic field ? Is the local condition in the immediate vicinity of the neutral point crucial to the build-up process, or are conditions far from the neutral point more important ? That is, have boundary conditions a greater influence on the process under consideration ? One of these boundary conditions is the shape of the boundaries, the widths of the entrance and exit of the flow, that determine the overall flow pattern away from the site where reconnection takes place. Another such boundary condition is the speed of inflow, which may be specified in terms of the applied electric field driving the fluid at the entrance.

Acceleration of particles. One of the important functions of the reconnection process is the acceleration of charged particles. There are two types of acceleration in this context ; one is the increase of fluid bulk velocity and the other is the heating of particles through the Joule dissipation. The acceleration of the fluid in bulk is done through the formation of X-type configuration of magnetic field. If the X-type magnetic field extends over a scale sufficiently larger than the characteristic Alfvén wavelength, this type of acceleration may give what space-physicists usually anticipate in many situations. The other type of acceleration is done irreversibly by the action of the electric field at the neutral point and in the case

of the build-up process of the reconnection the electric field due to the rapidly changing magnetic field may heat up particles very efficiently. We seek to check on these types of acceleration quantitatively.

Diffusion region vs convection region. In analytical studies given to the steady states of the reconnection, the domain of interest used to be divided into the diffusion region and the convection region. As already mentioned, this approach is based on the well-established boundary layer technique in hydrodynamics. In the computational study, it is difficult to make such a clear-cut distinction between the diffusion region and the convection region from the outset. If there is in fact such a boundary layer to be formed, then it should manifest itself spontaneously with time in the computed flow and field patterns that have been obtained without such simplifying assumptions about the boundary layer.

The above are the points of interest that will be pursued in this chapter.

§ 2. Governing Equations

The differential equations to be used are the usual MHD equations where incompressibility as well as time dependence are considered. Namely,

$$\nabla \cdot u = 0 \ , \tag{5.1}$$

$$\nabla \cdot B = 0 \ , \tag{5.2}$$

$$\nabla \times E = - \frac{\partial B}{\partial t} \ , \tag{5.3}$$

$$\frac{1}{\mu} \nabla \times B = J \ , \tag{5.4}$$

$$E + u \times B = J / \sigma \ , \tag{5.5}$$

$$\rho \left\{ \frac{\partial u}{\partial t} + (u \cdot \nabla) u \right\} = J \times B - \nabla p$$

$$- \rho \nu \nabla \times \nabla \times u \ . \qquad (5.6)$$

The notations used are obvious. The situation considered is the same as that of the preceding chapter : σ and ν are constant everywhere ; and the phenomenon we study is two-dimensional, namely, every quantity depends only on x and y coordinates and not on z.

Using potential functions $A(x, y)$ and $\Phi(x, y)$, the equations to be solved are scaled to the nonlinear, simultaneous equations

$$\frac{\partial A}{\partial t} = - \frac{\partial \Phi}{\partial y} \frac{\partial A}{\partial x} + \frac{\partial \Phi}{\partial x} \frac{\partial A}{\partial y} + \frac{1}{R_m} \nabla^2 A \ , \qquad (5.7)$$

$$\nabla^2 \frac{\partial \Phi}{\partial t} = - \left[\frac{\partial \Phi}{\partial y} \frac{\partial}{\partial x} - \frac{\partial \Phi}{\partial x} \frac{\partial}{\partial y} \right] \nabla^2 \Phi$$

$$+ \left[\frac{\partial A}{\partial y} \frac{\partial}{\partial x} - \frac{\partial A}{\partial x} \frac{\partial}{\partial y} \right] \nabla^2 A + \frac{1}{R} \nabla^4 \Phi \ . \qquad (5.8)$$

The induction electric field is known by relation

$$E = E_z = - \frac{\partial A}{\partial t} \ . \qquad (5.9)$$

§ 3. Assumptions and Procedure of Numerical Experiment

We first describe our somewhat simplified assumptions concerning boundary and initial conditions and then discuss the procedure of computation. The difference scheme adopted is described in Appendix B.

3.1 Boundary conditions

We assume that there exists an antiparallel magnetic field in the y direction, and that in the z direction there is no magnetic field or fluid velocity, since Eqs. (5.7) and (5.8) can be solved independently of the other set of equations which determine the variables u_z, B_z, E_x and E_y. For simplicity we impose a symmetry condition on both x and y axes and solve for the first quadrant only. A schematic picture of the region of analysis with the initial profile of the magnetic field is shown in Fig. 22 . There is a sudden injection of fluid from the boundary at x = 0.4 with a velocity profile also shown in the figure. This profile is a wavelength of a cosine function, having the maximum value U at y = 0 and minimum zero at y = ± 0.7. The origin will be the neutral point in the magnetic field as well as the stagnation point in the velocity field, at which the reconnection of magnetic lines of force will progress. The rectangular domain enclosed by thick lines is 0.8 × 0.4 by size and is replaced by 80 × 80 rectangular meshes for computation. The length ratio of two

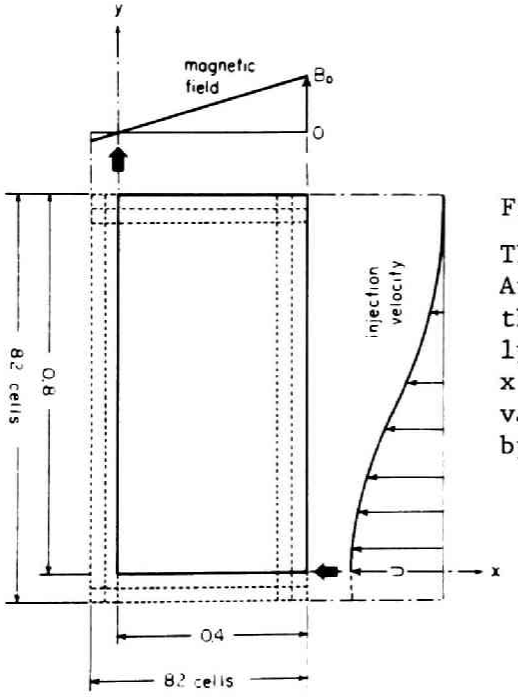

Fig. 22

The configuration for computation. Arrows with a cosine envelope shows the velocity profile of the initially injected fluid at the boundary x = 0.4. The intensity of linearly-varying magnetic field is also shown by a right-angled triangle.

sides of the mesh is, therefore, such that $\Delta x / \Delta y = 1 / 2$. To preserve the symmetry condition we need two outermost rectangular meshes. Thus we have 82×82 mesh points in all. The values of A and Φ on the boundaries of the inlet and outlet sides are extrapolated from within in terms of a third-order algebraic expression satisfied by the four nearest points, either aligned vertically or horizontally, so that the point of departure of each line of force or streamline may vary from time to time.

3.2 Initial conditions

In the case of vanishing zero-order velocity and uniform resistivity, the following condition is met by the zero-order magnetic field B_o :

$$\nabla^2 B_o = 0 . \tag{5.10}$$

This condition becomes

$$\frac{d^2 B_{oy}(x)}{dx^2} = 0 . \tag{5.11}$$

Thus $B_{oy}(x)$ varies linearly with x, which is the initial configuration of our model shown in Fig. 23 . This magnetic field might be sustained by the uniform current or the static electric field in the z direction. We will, however, leave the static field out of consideration, since the current decays resistively in the form of Joule dissipation in time τ_L, under the condition $\tau_L / \tau_A = R_m >> 1$. In the interval of about $0.1\tau_A$, during which the numerical experiment proceeds, the current or the pervading magnetic field seems to remain unchanged in view of the above condition. There is then an influx of fluid from both sides, transverse to the antiparallel magnetic lines of force. An

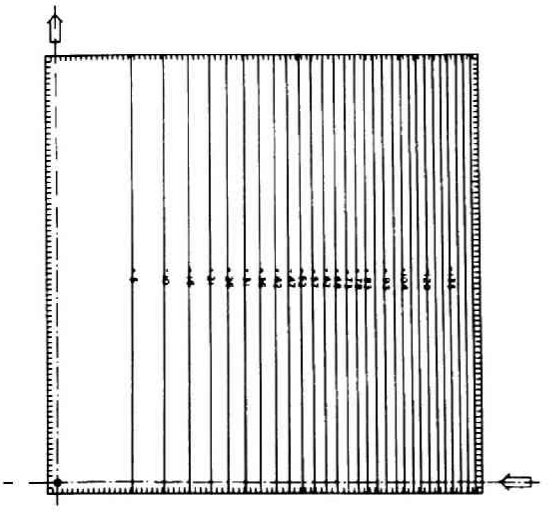

Fig. 23

The antiparallel magnetic field that there was at the start. Lines are contour A = constant ; the value of this constant is shown on each line, scaled by 10^3. The dot at the left bottom corner is the position of the neutral point, and the thick arrows are to show the injection and ejection of fluid.

unavoidable difficulty appears in this respect. Since the present model is incompressible, the velocity of sound is infinite. This means that we cannot inject a fluid as shown in Fig. 22 without considering the fluid that is ejected from the domain at the same time to maintain the continuity relation. We therefore simply " indent " a flow pattern shown in Fig. 24 on the antiparallel magnetic field shown in Fig. 23 at time t = 0. Figures 23 and 24 are reduced in length in the direction of y axis by a factor of 2. All the other square figures that will be shown later are also reduced in the same way.

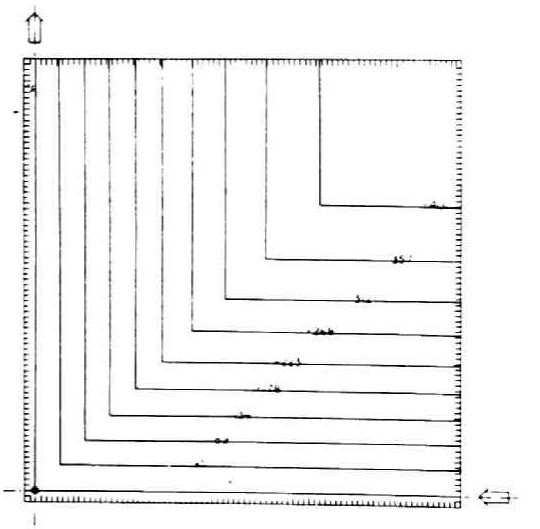

Fig. 24

Initial flow pattern to be indented on the antiparallel magnetic field shown in Fig. 23. Lines are contour Φ = constant ; the value of this constant is shown on each line, scaled by 10^3.

3.3 Procedure of computation

The algorithm of computation is : (1°). We compute the rhs of Eq. (5.7) from the initial condition or presently given condition ; (2°) we estimate the variation of A from Eq. (5.7), given its rhs ; (3°) we compute the rhs of Eq. (5.8) as step (1°) ; (4°) we solve Eq. (5.8), a Poisson-type equation, for $\partial\Phi / \partial t$, given its rhs ; and (5°) find the variation of Φ from thus obtained $\partial\Phi / \partial t$. And then the cycle restarts with step (1°).

There are two possible numerical difficulties. One is with procedures (2°) and (5°) where we may have an instability of initial-value-problem type. When this occurs, the line of force (A = constant) usually becomes irregular like saw-toothed waves with a period of the order of the mesh size. This numerical instability can be averted by using the difference scheme of Friedrichs and Lax and by taking a time step carefully considered. In the actual computation we checked that the results do not vary much even when we used different time steps. The other is in the stage of (4°) where a relaxation method is used to solve the boundary-value problem. The convergence criterion of the relaxation was also carefully considered to guarantee the accuracy.

The parameters of computation are R_m, R, and U (maximum injection speed). We could not get around the numerical difficulties in cases of R_m and R smaller than a few hundreds. This seems to be because when R_m^{-1} and R^{-1} are large, the effect of smoothing out errors during the relaxation (4°) could not overcome the errors due to higher-order numerical differentiation involving the terms on the extreme right of Eqs. (5.7) and (5.8).

The physical quantities to be measured in the present numerical experiment are, for example, the position and displacement of each individual line of force, the instantaneous position of streamlines, the current density not only in the neighborhood of the neutral point but anywhere including the convection region, the distribution of the

induction electric field and so forth. The results of these observations will be presented in the next section and the implications and interpretations of these results will be compared in section 5 with the points mentioned in the Introduction.

§ 4. Numerical Results

The numerical diffusion involved in our difference scheme is virtually comparable with the other terms in the rhs of Eqs. (5.7) and (5.8) and as much as $10 - 10^2$ times larger than the actual resistive and viscous diffusions of the fluid. Hence, the magnetic field does not interact strongly with the flow and the calculated patterns of the magnetic field are found to be very diffusive. It is, however, revealed that the variables such as E_z and J_z or the vorticity ω_z which are given by differentiating A or Φ are sensitively dependent on R_m's and R's, although A and Φ, respectively, are scarcely different. Therefore, we can say that the numerical diffusion is moderate in the sense that it never screens, though it exerts a considerable influence upon, the essential features of the reconnection of magnetic lines of force.

All the results presented in this section are, unless otherwise specified, for U = 1, i.e., the peak value of the injection speed is one Alfvén Mach. This choice of U reflects the consideration that we want to keep the number of independent parameters as small as possible and that flow coming in even a smaller magnitude of U will eventually reach a region where U = 1 before approaching close to the neutral point.

Figures 25 (a) - (e) are the time-sequential behavior of magnetic lines of force for the case of $R_m = R = 5 \times 10^3$. The fluid is continually injected from the right bottom of the figure and ejected from the left top. Figure 25 (e) is a piece of tangible evidence of reconnected lines of force. Of course in (d) of the figure, a reconnected line of force should already have appeared, if a contour

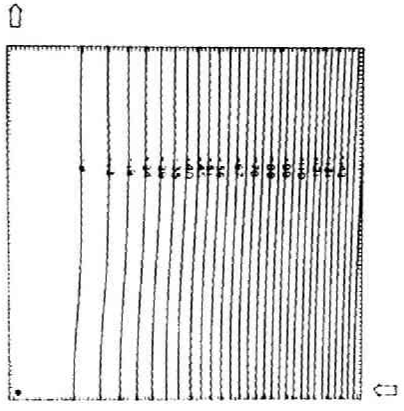

(a)

Fig. 25

Computer-drawn temporal behaviour of magnetic lines of force for the case $R_m = R = 5 \times 10^3$ and $U = 1$ at times $t = 10^{-2} - 6 \times 10^{-2}$. The neutral point is shown by a dot. Note that the length scale is reduced to half in the direction from top to bottm. The value of potential is shown on each line scaled by 10^3. Hereafter, unless otherwise specified, all the figures that will appear are for the same case.

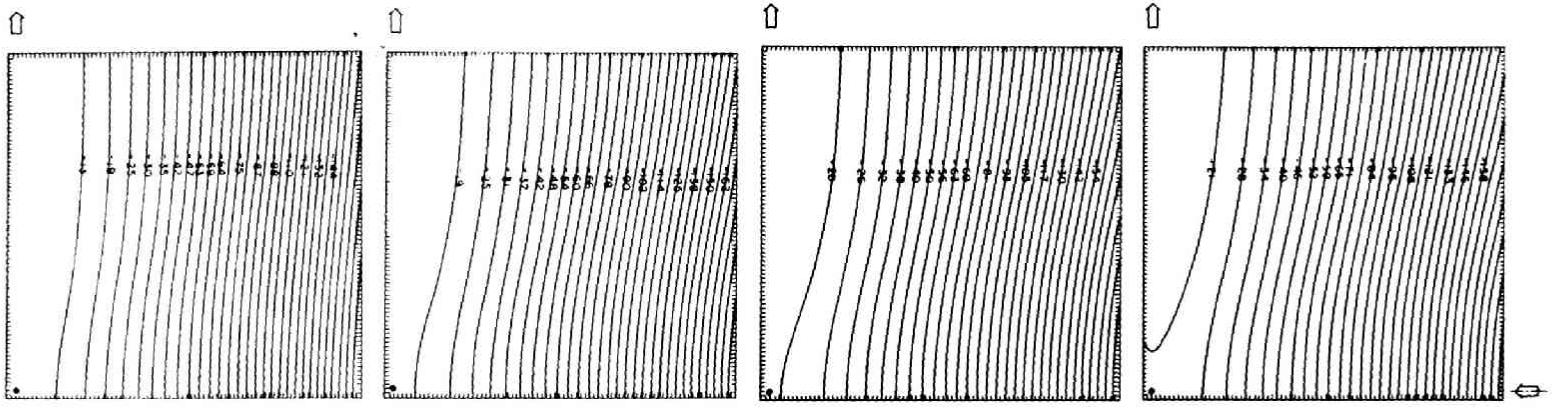

(b) (c) (d) (e)

interval somewhat smaller were used. We thus see that reconnection in fact takes place at the existing neutral point, immediately after a fluid is injected. There are two important features observed. One is that the front tip of the reconnected magnetic line of force does not become flattened as it zips back upward and that the bordering regions continue to maintain their thinness with time. The other feature is that, although the fluid injection is done virtually under a frozen-in condition (see Fig. 29 shown later), the ejection speed of the front tip is far faster than that of the fluid. This point will be discussed at length shortly.

In Fig. 26 the stream lines at two different times are shown as examples. We can readily see that the successive configurations of the flow are not altered much from the initial one, except that the greater time makes a slightly wider turn near the point of stagnation.

From Fig. 25 , it can be seen that the reconnection builds up immediately after the injection of fluid. To see this more quantitatively, it is interesting to plot B_x along the y axis at different times (B_x has been scaled by B_o, the magnetic field carried by the

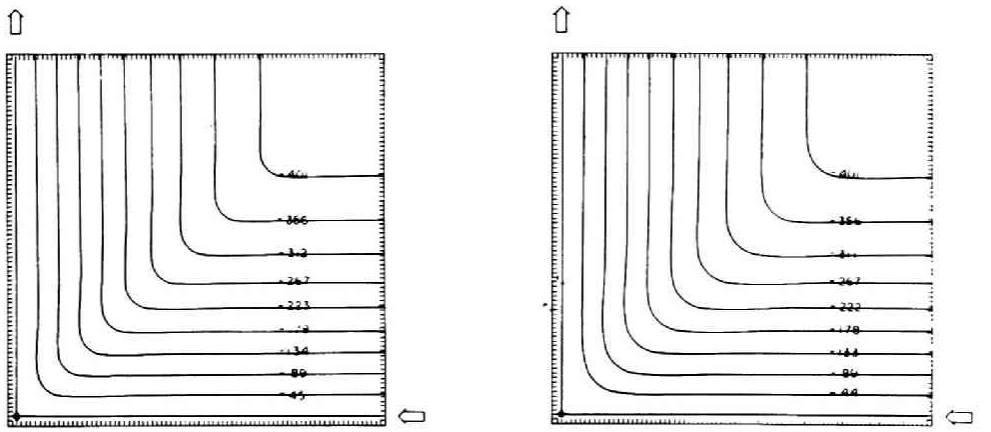

(a) (b)

Fig. 26 Computer-drawn streamlines at : (a) $t = 10^{-2}$ and (b) $t = 5 \times 10^{-2}$. The dot at the left bottom corner is the position of the neutral point.

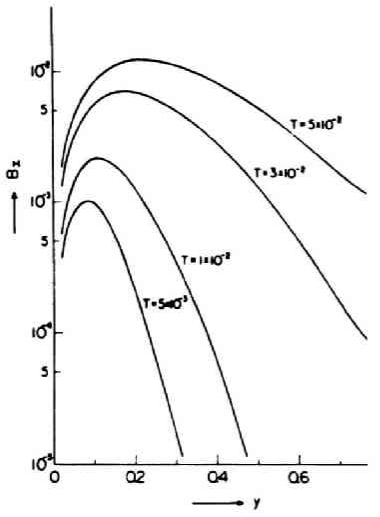

Fig. 27 B_x along the y axis plotted for different times.

incoming fluid). This is shown in Fig. 27 . Thus the transverse component of the magnetic field rapidly reaches as high as 10^{-2} in a matter of time 5×10^{-2}.

Since the magnetic field is frozen, although in fact partially in the fluid, it is convected to the inner region with the flow. We can see it in Fig. 28 (a) and more clearly in (b) where U = 5. The magnetic flux density is enhanced especially near the turning points of the stream lines, forming a sort of shock front, and then flattened far from the points. As already shown in the study of

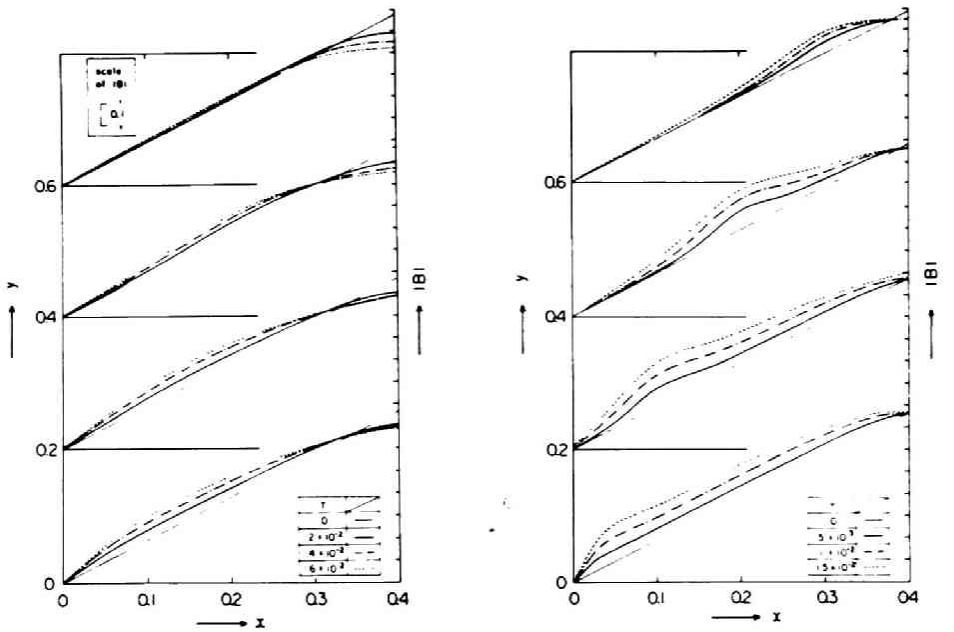

(a) (b)

Fig. 28 Variation of the magnetic flux density $|B|$ with time along the x axis and along a few lines parallel to it. The origin of $|B|$ is shifted by 6.0 for successive curves. (b) is for the same R_m and R, except U = 5.

the stationary-state solution, the variation of the magnetic field may be such that it is diffusive near the neutral point, enhanced considerably in the intermediate region where the shock waves are excited and then tends asymptotically to a constant. Comparing the magnetic lines of force between the cases of U = 1 and 5, it is readily seen that the more intensely a fluid is injected, the greater is the inward convection of the front tips. Therefore, the wedge angle, made by the asymptotes of the magnetic lines of force which go through the neutral point, seems to extend wider for larger U's.

Figure 29 shows the fluid velocity along the x and y axes. There is local acceleration in the vicinity of the neutral point, but away from the neutral point the inlet and exit velocities are respectively 1.0 and 2.0. The velocity field as a whole is little altered even after the intensity of the reconnected field reaches 10^{-2} ; the length ratio of 2 : 1 of the area we consider certainly restricts the global flow pattern. In the vicinity of the neutral point, the rate of decrease of the injection velocity is equal to that of increase of

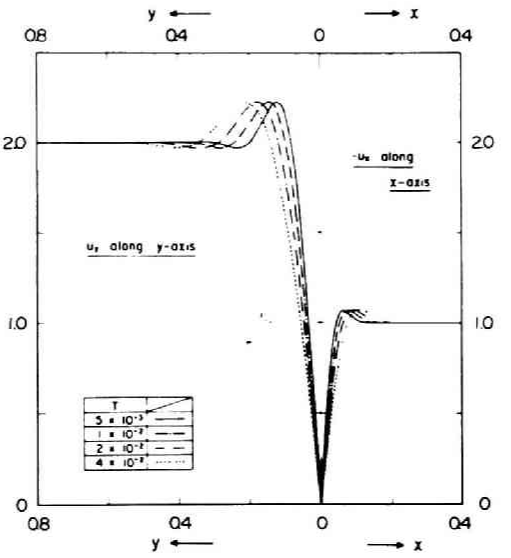

Fig. 29 $-u_x$ along the x axis and u_y along the y axis at times $t = 5 \times 10^{-3} - 4 \times 10^{-2}$.

the ejection velocity. This is the same as those known in the usual stagnation flows. One may also notice that the rates become reduced with time. This indicates that viscous diffusion is much more effective near the neutral point, the characteristic length of which is the instantaneous thickness $\delta \sim \sqrt{t/R}$.

We show the current density as measured by $-\nabla^2 A$ in Fig. 30 . The overall pattern makes little change with time, but the current accumulates in the vicinity of the neutral point. As expected, the current in the vicinity of the neutral point becomes stronger for larger R_m's and/or the larger U's.

Figures 31 (a) - (f) show the cross sections of the current density respectively along the x and y axes and along a few lines parallel to each axis. One finds that the core of current grows over the neutral point with a conspicuous gradient, especially in the direction

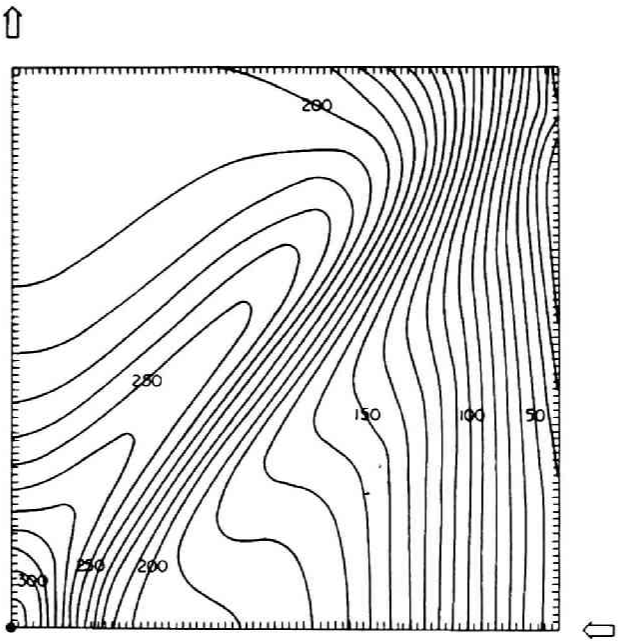

Fig. 30 Current density $J_z = -\nabla^2 A$ at $t = 3 \times 10^{-2}$. The dot at the left bottom corner is the position of the neutral point. Contours are shown for $-\nabla^2 A = 0.1 - 3.1$ with a contour interval of 0.1 scaled by 10^2.

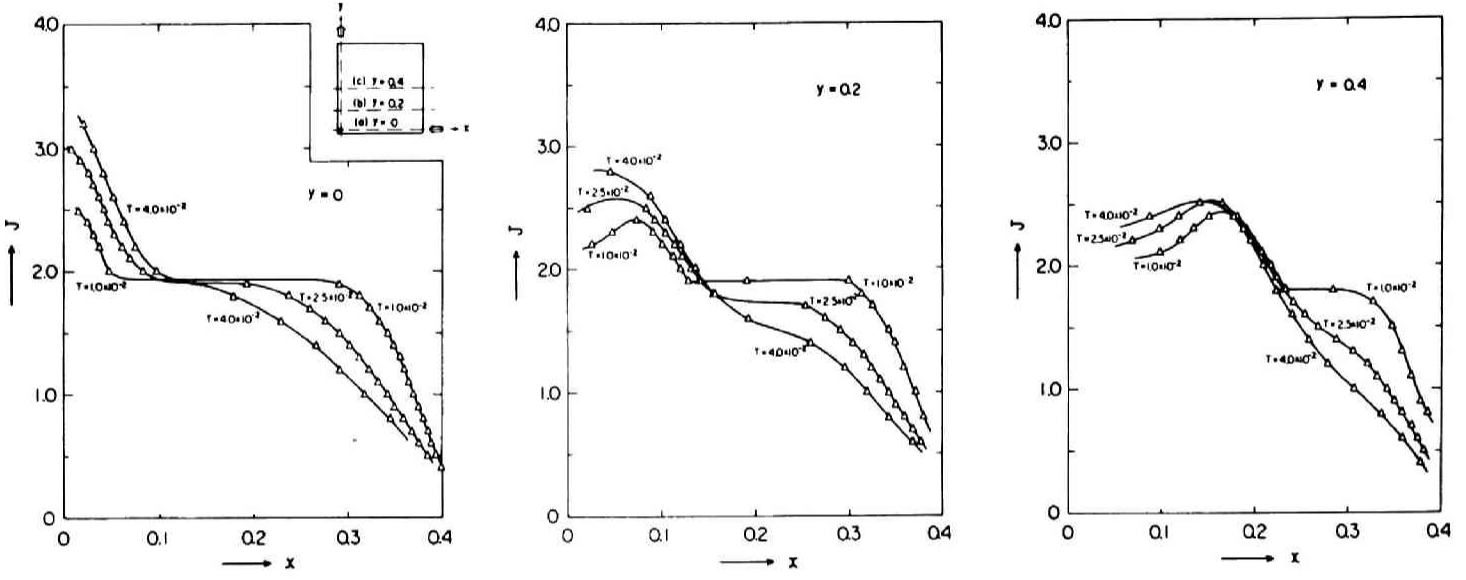

(a) (b) (c)

Fig. 31 Cross-sections of the current density plotted for different times along : (a) the x axis, (b) y = 0.2, (c) y = 0.4, (d) the y axis, (e) x = 0.2 and (f) x = 0.4. These were reproduced from contour maps such as those shown in Fig. 30.

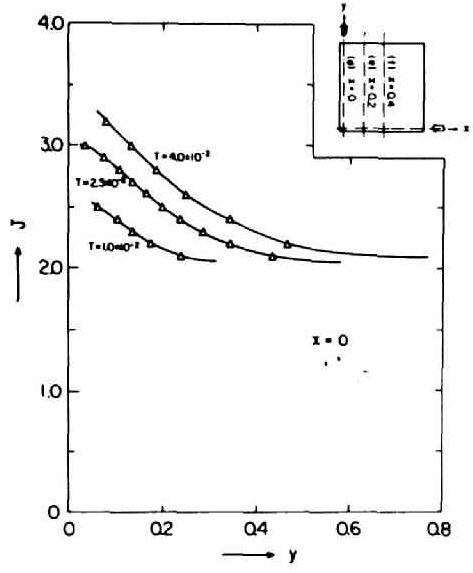
4.0
3.0
2.0
1.0
0
J
0
0.2
0.4
0.6
0.8
y
x = 0
T=4.0×10⁻²
T=2.5×10⁻²
T=1.0×10⁻²

(d)

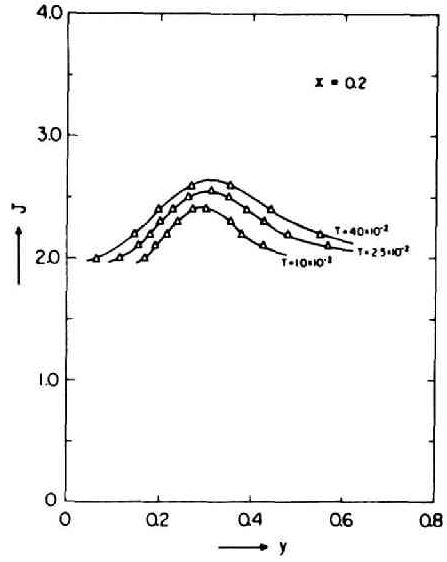
4.0
3.0
2.0
1.0
0
J
0
0.2
0.4
0.6
0.8
y
x = 0.2
T=4.0×10⁻²
T=2.5×10⁻²
T=1.0×10⁻²

(e)

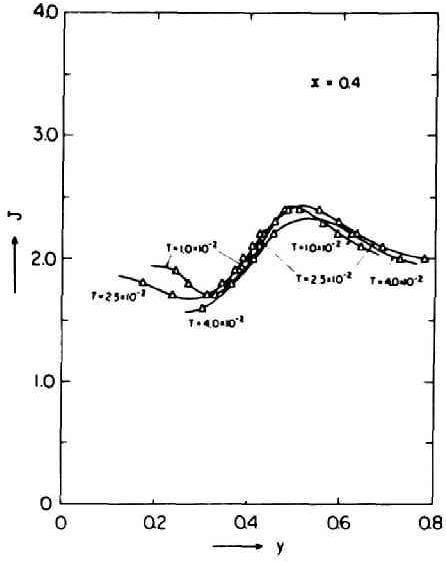
4.0
3.0
2.0
1.0
0
J
0
0.2
0.4
0.6
0.8
y
x = 0.4
T=1.0×10⁻²
T=2.5×10⁻²
T=4.0×10⁻²

(f)

of injection. The current also becomes intense along turning points of the flow, although the region spreads considerably. Similar features are also revealed for different R_m's and R's. We discussed in the analysis of the stationary-state solution that the intense current is concentrated in the vicinity of the neutral point, from which the transition layer of intense current extends outward ; it has been shown that this transition layer corresponds to Petschek's boundary layer and to the trailing wave of Sonnerup (1970). In the stationary-state reconnection, however, the negative current also flows along another transition layer (Sonnerup's leading wave), which stands contiguous to the positive-current layer. Concerning the current-core over the neutral point with the ridgelike extension along Petschek's boundary layer, the above figures suggest that it may eventually evolve into the one with sufficiently large amplitude. However, although the current is rapidly reduced in the inlet side, it is not clear whether the negative-current layer can really be formed or not.

Figures 32 (a) - (d) show the time-sequential variation of the electric field due to $\partial B / \partial t$ along the x and y axes and along a couple of lines parallel to the x axis. The injection of an Alfvénic flow induces the electric field at the boundary, as much as 0.7 for maximum velocity, which is transported to the inner region with a linearly-reduced intensity. A considerably large hump appears at the first instance and then becomes lowered with time, shifting its peak inside. As the reconnection proceeds, the electric field tends to be spatially uniform. Since the intensity of the magnetic field becomes uniform with time in the inlet side, we can say that the velocity of fluid there has a tendency to become uniform spatially. The rise and fall of the electric field coincides well with that of the current shown in Fig. 31 . Similar features are seen in the more conducting and/or less viscous fluid, where the increase or decrease are more rapid. Checking on the cases of different R_m's and R's, one finds that the time-sequential variations of the electric field at the neutral point are proportional to those of the current density as expected from Ohm's law.

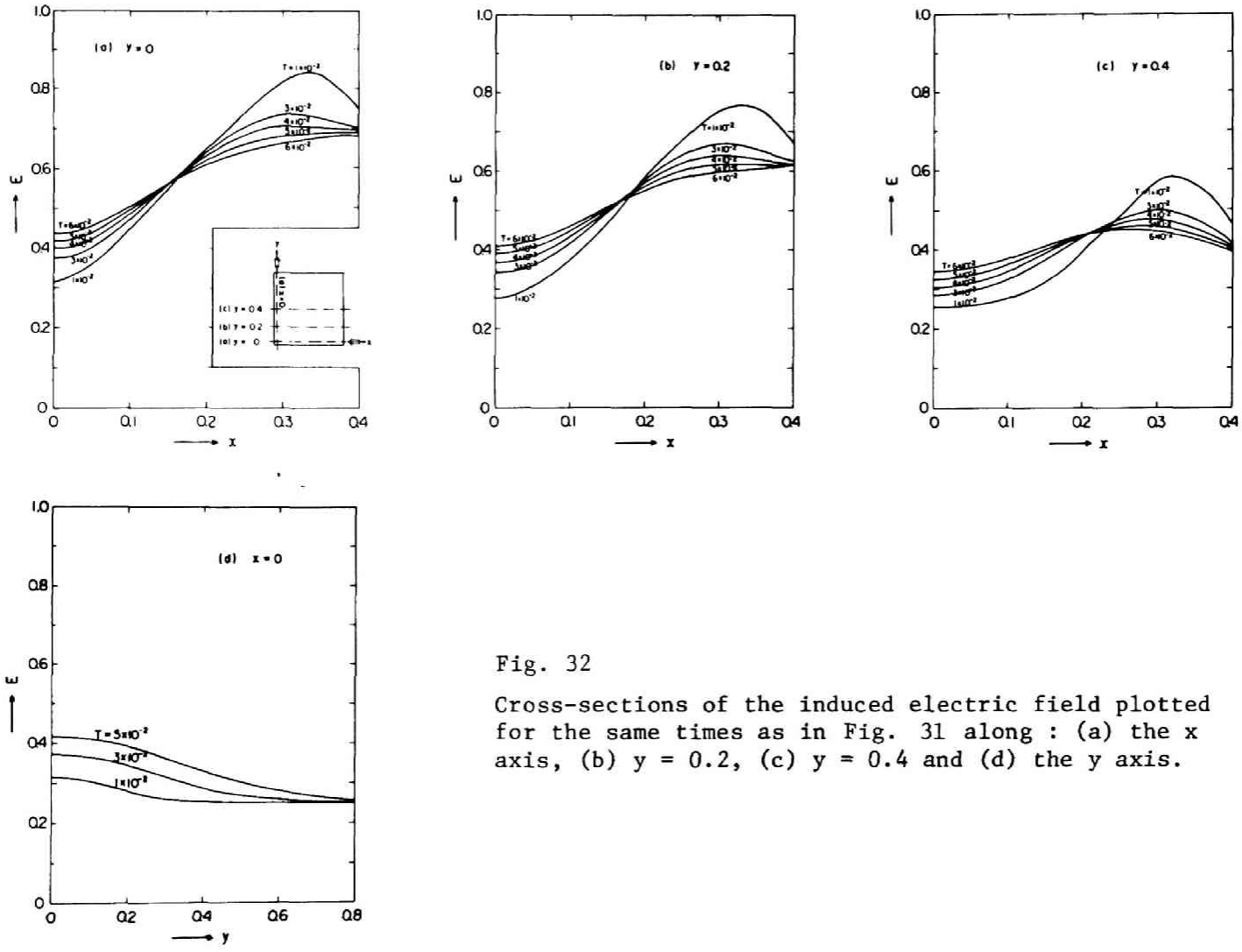

Fig. 32

Cross-sections of the induced electric field plotted for the same times as in Fig. 31 along : (a) the x axis, (b) y = 0.2, (c) y = 0.4 and (d) the y axis.

§ 5. Interpretation of the Results

We wish now to discuss those points of interest mentioned in the introduction.

5.1 Confirmation of reconnection

After extensive calculations over a range of Reynolds number, it is seen that reconnection can in fact take place. The results strongly suggest that reconnection can occur for any fluid with global Reynolds numbers $10^3 \leq R_m < \infty$, $10^3 \leq R < \infty$. Below these lower thresholds our numerical scheme fails for technical reasons already mentioned ; however, since there is reason to believe that at lower Reynolds numbers reconnection is more easily done, therefore our numerical experiment indicates that reconnection can be accomplished at any small or finitely large Reynolds numbers. This, together with the following statement on controlling conditions, seems to support the speculative conclusion put forward in chapter 4 that reconnection is not inhibited by the local condition at the neutral point, but rather the reconnection rate depends on the external conditions that set up the global flow pattern.

We may denote clearly that the magnetic lines of force would certainly grow to the X-type configuration through the reconnection in the region of existing neutral points. The bend or curvature of each line of force is expressed by the distance $\Delta\ell$ of its front tip on the x axis, measured from its x coordinate on the exit boundary (see Fig. 33) . This figure shows the time-sequential $\Delta\ell$'s of all lines of force that appeared in computer-drawn figures such as Fig. 25 . This might also be considered to indicate that the velocity of lines of force on the x axis differs from that on the exit boundary. The magnetic field imposed initially in a direction parallel to the existing neutral line (x = 0) tends to decline steeper with respect to the neutral point as the reconnection proceeds. It is especially steep

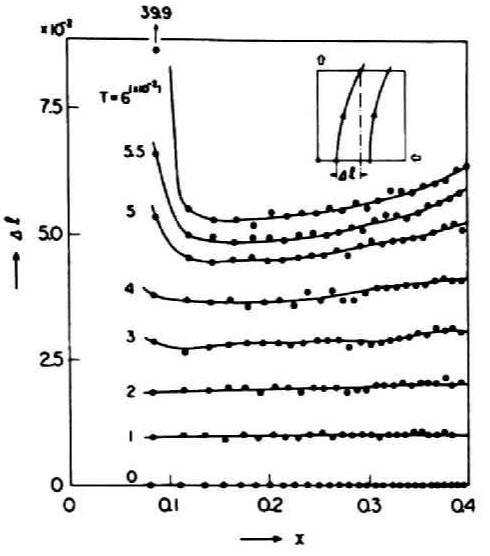

Fig. 33 Bend or curvature of each magnetic line of force plotted for different times.

far from the neutral point. Even at time $t = 6.0 \times 10^{-2}$, $\Delta\ell$'s still increase almost linearly and the stationary state might not be attained shortly. It is, however, quite probable that the magnetic field forms an X-type configuration, ultimately extending over the angle corresponding to the injection velocity as shown in the analysis of the stationary-state solution.

We add a few comments concerning the behavior of a line of force in the vicinity of the neutral point. The advance of the front tip is conspicuous there and its speed is remarkably enhanced just before and after the line of force becomes reconnected. This may be referred to the slippage of magnetic lines of force from the fluid, the velocity of which is given by (see Eq. (1.11))

$$w = \frac{1}{R_m} \frac{B \times (\nabla \times B)}{B^2} \quad . \tag{5.12}$$

Since we suppose the conductivity to be uniform in the whole region,

the enhancement of the slippage velocity should be referred to the local enhancement of the magnetic body force acting on the fluid there (see Fig. 29). There are, however, some grounds to expect that the enhancement of the slippage velocity might actually be more remarkable. We should note the fact that, as the reconnection proceeds, the current grows rapidly in the vicinity of the neutral point, forming a marked current-core with a steep shear or gradient. The computed current, of course, was found to be so diffusive, but if the numerical scheme were more appropriate, the enhancement of currents might be appreciable. We pointed out before that in the stationary state the large current shear is really formed in the vicinity of the neutral point and that its effect is comparable with the other terms in the Ohm's law. Therefore, it is probable, in an appropriate circumstances, that the shear of currents may eventually evolve into the sufficiently large one in the vicinity of the neutral point and contribute to reduce effectively the electrical conductivity in the manner mentioned in chapter 4. The reduced conductivity also enhances the slippage velocity.

5.2 Speed of growth

From the preceding discussions, reconnection of magnetic lines of force at the existing neutral points or lines follows immediately after a flow, or a perturbation, sets up. The reconnection will, perhaps, be delayed in about the sound wave propagation time in a compressible fluid, although it may not differ essentially from that of an incompressible fluid. We observe that, as the reconnection proceeds, the transverse component of the magnetic field rapidly increases as high as 10^{-2}, and that the wedge angle extending in the exit side becomes wider in a matter of time 5×10^{-2}. In the analysis of the stationary-state solution, the transverse component becomes about 10^{-1}, or more corresponding to the velocity of incoming fluid. It will, therefore, require a time of a few τ_A's, before the full configuration of the

X-type magnetic field builds up, although the buildup is faster for a greater speed of fluid injection.

5.3 Controlling conditions

As stated in a preceding paragraph, the process of reconnection does not seem controlled by the local conditions such as electrical conductivity or viscosity. On the other hand, this process is controlled by the external conditions of the area under consideration. According to our numerical experiment, the buildup of reconnection is considerably dependent on the typical speed of injection U ; the larger U is, the buildup is the faster. The other important factor is the shape of the boundaries, i.e., the widths of the inlet and exit of fluids away from the location of the neutral point. In other words, it may be said that the distribution of pressure gradients near the boundaries that set up the global flow in the domain is important in determining the flow pattern, rather than the dissipation mechanisms near the neutral point.

5.4 Acceleration of particles

There are two types of particle acceleration in connection with the reconnection of magnetic lines of force. The first is the acceleration of fluid in bulk, which occurs as follows. The fluid comes in with a slow velocity and a high magnetic field in a wide wedge angle as viewed from the neutral point. The fluid turns round at the neutral point forming a narrower wedge angle, with a weaker magnetic field but with a faster fluid velocity. The increase of the kinetic energy comes from the dissipation of magnetic energy by the propagation of Alfvén waves in the incompressible case and switchoff shocks in the compressible case. Thus, the angle made by the asymptotes of the X-type

magnetic lines of force is essential in determining the degree of fluid acceleration. When the fluid is injected at a high rate, the wedge angle, in which the fluid is ejected, becomes wider. This illustrates the fact suggested by the stationary-state solutions in the preceding chapter. It was also shown by the stationary-state solutions that the ejection velocity is always constant, independently of the external conditions on the flow. However, we cannot make it clear by the present computer experiment because of the weak-coupling between the magnetic field and the flow due to a resistive diffusion introduced artificially. In the absence of this artificial diffusion, the flow may be strongly restricted by the magnetic field and ejection velocity may be altered to some extent, although it is not clear whether it coincides with that of the stationary-state solution. However, it is the first essential to this type of acceleration that the X-type configuration of the magnetic field can really be set up in the region where there have been no flows before and that it extends, at least, over a characteristic Alfvén wavelength. The rate of acceleration is, in this sense, considered to be infinitely large. However, we can raise three questions concerning this process. First, as already mentioned, the X-type configuration of the magnetic field must extend over a considerably large region. If the scale of the system is large enough in favorable circumstances, the acceleration will efficiently yield high energy particles as observed in space, while if the system is smaller than the characteristic Alfvén wavelength, the increase of fluid kinetic energy will be soon spread over areas many times larger than the size of the reconnection region. The second question is, as suggested by Yeh and Axford (1970), that the fluid accelerated in this manner must escape from the system, otherwise the energy will again be converted to the energy of the magnetic field and then it will merely oscillate. The third question, closely related to the first, is concerned with the limitations of the stationary-state solutions. If the whole configuration of magnetic lines of force is more or less controlled by the flow external to the

neutral point, then of course the evolution of reconnection itself must be influenced by the external flow. This suggests that a stationary-state solution that *does not* depend on various external conditions may be an isolated state that the actual evolving system may not reach. The present study is unsatisfactory in clarifying these points, but it can be said at any rate that this is the very promising type of acceleration that efficiently yields high-energy particles as observed in solar flares and in the geomagnetic tail.

The other type of acceleration is the heating of particles by Joule dissipation due to an electric field induced by changing magnetic field. The current seems to be concentrated near the neutral point, forming an intense current-core in its vicinity ; elsewhere the current density is much less because there the induction electric field is cancelled by the fluid motion. The Ohmic energy dissipation is given by

$$J \cdot E = J_z E_z = \frac{1}{\mu} \nabla^2 A \cdot E_z \qquad (5.13)$$

before normalization of the variables and this quantity becomes, after our scaling,

$$\frac{B_o^2}{2\mu} \cdot \frac{1}{\tau_A} [\ \nabla^2 A \cdot E_z\ ] , \qquad (5.14)$$

where $B_o^2 / 2\mu$ is the magnetic energy density of the incoming fluid ; quantities enclosed by the square brackets are those after normalization that can be known from Figs. 31 and 32 . They show $[\ \nabla^2 A \cdot E\ ] \sim 1$ at times $10^{-2} - 5 \times 10^{-2}$ for $R_m = R = 5 \times 10^3$ and at earlier times in less viscous and/or more conducting fluids. This indicates that the magnetic energy injected is dissipated locally at the neutral point. Since the disappearance of magnetic flux through resistive diffusion does not in itself impart momentum to the system, the energy dissipated must appear as heat (Stevenson, 1971 ; 1972).

In less dissipative fluids the region of enhanced currents is reduced in extent around the neutral point. This is, of course, an efficient way of heating particles where the electric field due to the rapidly changing magnetic field plays the essential role, but seems inferior to the other type of acceleration in bulk in view of the extent of the region available for the acceleration.

5.5 Diffusion region vs convection region

The region for the magnetic field to be frozen in the fluid is not so apparent, since the magnetic field interacts weakly with the flow due to the numerical diffusion. Notably in Fig. 25 , the velocity of zipping back the front tip of reconnected lines of force can be estimated. This velocity is about 40, whereas the background fluid has velocity of about 2, so that the lines of force zip back at a speed 20 times faster than the fluid. The front tip of the lines of force, moreover, maintains its small radius of curvature while contracting toward the exit side. These features are probable evidence for the magnetic lines of force being transported very diffusively. We have, however, mentioned before that the slippage velocity increases rapidly in the vicinity of the neutral point, and that the region should be separated from the less resistive region far from the neutral point. The diffusive region in the vicinity of the neutral point coincides well with the region of intense current where the current increases with time and also with the stagnation region of the flow. This might indicate that even in very highly conducting fluids the magnetic lines of force are dissipated locally by the resistivity which is naturally induced by the inertia of current in the vicinity of the neutral point and that the so-called diffusion region may be formed with time. The extent of the diffusion region is not, however, well defined, although it may be more or less similar to those of Petschek (1964) and others insofar as the shape of the

diffusion region is concerned. The above discussion suggests that in an actual, very highly conducting fluid the front tip of a reconnected line of force will become flattened with time as the effect of diffusion diminishes away from the neutral point.

§ 6. Concluding Remarks

We have numerically obtained time-dependent incompressible MHD solutions in two dimensions to study the evolutionary process involving a reconnection of magnetic lines of force. Given an initial antiparallel magnetic field, or a current sheet, to which there is an injection of fluid in a transverse direction, we saw how the process of reconnection builds up. In this numerical experiment, special considerations were given to the confirmation of reconnection, the formation of X-type magnetic field, the speed of growth, conditions that control the evolution, acceleration of particles, the structure of the diffusion region and so forth. The findings are : magnetic lines of force can reconnect and grow to the X-type configuration in fluids of any finitely large hydromagnetic and hydrodynamic Reynolds numbers ; the conditions local to the neutral point are less important than the external conditions that set up global flow patterns ; acceleration of fluid in bulk concerns whether the X-type configuration grows to the comparably large extent or not ; and the electric field at the neutral point due to the rapidly changing magnetic field is less efficient to accelerate charged particles.

Chapter 6

DISCUSSION AND CONCLUSIONS

§ 1. Comparison with Relevant Laboratory Experiments

We have mentioned that laboratory plasmas containing X-type magnetic neutral points have been studied by some workers (e.g., Bratenahl and Yeates, 1970 ; Syrovatsky et al., 1972 ; Ohyabu and Kawashima, 1972), but as yet we have few pieces of experimental evidence to compare with our numerical computation. The only material to be compared is the magnetic field or associated current distribution near the neutral point and the transition layers observed with a laboratory device known as the double inverse pinch (Bratenahl and Yeates, 1970). In the double inverse pinch shown schematically in Fig. 34(a) , dual currents are supplied to two rods by charged capacitor banks and the current returns to ground through the pre-ionized plasma. Initially the return current paths are cylindrical about both rods as shown in Fig. 34(b) . However, the $J \times B$ force requires each cylindrical current sheet to move outward, carrying plasmas as they move. After 3 microseconds, the inverse pinches meet and reconnection begins. Figure 34(c) is a resultant pattern of magnetic lines of force, in which an X-type neutral point has been established. During the reconnection which follows, lines are carried in from regions 1 and 2, reconnect at the neutral point and merge as a line in region 3. Although there is an important difference between the field topology considered by our computation in chapter 5 and the one

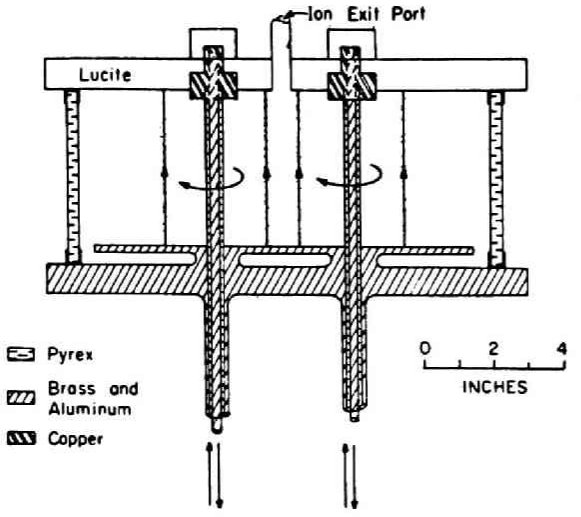

(a)

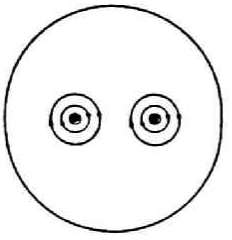

(b)

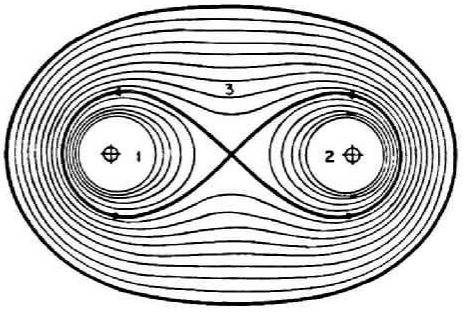

(c)

Fig. 34 (a) Schematic side view of the double inverse pinch device. Straight arrows : current flow ; curved arrows : magnetic field ; stipple : luminosity ; energy source : two 150 μF capacitor banks, 20 kV Max. (b) Top view and initial inverse pinch waves. (c) Top view of the magnetic lines of force. The dark line is the separatrix which divides the flux into three regions. Region 3 is accessible from regions 1 and 2 by reconnection at the origin.

considered here, it is common to both of the two that a pair of magnetic fluxes are injected from outside. The double inverse pinch is distinguished from the other experiments in that the induced electric field developes self-consistently from the plasma flow, while the electric field must be applied in the other experiments. As noted in the general introduction, the actual reconnection process is always accompanied by the induced electric field.

Figure 35 (a) shows contours of constant current density J_z observed by the double inverse pinch (Bratenahl and Yeates, 1970). The contours of constant density show a maximum at the X-type neutral point with ridgelike extensions running out along lines just downstream of the separatrix. The upstream side of this distribution has sharp gradients and the downstream side, gradients which are comparably gentle, resulting in a very strong concentration of current in the pinch and the associated ridgelike extensions.

These features bear remarkable resemblance to our computational results where the simulation was made of an evolution of the X-type magnetic neutral point (Baum, private communication, 1973). Note the similarity of the constant density contours of Bratenahl and Yeates to that of our computation shown in Fig. 35 (b) (redrawn from Fig. 30).

It is worthy of notice that slow mode shocks actually exist along the separatrices (Bratenahl and Yeates, 1970), and that plasmas are observed to be ejected from the downstream sides of the neutral point region, with the local magnetic Mach number which is nearly independent of the plasma conductivity and the passage of time (Baum and Bratenahl, 1973a).

§ 2. Effective Electrical Conductivity in the Diffusion Region

In a stationary-state analysis, it is necessary to attain a high rate of reconnection that the electrical conductivity is reduced

Fig. 35 Contours of constant current density J_z : (a) Experimental result with the double inverse pinch (redrawn from Fig.4 of Bratenahl and Yeates, 1970) and (b) our computer calculation (redrawn from Fig. 30).

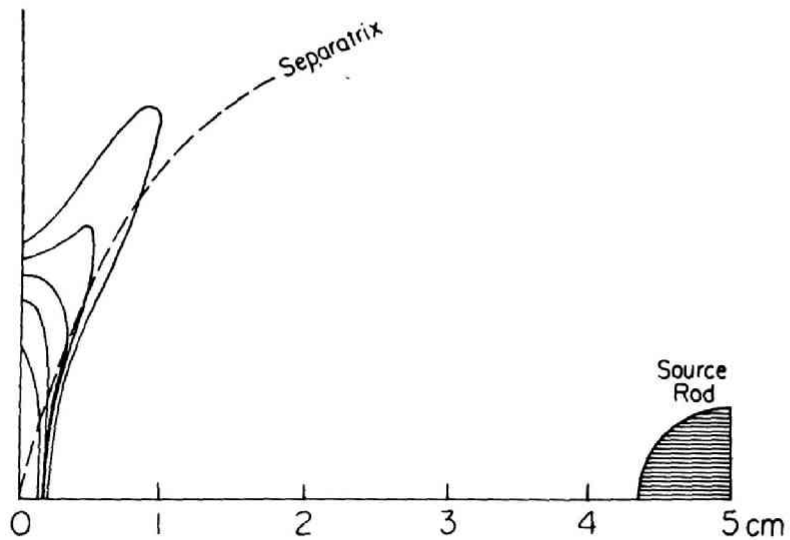

(a)

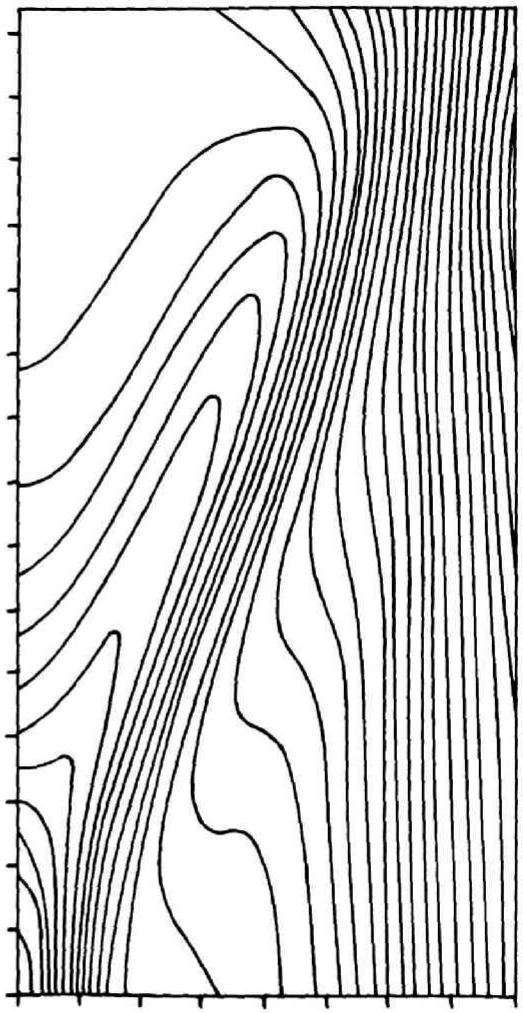

(b)

selectively in the vicinity of the neutral point. It is not allowed for the reduction mechanisms to disturb much the surrounding field and flow. We argued that, in the absence of particle-particle collisions or wave-particle interactions, inertia of a particle is responsible for reducing the conductivity. In this case the lifetime of a particle in the system replaces the collisional mean free time in the expression for the conductivity. The inertial conductivities may be efficient in space, especially in the current sheet in the geomagnetic tail where they are about 8 - 11 orders of magnitude smaller than the collisional conductivity (Speiser, 1970). Dungey and Speiser (1969) showed that two stream instability exerts only a small influence on the effective conductivity.

This is not to say that small-scale instabilities are not important or that there are no wave-particle interactions in the current sheet. In fact, there may be small-scale effects which enhance the dissipation. For instance, Jaggi (1963) has pointed out that the steep field gradient across the diffusion region produces small-scale resistive instabilities (see, e.g., Furth et al., 1963 ; Coppi and Friedland, 1971 ; Schindler and Soop, 1968 ; Biskamp and Schindler, 1971) which effectively reduce the local size of the diffusion region and greatly enhance the effective dissipation. If the current sheet becomes so concentrated that the drift velocity exceeds the electron thermal velocity, the Alfvén-Carlqvist instability (Alfvén and Carlqvist, 1967 ; Carlqvist, 1969) and two-stream instability (Stringer, 1964 ; Buneman, 1959) arise, enormously increasing the effective resistivity and the diffusion of the fields (Hamberger and Jancarik, 1972).

Concentration of current into thin sheets has been verified also by laboratory experiments (Bratenahl and Yeates, 1970 ; Nardi, 1970), and Baum and Bratenahl (1973c) actually observed the ion-acoustic-wave spectrum of Kadomtsev (1965) at the X-type magnetic neutral point.

Parker (1973a), on the other hand, points out that the fluid between the opposing antiparallel fields perhaps escapes via the

interchange and kink instabilities, permitting rapid close approach of the fields, with or without small-scale instabilities.

As yet, we can neither say quantitatively which mechanism plays a dominant role in actual astrophysical and geophysical phenomena, nor answer, in a convincing manner, even to the question whether the anomalous dissipation is the direct cause or an outcome of the reconnection process. It remains unsolved as a three dimensional problem in which magnetohydrodynamic aspect of the convection region should be simultaneously studied with the particle aspect of the diffusion region.

§ 3. Complementary Remarks to Particle Acceleration

As already mentioned, conducting fluid is always ejected at a velocity several times greater than the injection velocity, regardless of the magnitude of the injection velocity. This may successfully describe the ejection of plasma during the explosive phase, which accounts for the dominant part of energy emitted by a solar flare.

In highly conducting fluids, heating of particles by Joule dissipation seems inefficient in view of the extent of the region available for the acceleration. However, the electric field induced by the rapidly changing magnetic field works, in the vicinity of the neutral point, for the acceleration of ions to very high energies such as those observed following intense solar flare activity.

The particle orbit in the current sheet can be classified into two types (Speiser, 1965 ; Hoh, 1966). In one type the ion does not cross the neutral plane. It gyrates and drifts in the magnetic field. The second type of orbit is one in which the ion crosses the neutral plane and moves in a " serpentine " path. It is the ions having the second kind of orbit that will be accelerated by the electric field. Friedman (1969) has shown that ions can gain high energies in the Petschek's model of the magnetic field, and that

energy distributions similar to those observed can be obtained. He has also shown in a qualitative way that plasma turbulence prevents electrons from gaining high energy, consistent with cosmic-ray observations.

This mechanism of acceleration can be classified as Fermi-type acceleration, since an ion gains energy in the event of " collisions " between two moving magnetized plasmas. In the Fermi mechanism, however, it is necessary for an ion to gain an energy of, for instance, 10 GeV, that the plasma between these moving regions is compressed 10^5 times, which seems unreasonable. Using reconnection model, it can be seen that difficulties of this sort are avoided by allowing the plasma to escape from the region of acceleration.

§ 4. Concluding Remarks

We have been concerned with a theoretical investigation on the reconnection of magnetic lines of force with a view to applying it to the acceleration of solar and terrestirial plasmas.

In chapter 1, we first discussed a concept and kinematics of magnetic lines of force. Then, a pair of antiparallel magnetic lines of force were schematically shown to be broken off and reconnected with each other at a magnetic neutral point. Then we mentioned that the reconnection of magnetic lines of force is considered as of major importance in : acceleration and heating of plasmas due to the annihilation of magnetic energy and quasi-stationary penetration of an electric field parallel to a plane at rest. Finally, we referred to some astrophysical and geophysical phenomena, especially to those of the earth's magnetosphere and solar flares, in which the reconnection process is likely to play a crucial role.

Chapter 2 was devoted to the classification of magnetic neutral points in an infinitely conducting fluid. The so-called X- and O-type magnetic fields as well as the one with a magnetic neutral

line were classified appropriately. The possible existence of some other types of neutral points, e.g., spiral and node types, was pointed out for the first time. Then, the volume force acting on the fluid was described by the similar topological analysis. Finally, we discussed, though in a very qualitative manner, an evolutionary process which may account for the higher rates of energy conversion than those expected in X-type neutral points.

Chapter 3 concerned with a critical survey of current models for the stationary-state reconnection at an X-type neutral point, examining whether the reconnection rate of each model might be large enough for the explosive phase of largest solar flares. There have been two opposing points of view concerning what determines the rate of reconnection. One is that the rate is essentially dependent on the effective electrical conductivity near the X-type neutral point, while the other is that it is likely to be determined by conditions far from the neutral point where reconnection actually takes place. They regarded the anomalous resistivity in the vicinity of the neutral point, respectively, as the direct cause of a reconnection process and as an outcome of the process. These views said it possible to account for the time and energy of the explosive phase, however, we cannot approve of their results, since they could not completely succeed in the matching of the solutions which were investigated separately in the diffusion region and in the convection region.

Therefore, in chapter 4, we studied numerically the magnetic field and flow with an X-type neutral point in a finitely conducting fluid which has no such a clear-cut distinction between the two regions. Although the Reynolds numbers used are much smaller than the actual ones, the resulting solutions exhibit that the magnetic field and flow make a smooth transition in their properties from the diffusive in the vicinity of the neutral point to the convective far from it. The electric currents are concentrated in the vicinity of the neutral point and along the transition layers. The magnetic field is regarded as almost frozen in the fluid in other current-free

regions, even in the case of moderate conductivities. The current-core over the neutral point is accompanied by a remarkable shear of currents, which may contribute to reducing the local electrical conductivity effectively. The reduction may be more remarkable as the conductivity is larger. Thus the reconnection of magnetic lines of force may be possible even in very highly conducting fluids. It has also been shown that the overall features are not essentially influenced by dissipations due to finite electrical conductivity or viscosity, but definitely by external conditions such as the applied electric field in the magnetic field and flow.

Chapter 5 was given to the numerical study of time-dependent incompressible MHD solutions in two dimensions which describe the evolutionary process involving a reconnection of magnetic lines of force. Given an initial antiparallel magnetic field, or a current sheet, to which there is an injection of fluid in a transverse direction, we sought to see how the process of reconnection builds up. In this numerical experiment, special considerations were given to the confirmation of reconnection, the formation of X-type magnetic field, the speed of growth, conditions that control the evolution, acceleration of particles, the structure of the diffusion region and so forth. The calculated contour of constant current density showed the good similarity to that of the laboratory experiment with the double inverse pinch. The findings are : Magnetic lines of force can reconnect and grow to the X-type configuration in fluids of any finitely large hydromagnetic and hydrodynamic Reynolds numbers ; the conditions local to the neutral point are less important than the boundary conditions that set up global flow patterns ; acceleration of fluid in bulk only concerns whether the X-type configuration grows to the comparably large extent or not ; the electric field at the neutral point due to the rapidly changing magnetic field is less efficient in accelerating charged particles.

Finally, the correct picture for a complicated phenomenon such as the reconnection problem can be obtained only through a balanced

interplay between observational evidence and physical insight with mathematical reasoning based upon acceptable and tractable model. In this context, the computer calculations and the laboratory experiments will be the promising girders of the bridge spanned between the distant banks, or between the observational evidence in actual space and the purely physical insight.

Appendices

A. Method of computation

In Fig. 15 the origin is the null point in the magnetic field, as well as the stagnation point of the flow. The rectangular domain enclosed by thick lines is 0.70×0.35 in size and is replaced by 70×70 rectangular cells for computations. The length ratio of two sides of the cell is, therefore, such that $\Delta x / \Delta y = 1 / 2$. Though there are several kinds of difference schemes for a differential equation, we will use the most familiar form, such as

$$\left(\frac{\partial \Phi}{\partial x}\right)_{i,j} = \frac{1}{2\Delta x} \left(\Phi_{i+1,j} - \Phi_{i-1,j} \right) , \qquad (A.1)$$

where $\Phi_{i,j}$ indicates the approximation to the value of Φ at the cell point $(i\Delta x, j\Delta y)$. The central difference form is adopted for second-order differential coefficients, and $\left(\frac{\partial^2 \Phi}{\partial x^2}\right)_{i,j}$ is given by e.g.

$$\left(\frac{\partial^2 \Phi}{\partial x^2}\right)_{i,-j} = \frac{1}{(\Delta x)^2} \left(\Phi_{i+1,j} - 2\Phi_{i,j} + \Phi_{i-1,j} \right) . \qquad (A.2)$$

The fourth-order differential coefficient at some point is therefore approximated by the value there and those at the nearest four points, two each in the left and right cells (or in the upper and lower). So we need two outermost rectangular cells, and we have 74×74 cells in all (as is shown in Fig. 15). The values at points outside the axes are determined by symmetry conditions such that

$$\Phi_{-i,j} = -\Phi_{i,j} , \quad A_{-i,j} = A_{i,j} \quad (i = 1, 2) \qquad (A.3a)$$

for the y-axis, and

$$\Phi_{i,-j} = -\Phi_{i,j} \ , \quad A_{i,-j} = A_{i,j} \qquad (j = 1, 2) \tag{A.3b}$$

for the x-axis. On the other hand, values at the cell points outside the other two boundaries (where conducting fluid as well as magnetic lines of force are either injected or ejected) are extrapolated in terms of a third-order algebraic expression satisfied by the four nearest points inside, such that

$$\Phi_{i,j} = 4\Phi_{i,j-1} - 6\Phi_{i,j-2} + 4\Phi_{i,j-3} - \Phi_{i,j-4}$$
$$(i = 0,\ldots,69 \ ; \ j = 70, 71). \tag{A.4}$$

It is the same for $\Phi_{i,j}$'s (i = 70, 71 ; j = 0,.....,69)*. These two non-axis boundaries are for computational purposes, and are rather lacking in physical reality. One should note, however, that the computed results approximately satisfy the condition $E + v \times B = 0$ throughout the domain of these artificial boundaries.

When we assign suitable values to each cell point as a starting approximation, we can solve the simultaneous difference equations approximating the differential equations (4.25) and (4.26) by the over-relaxation method. If the starting approximation is appropriate, it will converge very rapidly to the exact solution, though principally it will be reached from any starting approximations in the case that the equations have a unique solution.

Sonnerup (1970) and Yeh and Axford (1970) observed that in the ideal hydromagnetic fluid (perfectly conducting and inviscid fluid free from thermal conduction) there are two rotational discontinuities dividing the domain into three regions each of which contains a

---

* The extrapolation was not complete, and it sometimes impeded the calculation, especially near the inlet and exit boundaries. To suppress unphysical irregularities, we carried out a sort of smoothing for values of A and Φ near the boundaries, and connected them smoothly to those of the outer regions.

uniform flow and magnetic field when the hydrodynamic pressure is uniform. There are jumps in neither mass density nor mass flow ; thermodynamical quantities are continuous across them, and the magnetic field rotates around their normal directions without changing its magnitude. The tangential component of the fluid velocity is changed according to the discontinuity of the magnitude of the magnetic field. As shown in Figs. 16 (a) and (b), the potential functions of the magnetic field and flow in regions 2 and 3, and the wedge angle between the two discontinuities are determined by virtue of the boundary conditions in terms of the Alfvén Mach number M of the incident flow in region 1. Here M is equal to E / B (normalized) and then identical with E (normalized) in region 1. The potential functions for each region, which are only another transformed expression of Sonnerup's solution, are

$$\left.\begin{aligned} \Phi &= -My \\ A &= -x \end{aligned}\right\} \quad \text{for } y \le \frac{1}{M}\,x \quad (\text{ region 1 }), \tag{A.5}$$

$$\left.\begin{aligned} \Phi &= -\frac{M}{2+\sqrt{2}}\,y - \frac{1}{\sqrt{2}}\,x \\ A &= \frac{M}{\sqrt{2}}\left(y - \frac{1+\sqrt{2}}{M}\,x \right) \end{aligned}\right\} \quad \text{for } \frac{1}{M}\,x < y \le \frac{1+\sqrt{2}}{M}\,x \quad (\text{ region 2-1 }) \tag{A.6}$$

$$\left.\begin{aligned} \Phi &= -\frac{M}{2+\sqrt{2}}\,y - \frac{1}{\sqrt{2}}\,x \\ A &= \frac{M}{(\,1+\sqrt{2}\,)(\,2-\sqrt{2}\,)}\left(y - \frac{1+\sqrt{2}}{M}\,x \right) \end{aligned}\right\}$$

$$\text{for } \frac{1+\sqrt{2}}{M}\,x < y \le \frac{(\,1+\sqrt{2}\,)^2}{M}\,x \quad (\text{ region 2-2 }), \tag{A.7}$$

$$\left.\begin{aligned} \Phi &= -(1+\sqrt{2})x \\ A &= \frac{M}{1+\sqrt{2}}\, y \end{aligned}\right\} \quad \text{for } y > \frac{(1+\sqrt{2})^2}{M}\, x \quad \text{(region 3)} . \tag{A.8}$$

Figures 16 (a) and (b) show, respectively, the magnetic lines of force and stream lines in the case of M = 0.5.

We adopt Sonnerup's solution as the starting approximation, then solve the simultaneous equations (4.25) and (4.26) by the over-relaxation method. We define two parameters

$$s1 = \frac{1}{K^2} \sum_{i,j}^{k} \left| \frac{A_{i,j}^{m+1} - A_{i,j}^{m}}{A_{i,j}^{m}} \right| , \tag{A.9a}$$

and

$$s2 = \frac{1}{K^2} \sum_{i,j}^{k} \left| \frac{\Phi_{i,j}^{m+1} - \Phi_{i,j}^{m}}{\Phi_{i,j}^{m}} \right| , \tag{A.9b}$$

where K is the total number of cells in a column (or row) of the rectangular cell space (here K = 70), and the index m counts the number of iterations. Convergence is considered to have been attained when

$$s1 < \varepsilon \qquad \text{and} \qquad s2 < \varepsilon \tag{A.10a,b}$$

where ε is a sufficiently small constant and assumed to be 10^{-3} - 10^{-4}.

B. Difference scheme of Eqs. (5.9) and (5.10)

The conservative MHD equations are written generally in an (N+1)-dimensional rectangular space-time as

$$\frac{\partial u}{\partial t} + \nabla \cdot F = 0 , \tag{B.1}$$

where, for example, u is the six-component vector

$$u = (u, B)$$

in the incompressible fluid and $F = F(u)$ a flux tensor. The Friedrichs-Lax scheme, which is adopted in our computation, approximates the differential coefficient $\partial u/\partial t$ by such a difference form as

$$\frac{\partial u}{\partial t} = \frac{u^{n+1} - \overline{u^n}}{\Delta t} , \tag{B.2}$$

where $\overline{u^n}$ is the spatial average in the neighborhood of the points where the flux is evaluated. This introduces a numerical diffusion, or correctly, a linear viscous term and the scheme really represents an approximation to the differential equation

$$\frac{\partial u}{\partial t} + \nabla \cdot F = \frac{\Delta^2}{2N\Delta t} \nabla^2 u - \frac{\Delta t}{2} \frac{\partial^2 u}{\partial t^2} \tag{B.3}$$

where Δ is the mesh size. If c is the maximum propagation velocity,

$$\frac{\partial^2 u}{\partial t^2} \leq c^2 \nabla^2 u \tag{B.4}$$

and the scheme should be stable if the condition

$$\Delta t < \Delta / (c\sqrt{N}) \tag{B.5}$$

is satisfied. It is, however, inevitable that the artificial diffusion

thus introduced causes any initial conditions to be smoother in the course of time and so we must say that some important features expected to be revealed in the evolution of the reconnection of magnetic lines of force have been lost during our numerical experiment.

REFERENCES

Alfvén, H., and P. Carlqvist, *Solar Phys.*, 1, 220, 1967.

Arnoldy, R. L., *J. Geophys. Res.*, 76, 5189, 1971.

Aubry, M. P., C. T. Russell, and M. G. Kivelson, *J. Geophys. Res.*, 75, 7018, 1970.

Axford, W. I., *Space Sci. Rev.*, 7, 149, 1967.

Axford, W. I., *Rev. Geophys.*, 7, 421, 1969.

Baum, P. J., and A. Bratenahl, *J. Plasma Phys.*, In press, 1973a.

Baum, P. J., and A. Bratenahl, *Phys. Fluids*, In press, 1973b.

Baum, P. J., and A. Bratenahl, In preparation, 1973c.

Biskamp, D., and K. Schindler, *Plasma Phys.*, 13, 1013, 1971.

Bratenahl, A., and C. M. Yeates, *Phys. Fluids*, 13, 2696, 1970.

Buneman, O., *Phys. Rev.*, 115, 503, 1959.

Carlqvist, P., *Solar Phys.*, 7, 377, 1969.

Chapman, S., and P. C. Kendall, *Proc. Roy. Soc. Lond.*, A271, 435, 1963.

Chapman, S., and P. C. Kendall, *Phys. Fluids*, 9, 2306, 1966.

Coppi, B., and A. B. Friedland, *Astrophys. J.*, 169, 379, 1971.

Domingo, V., and D. E. Page, *J. Geophys. Res.*, 76, 8159, 1971.

Dungey, J. W., *Phil. Mag.*, 44, 725, 1953.

Dungey, J. W., *Cosmic Electrodynamics*, Cambridge Univ. Press, p.98, 1958.

Dungey, J. W., *Proc. 1962 Les Houches Summer School*, Gordon and Breach, p.503, 1963.

Dungey, J. W., and T. W. Speiser, *Planet. Space Sci.*, 17, 1285, 1969.

Elsasser, W. M., *Phys. Rev.*, 95, 1, 1954.

Evance, L. C., and E. C. Stone, *EOS. Trans. Amer. Geophys. Union*, 52, 904, 1971.

Friedman, M., *Phys. Rev.*, 182, 1408, 1969.

Friedman, M., and S. M. Hamberger, *Astrophys. J.*, 152, 667, 1968.

Fukao, S., and T. Tsuda, *J. Plasma Phys.*, 9, 409, 1973a.

Fukao, S., and T. Tsuda, *Planet. Space Sci.*, 21, 1151, 1973b.

Fukao, S., M. Ugai, and T. Tsuda, In preparation, 1974.

Furth, H. P., J. Killeen, and M. N. Rosenbluth, *Phys. Fluids*, 6, 459, 1963.

Giovanelli, R. G., *Mon. Not. Roy. Astron. Soc.*, 107, 338, 1947.

Gold, T., and F. Hoyle, *Mon. Not. Roy. Astron. Soc.*, 120, 89, 1960.

Green, R. M., *Proc. IAU Symp. on Solar and Stellar Magnetic Fields*, Amsterdam (ed. R. Lüst), p.398, 1965.

Green, R. M., and P. A. Sweet, *Astrophys. J.*, 147, 1153, 1967.

Hamberger, S. M., and J. Jancarik, *Phys. Fluids*, 15, 825, 1972.

Hoh, F. C., *Phys. Fluids*, 9, 277, 1966.

Jaggi, R. K., *J. Geophys. Res.*, 68, 4429, 1963.

Jaggi, R. K., *Proc. AAS-NASA Symp. on the Physics of Solar Flares*, Greenbelt (ed. W. N. Hess), NASA SP-50, p.423, 1964.

Kadomtsev, B. B., *Plasma Turbulence*, Academic Press, New York, p.71, 1965.

Meng, C. I., *J. Geophys. Res.*, 75, 3252, 1970.

Mestel, L., and P. A. Strittmatter, *Mon. Not. Roy. Astron. Soc.*, 137, 95, 1967.

Morfill, G., and J. J. Quenby, *Planet. Space Sci.*, 19, 1541, 1971.

Morfill, G., and M. Scholer, *J. Geophys. Res.*, 77, 4021, 1972.

Nardi, V., *Phys. Rev. Letters*, 25, 718, 1970.

Newcomb, W. A., *Ann. Phys.*, 3, 347, 1958.

Nishida, A., and K. Maezawa, *J. Geophys. Res.*, 76, 2254, 1971.

Nishida, A., and N. Nagayama, *J. Geophys. Res.*, 78, 3782, 1973.

Northrop, T. G., *Rev. Geophys.*, 1, 283, 1963.

Ohyabu, N., and N. Kawashima, *J. Phys. Soc. Japan*, 33, 496, 1972.

Parker, E. N., *Phys. Rev.*, 107, 830, 1957.

Parker, E. N., *Astrophys. J. Suppl. (77)*, 8, 177, 1963.

Parker, E. N., *Proc. XI COSPAR Symp. on Solar Flares and Space Research*, Tokyo (ed. C. de Jager and Z. Svestka), p.412, 1969.

Parker, E. N., *Astrophys. J.*, 180, 247, 1973a.

Parker, E. N., *J. Plasma Phys.*, 9, 49, 1973b.

Petschek, H. E., *Proc. AAS-NASA Symp. on the Physics of Solar Flares*, Greenbelt (ed. W. N. Hess), NASA SP-50, p.425, 1964.

Petschek, H. E., and K. S. Thorne, *Astrophys. J.*, 147, 1157, 1968.

Pneuman, G. W., *Solar Phys.*, 2, 462, 1968.

Priest, E. R., *Astrophys. J.*, 181, 227, 1973.

Russell, C. T., *Proc. Joint COSPAR/IAGA/URSI Symp. on Critical Problems of Magnetospheric Physics*, Madrid (ed. E. R. Dyer), p.1, 1972.

Schindler, K., and M. Soop, *Phys. Fluids*, 11, 1192, 1968.

Schmidt, H. U., *Proc. XI COSPAR Symp. on Solar Flares and Space Research*, Tokyo (ed. C. de Jager and Z. Svestka), p.331, 1969.

Sonnerup, B. U. Ö., *J. Plasma Phys.*, 4, 161, 1970.

Sonnerup, B. U. Ö., and L. J. Cahill, *J. Geophys. Res.*, 73, 1957, 1968.

Speiser, T. W., *J. Geophys. Res.*, 70, 4219, 1965.

Speiser, T. W., *Planet. Space Sci.*, 18, 613, 1970.

Stern, D. P., *Space Sci. Rev.*, 6, 147, 1966.

Stevenson, J. C., *J. Plasma Phys.*, 6, 125, 1971.

Stevenson, J. C., *J. Plasma Phys.*, 7, 293, 1972.

Stringer, T. E., *Plasma Phys.*, 6, 267, 1964.

Sturrock, P. A., *Proc. IAU Symp. on Structure and Development of Solar Active Regions*, Budapest (ed. K.O.Kiepenheuer), p.471, 1968.

Sturrock, P. A., and C. Barnes, *Astrophys. J.*, 176, 31, 1972.

Sturrock, P. A., and B. Coppi, *Astrophys. J.*, 143, 3, 1966.

Sweet, P. A., *Mon. Not. Roy. Astron. Soc.*, 110, 69, 1950.

Sweet, P. A., *Proc. IAU Symp. on Electromagnetic Phenomena in Cosmical Physics*, Stockholm (ed. B. Lehnert), p.123, 1958.

Sweet, P. A., *Ann. Rev. Astron. Astrophys.*, 7, 149, 1969.

Syrovatsky, S. I., *Soviet Astron.*, 10, 270, 1966.

Syrovatsky, S. I., *Proc. XI COSPAR Symp. on Solar Flares and Space Research*, Tokyo (ed. C. de Jager and Z. Svestka), p.346, 1969.

Syrovatsky, S. I., A. G. Frank, and A. Z. Khodzhaev, *Soviet Phys., JETP Lett.*, 15, 94, 1972.

Takayanagi, A., J. Sakai, and H. Washimi, *Kakuyugo-kenkyu Suppl. (4)*, 29, 1, 1973.

Uberoi, M. S., *Phys. Fluids*, 6, 1379, 1963.

Uberoi, M. S., *Phys. Fluids*, 9, 2307, 1966.

Uchida, Y., *Pub. Astron. Soc. Japan*, 21, 128, 1969.

Van Allen, J. A., J. F. Fennell, and N. F. Ness, *J. Geophys. Res.*, 76, 4262, 1971.

West, H. I., Jr., and A. L. Vampolar, *Phys. Rev. Letters*, 26, 458, 1971.

Yeh, T., and W. I. Axford, *J. Plasma Phys.*, 4, 207, 1970.

Yeh, T., and M. Dryer, *Astrophys. J.*, 182, 301, 1973.